BIOARTIFICIAL MATRICES TO MODULATE EPITHELIAL MORPHOGENESIS

A Dissertation
Presented to
The Academic Faculty

By

Nduka Obichukwu Enemchukwu

In Partial Fulfillment
Of the Requirements for the Degree
Doctor of Philosophy in Bioengineering in the
Woodruff School of Mechanical Engineering

Georgia Institute of Technology

December 2013

BIOARTIFICIAL MATRICES TO MODULATE EPITHELIAL MORPHOGENESIS

Approved by:

Dr. Andrés García, Advisor
School of Mechanical Engineering
Georgia Institute of Technology

Dr. Brandon Dixon
School of Mechanical Engineering
Georgia Institute of Technology

Dr. Thomas Barker
School of Biomedical Engineering
Georgia Institute of Technology

Dr. Asma Nusrat
School of Medicine
Emory University

Dr. David Collard
School of Chemistry and Biochemistry
Georgia Institute of Technology

Date Approved: September 4, 2013

To my wife, Chinyere, and my family, for regarding me according to the potential within me.

ACKNOWLEDGEMENTS

"...what is man that you are mindful of him, and the son of man that you care for him?"
Psalm 81:4

As I complete this document, I ask myself, "Who am I to be given such an opportunity to study at this level and in such a place?" I was born with ability I did not earn and with a supportive family I did not choose. Therefore, I begin by acknowledging God who knew all of my days before I was born and ultimately demonstrated his love for me in the person of Jesus Christ.

Next, I thank my best friend and wife, Chinyere. Her name literally translates from Igbo to English as "God has given". *Enyi mu onye a huru'm n'anya*, you are truly a gift that keeps on giving. Upon meeting you, I only hoped that I could call you a friend. I was certain that my character would be enhanced by being close to a person like you. Since then, I have known you as a remarkable encourager and teammate who takes my silliness in stride. Even before we were married, you endured long evenings on campus to keep me company and provided vital perspective during difficult times. This document stands as a testament to the countless ways that you have supported me personally and professionally.

I acknowledge my advisor, Dr. Andrés García, who has modeled for me a tremendous level of professional excellence while dealing patiently with the challenges of my development. Andrés, the recent series of awards and distinctions that have been bestowed on you clearly demonstrate what I observed over the years: you are among the best in the business. Thank you for giving me this opportunity to learn from you. I especially appreciate your approach to graduate school as a training ground where I could assemble strategies to build on my strengths and address my weaknesses with plenty of

encouragement. I am also grateful for your honest reflections on the rigors and rewards of academic careers. You put your family first and it has been a pleasure to glimpse your interactions.

Similarly, I thank my thesis committee members for their investments of time, reagents, and perspective toward a successful investigation. I thank Dr. Asma Nusrat for sharing reagents that significantly accelerated my studies. I thank Dr. Thomas Barker for the long and ranging conversations that have helped me to develop rigor in the investigations. I thank Dr. David Collard for sharing perspective on graduate school as a development process. I thank Dr. Brandon Dixon for modeling sincere concern for students and for the well-being of the campus community.

I thank the current and former members of the García Lab and Wing 2D for maintaining a vibrant and collaborative workplace. Particularly, I thank Kellie Templeman for consistently helping me to secure the tools I needed for success. I thank Dr. Asha Shekaran for articulating critical questions that helped me to focus my efforts. I thank Dr. Ed Phelps and Dr. Ted Lee for productive problem-solving consultations. I thank Chimdimnma Esimai and Dr. Imen Elloumi-Hannachi for timely words of encouragement.

I am grateful for the generous and professional service rendered by the staff of the Petit Institute for Bioengineering and Bioscience (IBB). Particularly, I thank the late Christopher Ruffin for going the extra mile to ensure my progress in the Bioengineering Program. Vivian Johnson, Deidra Johnson, Floyd Wood, James Godard, Alyceson Andrews, Allen Echols, and Johnafel Crowe all deserve acknowledgement for their

assistance and kindness. I thank the custodial staff, including Wilhelmina, Sharon, Greg and Henry for taking special interest in my success.

Several members of the broader Georgia Tech community deserve special acknowledgment for facilitating my matriculation and progress. I thank Dr. Felicia Benton-Johnson, Dr. Comas Haynes, Dr. Keith Oden, and Dean Gary May for supporting special professional development opportunities for me through the FACES Fellowship other venues. I thank Dr. Julia Babensee for patiently mentoring my teaching practicum. I thank Dr. Adegboyega Oyelere, Dr. Rudy Gleason, and Cornelius Ejimofor for taking special interest in my progress. I also thank Darren Nowell, Dr. Wayne Whiteman, and Nancy Hutton for extraordinary efforts in funding matters.

I am grateful for funding furnished by the National Institutes of Health, the GEM Fellowship, the NASA Harriet G. Jenkins pre-doctoral fellowship, and the UNCF-Merck Science Initiative.

I acknowledge technical support from Dr. Vazha Glonty and Matt Winfree of Nikon, and Dr. Anirban Datta of UCSF, and reagents from Randi Eisen and Dr. George Ojakian of SUNY Downstate. I thank Colin Walters of Merck and Cellgene for being an excellent mentor, going far above what was required of him and challenging me to do the same.

I acknowledge the valuable support of friends, student groups, and other communities around Georgia Tech and Atlanta. Particularly, I thank Chima Nwosu and Dr. Chibuzo Emenari for helping me to get established in Atlanta. I am grateful for the Fellowship of Christian Graduate Students, the Black Graduate Student Association, and the BBUGS organizations at Georgia Tech. I also acknowledge the pastors and

congregation at my church, the Assembly of Truth Family Worship Center, who have cheered my accomplishments and have challenged me to grow toward the character of Jesus Christ. I thank the Nnewi Union of Atlanta and Umu Igbo Unite for making me feel at home in Atlanta. I thank the late Dana Crenshaw, a remarkably godly and well-rounded man, for finding time to be my first mentor in Atlanta.

I give special recognition to my former summer research mentee Jacques Kumutima whose contributions are included in the Future Directions section of this thesis. I am also grateful for fun times with my Little Brother KaDarius Glenn, my mentee and ultra-competitive friend through Big Brothers Big Sisters of Metro Atlanta.

Finally, I am grateful for lifelong friendships forged at Massachusetts Institute of Technology. I particularly acknowledge Ojonimi Ocholi and Dr. Anderson Nnewihe for extraordinary support during my years at Georgia Tech.

I acknowledge my parents Dr. Obi and Chinwe Enemchukwu. You overcame tremendous obstacles to pursue education and me and my siblings without excuses. Mom, thank you for setting such high expectations for me. You believed that I could be excellent in every academic pursuit even when I didn't believe it. You challenged me to look in the mirror and examine my own actions when things went wrong and encouraged me to stand for what is right even if I had to stand alone. Although I chafed at the "pressure" at the time, today I am grateful that you called me to excellence. If I matured quickly, it was the result of your transparency. You did not conceal *all* the difficulties of single parenthood. I watched you stay up late to pray for me and my siblings, although your work schedules scarcely allowed you any rest. You made it seem normal to house relatives and help them toward their goals. What you did to establish a spiritual

foundation for us, to teach us healthy habits, and to educate us about our heritage would require page upon page to recount. Thank you, I love you, and I already know that you will call this dissertation your own. Dad, you have been a steadfast supporter and a sure source of encouragement during my graduate school years. Our travels together over these years have been especially valuable to me. Also, your text messages and voicemails have helped me to put my own issues in perspective of the countless blessings that I have received from God. I admire the way you consistently set aside your own challenges to seek the well-being of others. I am particularly grateful for your support for me and Chinyere.

To my siblings, thank you for sharing the journey with me. Over the years, you traveled great distances to see me and provide support. I particularly remember when you road-tripped into town to help me buy furniture, paint my home, and put on a housewarming party. Ekene, you continued your long record of looking out for me during your visits by taking me out for Thai food or putting groceries in my refrigerator. Chibuzo, you have consistently valued me enough to hit the road to see me and support my activities. Uche, you have always spoken such encouraging words to me. Aj, thanks for bearing with my long-windedness and being my workout buddy whenever we get together. Benny, conversations with you always allowed me to learn something new. That is, when I was not laughing hysterically

I acknowledge my extended family of aunts, uncles, cousins, and grandparents who invested significant energy in my upbringing. In particular, I thank my uncles Udoka Odunukwe, Uzo Odunukwe, and Dr. Ebube Odunukwe, my aunt, Dr. Joy Odunukwe

Oraka, and my grandparents, the late J.A. Odunukwe and Mercy Odunukwe for substantial investments at critical stages in my youth.

.

TABLE OF CONTENTS

LIST OF TABLES

LIST OF FIGURES

LIST OF SYMBOLS AND ABBREVIATIONS

2D	two-dimensional
3D	three-dimensional
AJ	adherens junction
ANOVA	analysis of variance
BM	basement membrane
Coll	collagen
DMSO	dimethyl sulfoxide
ECM	extracellular matrix
EdU	5-ethynyl-2´-deoxyuridine
EHS	Englebreth Holm-Swarm
EMT	epithelial-mesenchymal transition
ERK	extracellular signal-regulated kinase
FAK	focal adhesion kinase
FBS	fetal bovine serum
FN	fibronectin
GM130	golgi matrix protein 130
GPQ-A	GCRDGPQGIAGQDRCG
GPQ-W	GCRDGPQGIWGQDRCG
HA	hyaluronic acid
HGF	hepatocyte growth factor
JAM	junctional adhesion molecule
kDa	kiloDalton
LM	laminin
MDCK	Madin-Darby canine kidney
MEC	mammary epithelial cell
MET	mesenchymal-epithelial transition
MMP	matrix metalloproteinase
PEG	poly ethylene glycol
PEGDA	PEG-diacrylate
PEG-4MAL	four-arm PEG-maleimide
PEG-4VS	four-arm PEG-vinyl sulfone
PEG-4A	four-arm PEG-acrylate
PI3K	phosphoinositide 3-kinase
PIP2	phosphatidylinositol -4,5-bisphosphate
PIP3	phosphatidylinositol-3,4,5-triphosphate
Podxl	podocalyxin/gp135
PTEN	phosphatase and tensin homolog
RGD	arginine-glycine-aspartate
TEA	triethanolamine
TJ	tight junction
VEGF	vascular endothelial growth factor
wt%	weight percentage
ZO-1	zonula occludens 1

SUMMARY

Acute injury of major epithelial organ systems (kidney, liver, lung, etc.) is collectively a principal cause of death worldwide. Regenerative medicine promises to meet these human health challenges by harnessing intrinsic cellular processes to repair or replace damaged tissues.

Epithelial morphogenesis is a hard-wired, multicellular differentiation program that dynamically integrates microenvironmental cues to coordinate cell fate processes including adhesion, migration, proliferation, and polarization. Thus, epithelial morphogenesis is an instructive mode of tissue assembly, maintenance, and repair. Three-dimensional epithelial cell cultures in natural basement membrane (BM) extracts produce hollow, spherical cyst structures and have indicated that the BM provides the critical cell adhesion ligands to facilitate cell survival, stimulate proliferation, and promote polarization and lumen formation. However, the utility of natural BMs for detailed studies is generally limited by lot-to-lot variations, uncontrolled cell adhesive interactions, or growth factor contamination.

The goal of this thesis was to engineer bioartificial extracellular matrices (ECM) that would support and modulate epithelial cyst morphogenesis. We have engineered hydrogels, based on a multi-arm maleimide-terminated poly (ethylene glycol) (PEG-4MAL), that present cell adhesive molecules and enzymatic degradation substrates and promote polarized epithelial cyst differentiation *in vitro*.

To investigate the influence of matrix physical and biochemical signals on cyst morphogenesis, we independently varied the polymer weight percentage (wt%), the density of a cell adhesion ligand (RGD), and crosslink degradation rates of the hydrogels.

Then, we evaluated functional outcomes including Madin-Darby canine kidney (MDCK II) epithelial cell survival, proliferation, cyst polarization, and lumen formation. We found that cell proliferation, but not cell survival, was sensitive to the polymer wt%, which is related to elastic modulus and crosslink density. This result defined a working range of PEG-4MAL concentration (3.5% - 4.5%) that promotes robust proliferation. Analysis of mature cysts indicated that 4.0% and 4.5% gels produced cysts resembling those typically grown in type I collagen gels while 3.5% gels produced cysts with higher incidence of inverted polarity and multiple lumens. Perturbation of matrix degradability using a slow-degrading crosslink peptide or matrix metalloproteinase inhibitors showed that the rate of matrix degradation exerts major influence on cyst growth in PEG-4MAL gels. We employed 4.0% PEG-4MAL hydrogels with RGD ligand density ranging over 0 – 2000 uM to discover that (1) lumen formation was eliminated in the absence of RGD, (2) extent of lumen formation increased with increasing RGD concentration, and (3) cyst polarity was inverted below a threshold of integrin binding to RGD. Together, these results show that the biochemical and physical properties of the matrix, particularly integrin binding and matrix degradability, effectively modulate establishment of apico-basal polarity and lumen phenotypes in MDCK II epithelial cyst structures. Furthermore, these studies validate PEG-4MAL hydrogels as a powerful culture platform to enable detailed investigation of matrix-directed modulation of epithelial morphogenesis.

CHAPTER I: SPECIFIC AIMS

Introduction

Epithelial morphogenesis is an instructive mode of tissue assembly, maintenance, and repair. Three-dimensional cultures in natural basement membrane (BM) extracts produce spherical cyst-like epithelial structures and have indicated that the BM provides the critical cell adhesion ligands that facilitate cell survival, stimulate proliferation, and promote polarization and lumen formation. However, the utility of natural BMs for detailed studies is generally limited by lot-to-lot variations, uncontrolled cell adhesive interactions, or growth factor contamination. The objective of this project was to engineer bioartificial matrices to support epithelial morphogenesis. Our hypothesis was that protease-degradable, synthetic hydrogels optimized to present integrin-targeting cell adhesive motifs would support robust cyst differentiation in a manner similar to that observed in natural BM. The significance of this work is the development of synthetic microenvironments that modulate epithelial morphogenesis by controlling cell-matrix interactions. Toward this goal, we pursued the following specific aims:

Specific Aim 1: Quantitate the influence of PEG-4MAL polymer weight percentage on cyst morphogenesis in bioartificial hydrogels.

The purpose of this aim was to characterize the physical properties of synthetic matrices that support epithelial morphogenesis. Multi-arm poly (ethylene glycol)-maleimide (PEG-4MAL) macromers were functionalized via a Michael-type reaction with adhesive peptides and crosslinked with peptides containing matrix metalloproteinase

sensitive sequences in the presence of Madin-Darby canine kidney (MDCK II) epithelial cells.

PEG-4MAL-based hydrogel elastic moduli vary linearly with PEG-4MAL weight percentage over the range of 4.0% and 10% (w/v). Notably, gels fabricated at 4.0% exhibit elastic moduli that resembles type I collagen gels [1]. We show here that these engineered microenvironments permit high MDCK II cell viability and promote robust cyst morphogenesis over 10 days in a manner similar to that observed in type 1 collagen gels. We adapted immunofluorescence protocols and employed confocal microscopy to visualize lumen formation and markers of apico-basal polarity. Our results define a PEG-4MAL weight percentage regime that promotes robust polarized cyst morphogenesis and demonstrate modulation of apico-basal polarity and lumen phenotypes via adjustment of matrix degradability.

Specific Aim 2: Quantitate the influence of adhesive ligand density on cyst morphogenesis in bioartificial hydrogels.

The purpose of this aim was to characterize the biochemical properties of synthetic matrices that support epithelial morphogenesis. PEG-4MAL-based hydrogels exploit a highly-efficient maleimide-thiol Michael addition reaction that ensures rapid and complete incorporation of adhesive ligand added to the hydrogel precursor solution [1]. Thus, adhesive ligands can be incorporated with high precision. We titrated ECM-derived adhesive ligand arginine-glycine-aspartic acid (RGD) over the range of 0 μM to 2000 μM in PEG-4MAL gels and evaluated cyst morphogenesis on the bases of cyst size, lumen phenotype, and apico-basal polarity. Our results indicate that MDCK II cyst

morphogenesis is highly-sensitive to incorporated RGD concentration. We found that (1) lumen formation was eliminated in the absence of RGD, (2) extent of lumen formation increased with increasing RGD concentration, and (3) cyst polarity was inverted below a threshold of integrin binding to RGD.

Project Significance

Acute injuries of major epithelial organ systems (kidney, liver, lung, etc.) are collectively a principal cause of death worldwide [2-5]. Several organs, including the kidney, lung, intestine and liver, can recover from acute injury, provided that the host survives the initial trauma. For instance, in kidney regeneration, partially-denuded epithelial interfaces are repopulated by surviving epithelial cells that secrete a specialized matrix, transiently differentiate to a mesenchymal phenotype, and proliferate [5-9]. However, several debilitating diseases, including idiopathic pulmonary fibrosis (lung), Crohn's disease (intestine), and kidney fibrosis, involve permanent differentiation of epithelial cells to a fibrotic mesenchymal phenotype and ultimate loss of organ function [2, 10, 11].

Regenerative medicine promises to meet human health challenges by harnessing intrinsic cellular processes to repair or replace damaged tissues. Epithelial morphogenesis is a hard-wired, multicellular differentiation program that dynamically integrates microenvironmental cues to coordinate cell fate processes including adhesion, migration, proliferation, and polarization. Thus, it is an instructive mode of tissue assembly, maintenance, and repair. Learning how to modulate epithelial morphogenesis to control

cell proliferation, alter differentiation responses, and maintain cell polarity after acute injury could remarkably improve human health [5].

A potential strategy for controlling cell behavior in a multicellular context involves rationally-designed, ECM-mimetic biomaterials. Synthetic ECM analogues offer tunable elastic properties, controlled integration of cell adhesion ligands, and degradation by cell-secreted enzymes, all with minimal immunogenicity *in vivo* [12]. We have employed PEG-based hydrogels that controllably integrate cell adhesion ligands and protease-degradable crosslinks to effectively modulate epithelial cyst polarization and lumen formation. Thus, bioartificial matrices stand as an experimental and therapeutic platform offering remarkable control of the physical and biological properties of the microenvironment for studies of tissue morphogenesis. This work aims to marry the biology of the native epithelial tissue microenvironment with versatile synthetic biomaterials and may expose therapeutic strategies for epithelial organ regeneration.

CHAPTER II: LITERATURE REVIEW

Epithelial structure and function

In metazoans, from *Caenorhabditis elegans* to *Homo sapiens*, body compartments are separated for localization of critical organ functions, for protection from the outside world, and for establishment of passageways that transport fluids and other cargo [5, 13, 14]. The barrier between compartments is called an epithelium. Epithelia are contiguous sheets of cells that actively regulate movement of fluids and solutes between compartments. The skin and the lining of the gastrointestinal tract typify epithelial sheets. In glandular organs, epithelia exist in tubular forms and may feature branching morphology that terminates in hollow, spheroid structures surrounding a central lumen. Spherical epithelial monolayers are called acini, alveoli, follicles, or cysts in specific tissue contexts [14]. Epithelial cell sheets are polarized, in that each cell maintains three membrane surface types: (1) lateral cell-cell adhesion with neighboring cells; (2) a basal surface that adheres to underlying extracellular matrix (ECM); and (3) a free, apical surface that might border a lumen. In general, the lateral and basal membrane domains are continuous and are therefore called "basolateral" (**Figure 2.1**). Lateral cell-cell adhesion is mediated by cytoskeleton-linked transmembrane proteins and tight junction complexes and is critical to barrier functions. A specialized ECM called basement membrane is secreted and assembled by epithelial cells, and this provides critical survival and morphogenetic signals through cell surface receptors that also provide anchorage. In glandular epithelia, the lumen-facing apical surface might be characterized by microvilli for absorption or by cilia for movement of secretions.

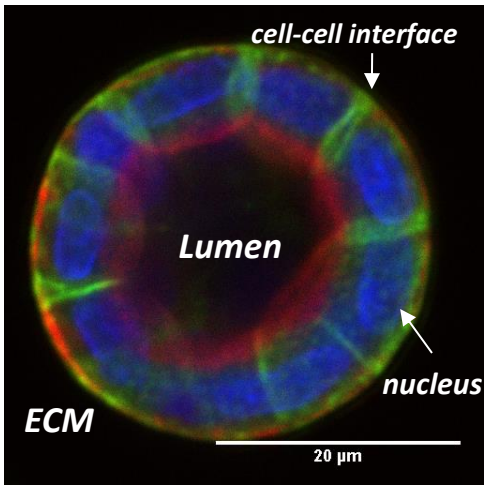

Figure 2.1. Confocal immunofluorescence image of polarized Madin-Darby Canine Kidney (MDCK) epithelial cell cyst grown in protease-degradable synthetic hydrogel matrix with cell adhesive peptides. Green = β-catenin, red = f-actin, blue = nuclear DNA.

Cell-cell adhesion and polarity

Cell-cell adhesion is a critical aspect of the sheet-like character and barrier functions of epithelia. Several proteins are involved in the variety of subcellular structures that maintain cohesiveness in cellular sheets. These structures provide physical anchoring between cells, link to the actin cytoskeleton, and modulate signaling pathways that regulate gene expression [15-18]. Furthermore, the asymmetric cellular localization and intramembrane diffusion limiting functions of particular cell-cell adhesion structures is critical to epithelial polarity [19].

Tight junctions (TJs) are located close to the apical surface of an epithelium and serve as tight seals between cells such that the cell layer is selectively permeable barrier to diffusion [18, 19]. Adherens junctions (AJs), located basally versus TJs, initiate and maintain the physical attachment between neighboring epithelial cells. On the molecular level, the AJ is made up of homotypically-interacting E-cadherin molecules [15]. Desmosomes are a third type of cell-cell adhesion structure. Located further toward the

basal surface versus TJs and AJs, desmosomes are distinguished by transduction of intermediate filament interaction across the cell membrane [20].

TJs are particularly versatile in that they mark the boundary between the apical and basolateral membrane domains and serve as a barrier to prevent diffusion of macromolecules between the apical and basolateral domains. Additionally, TJs are multi-protein signaling complexes that play critical roles in cell polarity, proliferation, and differentiation [19, 21]. Structurally, the TJ complex is made of transmembrane proteins and peripheral membrane proteins that function as scaffolding proteins to link the TJ to the actin cytoskeleton and signaling molecules. The transmembrane protein group includes occludins, claudins, and junctional adhesion molecules (JAMs). These proteins regulate flow of fluids and ions through the gap between cells between cells while preventing passage of large molecules. The peripheral membrane proteins include ZO-1 and Rab13 and facilitate organization of transmembrane proteins, allow transmembrane protein interaction with the cytoskeleton, and initiate cell signaling [18].

Given their apical localization relative the cell layer, TJs essentially define apico-basal polarity in epithelia. In a mature, polarized epithelium, the apical plasma membrane domain interfaces a free surface (like a fluid-filled lumen). Compositionally, the apical plasma membrane is characterized by phosphatidylinositol -4,5-bisphosphate (PIP2), podocalyxin, annexin-2, and a dense f-actin meshwork. Morphologically, the apical plasma membrane is often marked by microvilli and cilia. In contrast, the basolateral membrane domain is enriched in β1 integrin, phosphatidylinositol-3,4,5-triphosphate (PIP3), and phosphoinositide 3-kinase (PI3K), the kinase that converts PIP2 to PIP3 [5]. The system by which intracellular trafficking machinery target newly synthesized

membrane components to their designated location is complex and regulated by a variety of pathways [22-24]. Notably, the transition between apical and basolateral membranes is marked sharply by the TJ, as the structure bars intramembrane diffusion. The TJ also dictates apico-basal polarity by specific intermolecular interactions. As will be discussed later, orientation of polarity in a developing epithelium is followed by generation of membrane asymmetry that requires docking of polarity proteins at the TJs [18, 19, 25-27].

Basement membrane

The ECM is the non-cellular component of tissues that provides mechanical support while sequestering and presenting growth and differentiation factors, as well as adhesive ligands, which are essential for survival, proliferation, migration, and nutrient storage [28]. It is a hydrated meshwork of glycoproteins and proteoglycans that has nano-, micro-, and macro-scale organization [29]. Macro-scale features of ECM include folds, bends, invaginations, and protrusions formed by patterned matrix secretion, matrix swelling, and cell contractility [13]. The major components of the ECM are the large, insoluble macromolecules collagen, laminin (LM), fibronectin (FN), and proteoglycans, including hyaluronan, organized in fibrillar or isotropic networks with nano-scale order. The ECM is dynamic in that its secretion, assembly, and degradation by cells is regulated by developmental stage and is altered in disease and regeneration [13, 30, 31].

The basement membrane (BM) is a 20 – 100 nm thick layer of specialized ECM that underlies epithelia and provides ligands for anchorage and signaling via cell surface receptors. Furthermore, the BM physically isolates epithelia (as well as blood vessels,

muscle, fat, and peripheral nerve cells) from the surrounding connective tissue. From the early steps of embryogenesis, the basement membrane is critical for tissue development [32]. The BM is secreted and assembled by epithelial cells and is rich in type IV collagen and various LM isoforms [13, 32-35]. These two major components form independent, weakly interactive networks that are interconnected by minor BM components, namely nidogens [32, 33, 36-38]. Type IV collagen is thought to provide mechanical stability [33], whereas both LM and collagen provide cell adhesive motifs bound by integrins and dystroglycan [30, 33]. Much of what is known about BM composition, assembly, and function is derived from studies of the Englebreth-Holm-Swarm (EHS) mouse tumor basement membrane. The EHS tumor produces copious amounts of matrix from which individual macromolecular components can be purified [39-42].

As the collagen IV scaffold of the BM seems to depend on initial secretion and assembly of LM, it has been concluded that LM is the centerpiece of the BM [39]. The LM molecule is a large glycoprotein consisting of three polypeptide chains associated in a cross-shaped coiled coil. Each LM macromolecule is a heterotrimer containing one each of α, β, and γ chains. Five LM α, four β, and three γ genes have been identified in mammals, with two forms of α3 owing to alternative splicing. LM subunits are secreted in 15 combinations that are known to be stable (**Figure 2.2**). LM-332, for instance, is composed of α3, β3, and γ2 chains. There are three short arms in the cruciform macromolecule that correspond to N-terminal ends of each constituent chain while the long arm is the coiled-coil region made from the C-terminal ends of all three chains. At each terminus, several bioactive domains are found. These include cell surface receptor recognition motifs, enzyme degradation sites, homo- and heterotypic LM chain

interaction sites, and domains where LM binds other ECM molecules [43, 44]. Importantly, LM-111 contains an Arg-Gly-Asp (RGD) amino acid motif and mediates cell adhesion via cell surface integrin receptors [45].

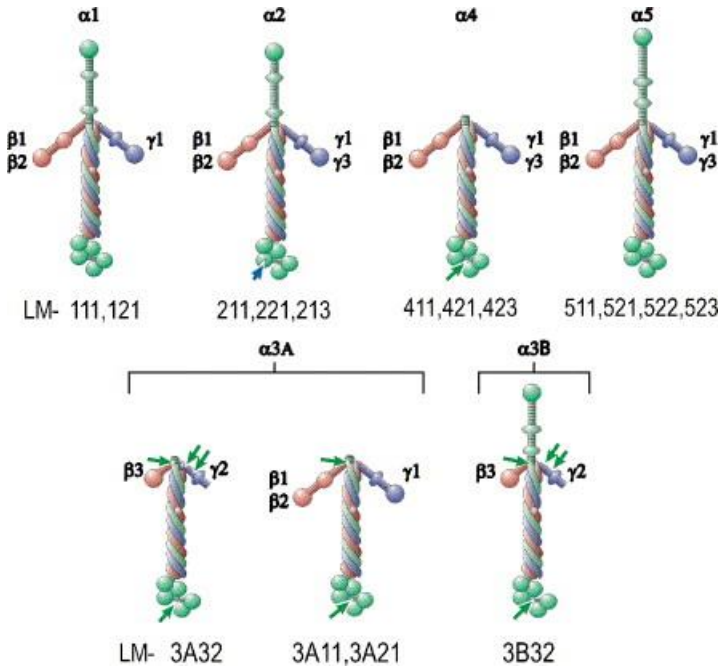

Figure 2.2. The human or mouse laminin (LM) heterotrimers. From [43].

While it is known that LM is deposited into the basement membrane by epithelial cells, its assembly into a network is not well understood [34]. Laminins are secreted as intact heterotrimers and some are then proteolytically processed in a way that might affect receptor binding [46]. It initially appeared that self-assembly of laminins into polymers and co-polymers *in vitro* requires that all trimer arms be full-length [38]. However, surface plasmon resonance has been used to observe interactions of LM-332, having a truncated β chain, with itself and with LM-511 that suggest that truncated-arm laminins may be involved in provisional matrices that are then stabilized by addition of full-length laminins [31, 47]. Nevertheless, pericellular polymerization of laminins occurs

as the trimers are bound to cell surface receptors [48, 49]. The α3β1 integrin modulates LM-332 deposition *in vitro* and α6β4 might also be involved [50-52]. Integrins are thought to regulate LM deposition via signaling by Rho GTPases including Rac1. After integrin binding activates Rac1 and inhibits rhoA, Rac1 causes integrins to organize secreted LM at the cell periphery [53-55]. The details concerning how integrins regulate LM deposition via Rac1 remain unclear but one model is that Rac1-induced actin reorganization causes integrins to move about on the membrane such that they alter the conformation of freshly secreted LM-332. A similar mechanism is observed in FN secretion and assembly [34, 56, 57].

Laminins have been shown to have profound impact on epithelial tissue morphogenesis *in vivo*, having roles in cell survival and polarization among others. The expression patterns of the various LM isoforms is tissue-specific and is dependent of developmental phase and disease state [44]. LM-111 was the first to be discovered and is also the most extensively studied of all the isoforms [30, 58]. Furthermore, LM-111 is perhaps the most widely distributed of the laminins and it has been shown to have critical roles in embryonic BM assembly [30, 32]. In mouse embryonic kidney development, LM-111 and LM-511 are found in the basement membrane surrounding the ureteric bud, the epithelial outgrowth that invades the metanephric mesenchyme and causes it to condense into an epithelium via a mesenchymal-epithelial transition (MET). Morphogenetic transitions of this epithelium give rise to the nephron, the functional unit of the kidney [44]. In *ex vivo* cultures of embryonic kidney, antibodies against the LM α1 chain block the nephrogenic MET [59]. Also, embryos lacking the gene encoding LM α5 chain show disrupted ureteric bud branching [60]. Whereas expression of LM-332 is

sparse in the healthy kidney, its expression is widespread during regeneration following ischemic renal injury and in polycystic kidney disease [31, 61]. *In vitro* studies with MDCK cells and *in vivo* studies in a rat model of ischemic renal injury indicate that LM-332 is required to stimulate cell proliferation and cell spreading in order to reconstitute an intact epithelium. MDCK cells synthesize and secrete LM-332 while sub-confluent, and spread on the provisional matrix via α6β4 and β1 integrins, and then subsequently degrade the matrix upon reaching confluence. In this context, polymerization of LM-511 is thought to be responsible for polarization of the regenerated epithelium [31]. Such studies suggest a role for LM-332 in normal regeneration of renal tubular epithelia after injury and in pathological generation of renal cysts.

In the lung, several LM isoforms are present during embryonic development and in the adult tissue. The LM α1 chain is critical for branching. Specifically, in human embryonic lungs, LM α1 is present specifically at the tips of advancing branch tips and not at proximal portions. Whereas LM α1 is present only during pre-natal lung development, LM α5 is present throughout organogenesis and is thought to be involved in epithelial cell differentiation. Whether LM-332 plays a critical role in wound healing following lung injury, as it does in kidney, is yet to be seen [62]. Observations are complicated by the lethal skin disease that affects mice that lack LM α3 [63]. Nevertheless, knockdown of LM α3 expression results in increased type I collagen deposition at the alveolar epithelial basement membrane, suggesting a role of LM α3 in inhibiting fibrosis [64].

Cell-ECM adhesion

Epithelial cells are anchored to the basement membrane via cell surface receptors that bind specific components of the basement membrane. These receptors include integrins, dystroglycans, syndecans, and less specifically classified receptors including the 67 kDa and 110 kDa LM receptors. The family of integrins represents the best understood class.

Integrins are transmembrane glycoproteins that link the cytoskeleton to the ECM with wide-ranging consequences for cell behavior in all metazoans [65]. Each integrin is a heterodimer, consisting of α and β chains. Of the 24 known integrin subunit combinations in mammals, epithelial cells typically express β_1, β_3, or β_4 subunits paired with any of a number or α subunits, thus allowing interaction with ECM components FN, LM, and collagens [66]. Most of the β_1 subunit-containing heterodimers ($\alpha_1\beta_1$, $\alpha_2\beta_1$, $\alpha_6\beta_1$, and $\alpha_3\beta_1$) are receptors for collagen and LM. Meanwhile, $\alpha_5\beta_1$ and $\alpha_V\beta_3$ are receptors for the RGD peptide of fibronectin and other adhesive proteins. Finally, $\alpha_6\beta_4$ is an epithelial-specific integrin that binds LM [65](**Figure 2.3**). Integrins function not only to provide anchorage but also to transduce signals bi-directionally [33, 50, 65, 67]. Upon binding extracellular ligand, integrin outside-in signaling involves assembly of multimeric signaling complexes at the short cytoplasmic tails of the heterodimer. These complexes initiate various signaling cascades that regulate survival, proliferation, and differentiation [65]. Inside-out signaling may involve association of actin-binding proteins with the cytoplasmic tails of bound integrins. Cell contractility then causes assembly or deformation of ECM networks [33, 51, 65].

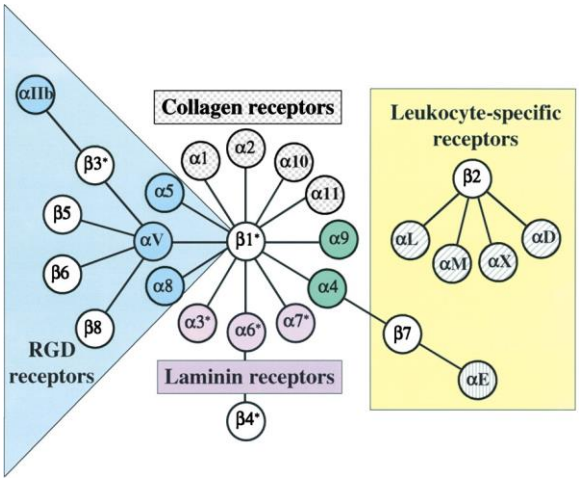

Figure 2.3. The family of integrin receptors. Laminin, collagen, and RGD motif binding integrins are grouped. From [65].

Epithelial morphogenesis

Epithelial morphogenesis refers to the dynamic integration of environmental stimuli in a hardwired genetic program that produces and maintains epithelial tissue structures [14]. *In vivo* development of epithelial tissues involves coordination of cell fate processes including proliferation, migration, cell death, and differentiation. Thus, epithelial morphogenesis is a valuable model that provides insights into many aspects of physiology that are relevant for tissue regeneration. Historically, epithelial morphogenesis has been observed *ex vivo* with embryonic kidney explants and in the morphological transitions of the adult mammary gland [68-73]. *In vitro*, two-dimensional cultures of epithelial cells on permeable filters has given way to three-dimensional cultures in natural or synthetic matrices and, together, have provided fruitful models for investigation [5].

In vitro models: Cyst morphogenesis

Monolayers of cultured epithelial cells were the first *in vitro* models of epithelial tissues. The Madin-Darby canine kidney (MDCK) cell line was derived from renal collecting tubules of a Cocker-Spaniel kidney and has been used extensively in research [74, 75], as have human mammary epithelial cell lines (e.g., MCF-10A) [76], and human intestine-derived cell lines (e.g., Caco-2) [77, 78]. Fluorescently-labeled antibodies and confocal microscopy have been used to visualize apically-, basally-, and laterally-segregated membrane proteins and cell surface receptors. As many proteins are targeted to both the basal and lateral membranes, the two surfaces are captured together in the term "basolateral" [14]. Polarized MDCK epithelial sheets feature ductal characteristics including solitary cilia, apical microvilli and tight junctions. Microvilli increase surface area for absorptive function. Tight junction complexes mark the apical-lateral border and serve to limit paracellular fluid transport across the monolayer. Early studies revealed that apico-basal polarity involves active segregation of membrane-associated proteins to distinct domains using intracellular trafficking machinery [23, 25].

Induction of epithelial cell polarity has been found to depend on both cell-cell and cell-ECM adhesion [14]. Three-dimensional (3D) cultures of MDCK and other epithelial cells in extracts of natural basement membrane trigger robust cyst development. Type I collagen gels and the complete EHS basement membrane extract, known as Matrigel^{TM}, have been used most extensively [14, 79-86]. These polarized cysts represent near-physiological epithelial tissue rudiments. Introduction of hepatocyte growth factor (HGF) to these cultures elicits epithelial-mesenchymal transitions (EMTs) that resemble tubulogenesis *in vivo* [87-89]. These 3D cultures have allowed perturbation of cellular machinery and have yielded tremendous insight into the mechanisms by which basement

membrane attachment-associated signals orient polarity and drive lumen formation to establish and maintain epithelial tissue architecture [14].

Type I collagen gels have been used extensively as substrates for 2D cell culture studies and as matrices for 3D cultures [90-92](**Figure 2.4**). For epithelial cells, collagen gels were initially used to observe histotypic growth and reorganization of mouse mammary and pig thyroid cells embedded within [81, 82, 84, 85, 93, 94]. The first reported 3D cultures of MDCK cells involved a fibrin clot in which MDCK formed polarized cysts with lumens [79]. When MDCK cells were grown in a monolayer on collagen gel and then overlaid with yet more collagen gel, small cysts formed via cell aggregation [83]. However when single MDCK cells were cultured dispersed in collagen gel, polarized cysts formed clonally with a single cell giving rise to each cyst [80]. The same group demonstrated that MDCK cysts could be extracted from collagen gels using collagenase and subsequently resuspended in collagen or dissociated and plated to form monolayers [80]. The flexibility of the collagen gel culture system and the resilience of MDCK cysts facilitated other studies that investigated reversal of cyst polarity upon change of extracellular environment. Whereas MDCK cysts cultured in collagen gels polarize such that the apical surface borders the lumen and the basal surface interfaces the collagen matrix, cysts formed in suspension culture show opposite polarization. In suspension-grown cysts, apical membrane proteins localize to the exterior of the cyst while basement membrane proteins are secreted into the lumen. Embedment of these suspension-grown cysts in collagen simultaneously provides an ECM interface and eliminates the free exterior surface. The result is reversal of polarity, as the cysts degrade the luminal basement membrane [93, 95-97] [55].

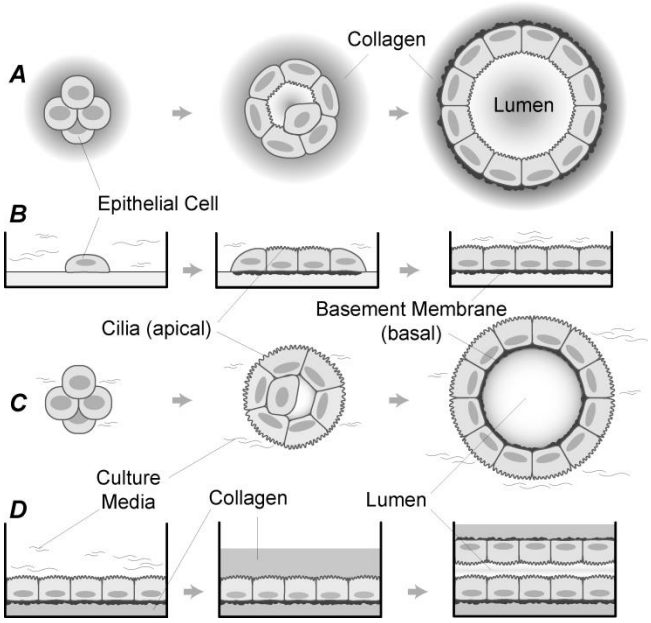

Figure 2.4. Epithelial cell growth characteristics in vitro. a, Cell division, apoptosis, and shape change over a period of several days in embedded culture often leads to a stable, lumen-containing cyst formed by a single layer of ECs. b, ECs plated on a layer of collagen (surface culture) typically generate a stable, uniform monolayer. c, Inverted cysts (cell polarity relative to that in *a* is inverted) form in suspension culture, with matrix deposited on the inside of the cyst. d, Lumens are frequently formed in collagen overlay experiments. From [98].

In 3D cultures, it has been shown that integrins have critical roles in survival, establishment of polarity, and lumen formation. MDCK bind to collagen via $\alpha_2\beta_1$ integrin [99]. Inhibition of $\alpha_2\beta_1$ integrin-mediated adhesion to type I collagen gels reduces cyst formation, increases apoptosis, and blocks HGF-induced tubulogenesis [100]. Furthermore, apical surfaces of MDCK cysts have a small pool of inactive $\alpha_2\beta_1$ integrins that are activated when overlaid with collagen and mediate signaling that results in polarity reversal [99, 101-103].

During the course of cyst development, MDCK cells in type I collagen secrete and assemble a basement membrane of LM and type IV collagen (Coll IV) with a layer of fibronectin, a ligand for integrin $\alpha5\beta1$. Ablation of the fibronectin matrix with siRNA

resulted in increased apoptosis [104]. Notably, as Matrigel™ is a basement membrane derived from a mouse tumor, it is a pre-assembled matrix consisting primarily of LM and type I collagen, and myriad other components in smaller quantities [105]. Thus, MDCK cells embedded in Matrigel™ encounter immediate presentation of α3β1- (LM) and α6β4-(Coll IV) integrin binding ligands. As will be discussed later, the quality and timing of basement membrane assembly, and subsequent integrin binding, are critical for establishment of epithelial cyst polarity.

Cells derived from intestine, mammary gland, and lung, also form hollow, polarized, cyst-like structures when embedded in natural ECM extracts, with some mechanistic variety [35, 106-109]. Normal mammary epithelial cells (MECs) form acini, single layers of polarized, growth-arrested cells surrounding a hollow lumen when grown in Matrigel™ [76]. Induction of oncogenes in these cultures have elucidated important roles for ECM properties in mammary tumor metastasis [110, 111]. Importantly, primary MECs from β1 integrin knockout mice were used to show that β1 integrin binding in the mammary gland triggers alignment of microtubules to facilitate cell membrane asymmetry and polarized localization of the golgi apparatus [24].

Establishment of polarity

It is critical that the polarity of each constituent cell is aligned with the overall tissue structure in order for the tissue to function [54]. Indeed, in the developing kidney, cells surrounding the ureteric bud aggregate and polarize before forming a lumen [112]. Mostov, Matlin, Nelson and many others have investigated the mechanisms by which integrin signaling aligns the axis of epithelial polarity to the overall tissue architecture [5, 25, 66, 113].

Today, epithelial tissue polarization is thought to occur in two steps: (1) an axis of polarity is selected; and (2) molecular asymmetry is generated along that axis [25].

(1) Selection of an axis of polarity

Beginning with the observation that classical Rho family GTPases (RhoA, rac1, Cdc42) play roles in polarization, Mostov and colleagues investigated the role of cell-ECM interactions in establishment of an axis of polarity. Rac1 along with other Rho family proteins (RhoA and Cdc42) are known to propagate polarization signals by remodeling the actin cytoskeleton near the cell membrane. Whereas mutant Rac1 does not alter polarity in MDCK monolayers, expression of dominant negative Rac1 causes inverted cyst polarity in 3D culture [16, 54]. Furthermore, mis-assembly of the pericellular LM basement membrane was observed. Exogenous LM was recruited to the cyst surface and rescued proper cyst polarity. Subsequent work in the same group identified the necessity of β_1 integrin in LM assembly and in signaling to allow polarized cyst morphogenesis [53]. Thus, Rac1 and LM comprise an autocrine pathway through β_1 integrin that orients the apical pole in cyst morphogenesis. The proposed mechanism is that intracellular Rac1 controls extracellular LM assembly via integrin-cytoskeleton interactions. Then, the extracellular LM acts on the cells via β_1 integrins to direct orientation of apical pole [54].

(2) Generation of membrane asymmetry

Mostov and colleagues used siRNAs and introduction of dominant negative proteins to alter expression and function, respectively, of phosphatase and tensin

homolog (PTEN), annexin 2 (Anx2), Cdc42, and atypical protein kinase C (aPKC), all proteins thought to be critical to MDCK apical (AP) plasma membrane (PM) and lumen formation [27, 114-118]. Additionally, proteins were added exogenously to the PM to investigate effects. From their findings that loss of function of any one of the aforementioned proteins prevents normal AP/PM and lumen formation, a mechanism that links MDCK epithelial cell AP/PM development to lumen formation was proposed. Initially, the phosphoinositides PIP2 and PIP3 are distributed throughout the cell membrane. Once tight junctions (TJs) are formed, PTEN, a phosphatase, is targeted to the TJs where it antagonizes the behavior of PI3K (the kinase that phosphorylates PIP2 to PIP3) and converts PIP3 to PIP2. The result is enrichment of PIP2 near the TJs. PIP2 is bound strongly by Anx2, a protein involved in apical transport that recruits Cdc42 to the now established apical domain. There, Cdc42 binds the Par6/aPKC polarity complex [27]. Lumen formation is believed to be tied to this process by the membrane protein trafficking machinery [119]. Specifically, apical membrane proteins are embedded in intracellular vacuoles called vacuolar apical compartments (VACs) that fuse with the designated region of cell-cell contact and exocytose fluid that makes up the lumen [120-122]. Depletion of Cdc42 causes intracellular accumulation of aPKC. Thus, VACs are never targeted to the cell membrane and, instead, fuse in the cytoplasm, resulting in cysts with multiple lumens. [27].

Thus, two pathways are at work in polarization of MDCK cysts. A Rac1–β_1 integrin–LM pathway determines the axis of polarity while a PTEN–PIP2–Anx2–Cdc42 pathway defines the AP surface and drives lumen formation. Although the connection is unclear,

the two pathways may be linked by Rac1 control of Par3/Par6/aPKC complex at TJs where PTEN is targeted [27].

Lumen formation

The hollowing mechanism of lumen formation described above is one of many observed in metazoans. Others include wrapping, budding, and cavitation [119]. Both hollowing and cavitation can be observed in MDCK cyst and tubule development in 3D cultures [89, 123]. Whereas hollowing involves exocytosis of vacuolar fluid to establish a lumen *without* cell loss, cavitation involves matrix-detachment associated apoptosis (anoikis) at the center of a solid cell cluster [119, 124]. Recent work by Mostov and colleagues has illustrated the relationship between rate of polarization and mode of lumen clearance. MDCK cells were cultured embedded in type I collagen or in Matrigel™, the type IV collagen- and LM-rich extract of EHS basement membrane widely used in 3D culture assays [40, 76]. In Matrigel™, MDCK cells rapidly formed polarized clusters and exhibit lumens within 24 – 48 hours without cell death. Laminin, provided by Matrigel™, provides a strong polarization signal through integrin binding, as discussed earlier. In type I collagen gels, there was an initial, low-polarization phase (1 – 3 days) followed by an apoptotic phase (4 – 10 days) in which cells polarized and luminal cells were eliminated by apoptosis. In Matrigel™ cultures, delay of polarization by blockade of Cdc42 induced apoptotic clearance of lumens. Thus, slow polarization necessitates apoptotic cavitation for lumen formation whereas rapid polarization induces a hollowing mode of lumen formation with reduced need for apoptosis [123].

In summary, 3D cultures of epithelial cells have uncovered design principles and mechanistic frameworks for alignment of epithelial polarity to overall tissue architecture and development of lumens. Epithelial cells sense environmental cues using cell surface receptors and then secrete and assemble basement membrane that provides integrin-mediated signals that establish an axis of polarity. Finally, membrane trafficking programs simultaneously distinguish membrane domains and establish the lumen. Nevertheless, there remains much to be learned about the mechanistic connections between extracellular ligand binding, polarization, and the various modes of lumen formation. The specific effects of binding particular integrins, the nature of cooperation between integrin and non-integrin receptors, and the specific signaling roles of minor BM component must be clarified. Also, the stimuli and signaling involved in the alterations of BM composition observed in injury and regeneration are not understood. Ultimately, a move from *observing* to *modulating* epithelial morphogenesis will be necessary in order to affect human health, particularly in acute injuries to epithelial organs. This requires strategies that leverage biological insights from 3D culture experiments to control proliferation, dictate EMTs and METs, and manipulate polarity for tissue and organ regeneration.

While natural BMs inherently provide biological recognition and susceptibility to proteolytic remodeling, they alone are not sufficient to develop therapeutic platforms that dictate specific morphogenetic programs [12]. Generally, natural BM extracts are limited by uncontrolled presentation of cell adhesive motifs, lot-to-lot variations in composition, unavailability of materials matching composition of cells' native BM, limited control of mechanical properties, and immunogenicity *in vivo*. Cell-matrix interactions in

Matrigel^{TM}, even with growth factor-reduced varieties, are complicated by the presence of a host of growth factors including IGF-1, TGF-β, and EGF. Type I collagen, for all its value in 3D culture of MDCK cells, only ligates integrin α2β1, leaving the roles of other integrins unexplored.

Synthetic matrices for epithelial morphogenesis

A recently-advanced strategy for controlling cell behavior in a multicellular context involves rationally-designed, ECM-mimetic biomaterials. Synthetic ECM analogues offer tunable elastic properties, controlled integration of cell adhesion ligands, and degradation by cell-secreted enzymes, all with minimal immunogenicity *in vivo*. These bioartificial matrices are finding application as *in vitro* cell culture materials, implantable vehicles for tissue rudiments constructed *ex vivo*, and as implanted niches that induce ingrowth from surrounding tissues [12].

Whereas some natural ECM-derived materials are approved for therapeutic applications, for example fibrin glue for wound healing and collagen as tissue sealant, many of the priority cell biological investigations and regenerative medicine applications will require customized matrices with precise control over their physical and biochemical properties [12, 125, 126]. Of synthetic ECM-mimetics, there are several classes. Self-assembled nano-fibrillar matrices formed in situ recapitulate a key structural feature of the ECM. However, few of these materials assemble under conditions that are amenable to cell survival. Of those, supramolecular gels of self-assembled oligomeric amphiphiles that incorporate biomolecular ligands have shown promise [127]. The major limitations of self-assembled fibrillar gels include high cost, harsh reaction conditions, weak

mechanical properties, and lack of control of degradation. Synthetic polymer hydrogels are a logical choice for biomedical applications, as hydrogel character is a key feature of natural ECMs. In addition to recapitulating viscoelasticity and transport properties of natural ECM, synthetic polymer hydrogels can be formed in situ in the presence of cells and even *in vivo* [128].

Poly (ethylene glycol) (PEG) hydrogels are the gold standard for cell- and tissue-interactive synthetic biomaterials, owing to hydrophilicity that results in highly-swollen gels with tissue-like properties, non-fouling character that presents a "clean slate" to biological systems, and excellent acceptance *in vivo* [129]. For this reason, cell-encapsulating PEG hydrogels that present cell adhesion ligands and protease-sensitive crosslinking peptides have found broad experimental applications including regulation of cell migration, therapeutic vascularization, and stem cell differentiation [130-136]. In general, PEG-based bioartificial matrices are modular systems that comprise linear or multi-armed PEG chains that are crosslinked into a network. To confer bioactivity, the PEG macromers may be functionalized with ECM-derived proteins or peptides or tethered growth factors. To allow cell-mediated degradation, protease-sensitive oligopeptides derived from ECM may be incorporated into the network, often as the crosslinking molecule. For cell encapsulation, the crosslinking step is conducted while cells are suspended in the precursor solution.

PEG-based bioartificial matrices can be broadly classified by crosslinking chemistry. The two most popular approaches are photo-initiated radical polymerization and Michael-type addition. In radical polymerization, a photo-sensitive radical initiator is added to a solution of acrylate-terminated PEG macromers and activated by ultraviolet

(UV) light irradiation. The initiator fragments into a pair of radicals that attack the acrylate, converting it to a radical, and the free-radical propagation results in covalent bonds between acrylate groups for the duration of irradiation [137]. The result is a three-dimensional crosslinked network. Conjugation of PEG-acrylates to adhesive peptides and protease-sensitive peptides prior to photo-initiation confers bioactivity to the engineered hydrogel. Photo-initiated crosslinking schemes are attractive in that they offer controlled initiation and termination of the crosslinking reaction, rapid reactions, and spatial control [137]. These features enable remarkable versatility and interesting experimental approaches. One of the most interesting features is the potential to spatially pattern bioactivity in 3D [138-141]. Specifically, gradients of cell adhesive ligands can be produced using graded irradiation via masks and other techniques [139]. Also, cell adhesive features can be localized with nano-scale resolution using two-photon laser-irradiation techniques [141]. Thus, after encapsulating cells, additional adhesive ligands can be added into the matrix. Alternatively, crosslinks may be added or degraded during the course of 3D cell culture to change the structure and properties of the microenvironment [138, 139]. Generally, the disadvantages of free-radical polymerized hydrogels are use of cytotoxic UV irradiation, potentially harmful initiator reagents, and uncertainty about the safety of degradation products and initiator residues [137]. Furthermore, in therapeutic applications, photo-crosslinking in situ is limited to implantation sites where proper irradiation is feasible. Nevertheless, with the development of blue- or white-light irradiation systems paired with eosin Y photoinititator, free-radical polymerization remains an appealing strategy for fabrication of hydrogels for cell encapsulation [142]. For instance, West and colleagues recently used

white light and eosin Y to fabricate an enzymatically-degradable, PEG-diacrylate-based system with RGD to investigate the influence of microenvironment on lung cancer spheroid morphogenesis [143].

The Michael-type addition reaction is high-yield conjugation reaction between a nucleophile (e.g. thiol or amine) and an unsaturated alkene group (e.g. maleimide, acrylate, vinyl sulfone) that has been employed extensively in bioconjugate chemistry. In the context of fabricating PEG hydrogels, Michael-type addition with thiols offers rapid, efficient reactions that proceed at physiological temperature and pH without toxic reagents or side-products. Additionally, with tunable reaction kinetics, the rate of gelation can be controlled to facilitate rapid cell encapsulation without sedimentation and to allow direct application at an implant site. One way to conjugate PEG to peptides and proteins is to use *N*-hydroxysuccinimide esters of PEG carboxylic acids (PEG-NHS) and similar approaches. However, such PEGs react non-selectively with amines and thiols on the target protein or peptide and result in a mixture of products [144]. Notably, this is the general approach to prepare bio-functional PEGs for fabrication of photo-crosslinked PEG hydrogels [136, 143]. In contrast, the unsaturated alkene-terminated PEGs used in Michael-type addition react selectively, with thiols reacting at least one order of magnitude faster than amines [145]. Furthermore, with reduced thiols being rare in the extracellular milieu, the thiol Michael addition is potentially bio-orthogonal, proceeding without side reactions *in vivo* [146]. To make hydrogels with Michael-type addition, Hubbell and colleagues reacted a vinyl sulfone-terminated four-arm PEG (PEG-4VS) with bis-cysteine peptide to form a cross-linked network [147]. Functionalization of the PEG-4VS with adhesive peptide (e.g., GRGDSPC) and inclusion of a protease-sensitive

amino acid motif (e.g., GPQGIWG) in the bis-cysteine crosslinking peptide conferred bioactivity and cell-mediated degradation [131, 148, 149]. When primary human fibroblasts were encapsulated in these hydrogels, the speed and extent of migration were modulated by the adhesive ligand density, the amino acid sequence of the crosslinking peptide, and the length of the PEG arms in the PEG-4VS [130]. We adapted these bioartificial hydrogels as a model ECM for modulation of epithelial morphogenesis and showed that integration of RGD peptide or LM-111 significantly enhanced formation of polarized MDCK cysts with lumens [150].

Michael-type addition kinetics can be modulated by the type of alkene, the pK_a of the thiol, pH of the buffer, and the concentration of base (often triethanolamine, TEA) in the buffer. Under a given set of conditions, the Michael reactivity of unsaturated alkenes is as follows:

$maleimide > vinyl\ sulfone > acrylate > methacrylate, acrylamide$ [1, 144]

In the initial studies by Hubbell and colleagues, 300 mM TEA and pH 8.0 was used to fabricate PEG-4VS hydrogels [130]. Such levels of TEA cause toxicity for sensitive cell types like thyroid follicles and human umbilical vein endothelial cells [1, 151]. We recently demonstrated that a commercially-available, maleimide-terminated four-arm PEG (PEG-4MAL) enables rapid and complete functionalization and improved crosslinking versus PEG-4VS and acrylate-terminated PEG (PEG-4A), all with low (2 – 4 mM) TEA at pH 7.4. With reactions that proceed to completion, as evidenced by consumption of free thiols, PEG-4MAL hydrogel fabrication is a stoichiometric combination of three modules: PEG macromer, adhesive ligand (any cysteine-containing

protein or peptide), and bis-cysteine crosslinking peptide [152]. We also found that high reaction efficiency had significant implications for hydrogel structure and allowed rational tuning of swelling and elastic modulus [152]. PEG-4MAL hydrogels have also been used *in vivo* for cell-demanded therapeutic growth factor release and for pancreatic islet transplantation and vascularization [152, 153]. Specifically, PEG-4MAL gels that released incorporated vascular endothelial growth factor (VEGF) and hepatocyte growth factor were applied directly to myocardial infarcted rat hearts and improved cardiac function over weeks as growth factor was released in response to cell-secreted proteases [153]. PEG-4MAL hydrogels functionalized with VEGF-A and RGD were used to encapsulate mouse pancreatic and then transplanted into diabetic mice. The recipient mice showed complete reversal of diabetic hyperglycemia, and exhibited improved weight gain, regulation of glucose challenge, and islet engraftment versus diabetic mice receiving injected islets, all with a smaller number of islets [152]. Thus, PEG-4MAL hydrogels can be engineered to maintain and structure and function of complex, multicellular tissue modules. In summary, bioactive hydrogels formed via Michael-type addition, particularly with PEG-4MAL, have clear advantages over alternative chemistries. These include commercially-available starting material, rapid stoichiometric reactions, and bio-orthogonality, all at physiological pH and temperature, without toxic additives.

With increasing emphasis on understanding tissue development processes, engineering cell fate, and therapeutic delivery of functional tissues, engineered ECM mimics like PEG-4MAL may become key platforms for fundamental investigations of tissue morphogenesis.

CHAPTER III: INFLUENCE OF POLYMER WEIGHT PERCENTAGE ON CYST MORPHOGNESIS OF MDCK II EPITHELIAL CELLS IN A BIOARTIFICIAL MATRIX

Summary

Three-dimensional (3D) cell cultures in natural ECM extracts, including type I collagen (Coll I) , enable observation of epithelial morphogenesis, a hard-wired, multicellular differentiation program that integrates cell-ECM adhesion, cell proliferation, and ECM remodeling to achieve functionally differentiated structures like hollow cysts and tubules [154]. Nevertheless, critical limitations of natural ECM extracts, including clinical incompatibility, lot-to-lot variability and undefined presentation of cell adhesion motifs motivated development of a synthetic ECM platform for detailed studies. Here, a multi-arm poly (ethylene glycol) (PEG)-maleimide macromer (PEG-4MAL) is covalently functionalized with adhesive peptides and crosslinked with proteolytically-cleavable structural peptides in the presence of epithelial cells. A highly-efficient Michael-addition reaction enables fabrication of hydrogel with elastic properties resembling natural ECMs [1]. By culturing MDCK II epithelial cells in these engineered PEG-4MAL matrices over a range of polymer wt%, we showed that the physical properties of the matrix such as elastic modulus, network crosslink density and degradability effectively modulate establishment of apico-basal polarity and lumen phenotypes in MDCK II cysts.

Introduction

Organization of epithelial cells into polarized, 3D tissue structures is critical to the barrier, secretion, and exchange functions of organs including lung, kidney, intestine and salivary gland. Disruption of the 3D structure or dysregulation of the polarity in epithelial tissues occurs with significant morbidity and mortality [155]. When epithelial cell lines like MDCK are encapsulated in Coll I gels, hollow spherical monolayer structures called cysts form within 10 days and bear the hallmarks of epithelial polarity [92, 95, 96, 156]. Such 3D cultures of epithelial cells in natural ECM extracts have revealed that development and maintenance of intricately ordered epithelial structures (a process termed epithelial morphogenesis) involves coordination cell fate processes including adhesion, migration, differentiation, polarization, and apoptosis. Furthermore, these studies have exposed a powerful role of ECM in a framework of bi-directional signaling where cells embedded in matrix sense the adhesive signals and mechanical properties of the matrix while actively remodeling the matrix via proteolytic degradation and secretion of new matrix [24, 35, 53, 65]. Thus, 3D culture of epithelial cells in natural ECM extracts is a critical tool for studying development and maintenance of tissue architecture and their implications in organ function.

Nevertheless, studies of epithelial morphogenesis in natural ECMs are limited by the uncontrolled presentation of adhesive ligands, limited control of elastic properties, lot-to-lot variability, and concerns over clinical use of animal-derived materials. In contrast, an engineered matrix that specifically and controllably presents biological functionalities, with tunable elastic properties, could be a useful platform for elucidating key influences of ECM properties in tissue morphogenesis. PEG hydrogels are the gold standard for cell- and tissue-interactive synthetic biomaterials, owing to hydrophilicity

that results in highly-swollen gels with tissue-like properties, non-fouling character that presents a "clean slate" to biological systems, and excellent acceptance in vivo [129]. For this reason, cell-encapsulating hydrogels that present cell adhesion ligands and protease-sensitive crosslinking peptides have found broad experimental applications including regulation of cell migration, therapeutic vascularization, and stem cell differentiation [1, 130-133, 136, 152]. We previously showed that PEG-based hydrogel systems could support MDCK cyst morphogenesis [150]. Here, we present a four-arm PEG-maleimide (PEG-4MAL)-based system that offers superior reaction efficiency, a wide range of achievable elastic properties, and cell-responsive degradation as a bioartificial matrix to modulate epithelial morphogenesis. By culturing MDCK II epithelial cells in these engineered PEG-4MAL matrices over a range of polymer weight concentrations, which results in variations in elastic moduli and network crosslink density, and observing apical polarity and lumen phenotypes in the resulting cysts, we demonstrate a versatile platform for modulating epithelial morphogenesis.

Results

To demonstrate the functionality and flexibility of PEG-4MAL-based hydrogels as an ECM analogue and 3D culture system for epithelial cyst morphogenesis studies, we embedded MDCK II epithelial cells in PEG-4MAL matrices and monitored cyst development over several days (**Figure 3.1a**).

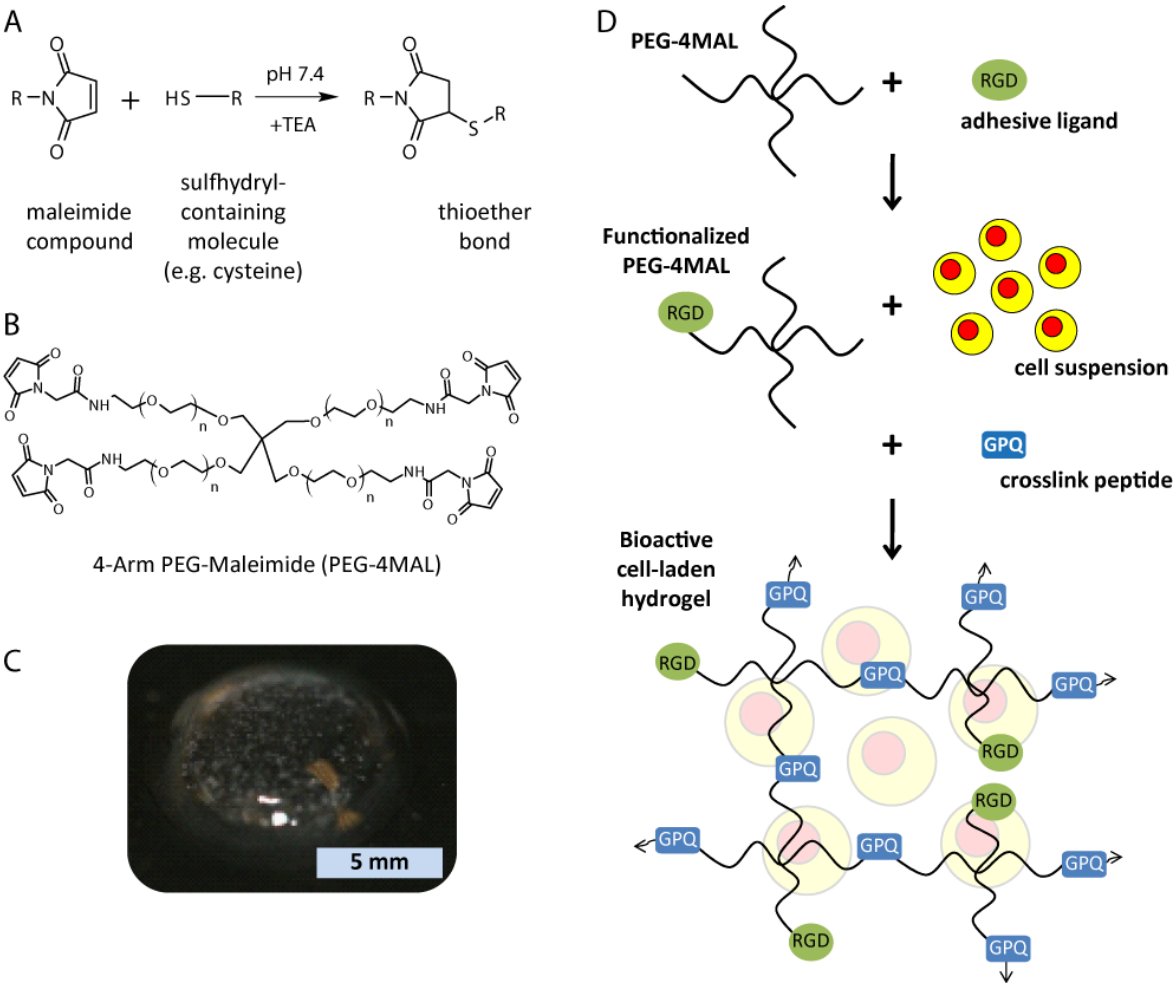

Figure 3.1. PEG-4MAL hydrogel chemistry and cell encapsulation scheme. a, Michael-type addition reaction. TEA, triethanolamine. b, 4-arm PEG Maleimide macromer. c, Sample cell-laden PEG-4MAL hydrogel. d, Cartoon of cell encapsulation scheme in bioactive PEG-4MAL hydrogel. First, PEG-4MAL macromers are functionalized with GRGDSPC adhesive ligand. Next, living cell suspension is added to precursor mixture and followed by crosslinking upon addition of cysteine-flanked protease-cleavable peptide.

First, we varied the macromer concentration (or polymer wt%). In previous work, we showed that the elastic modulus of PEG-4MAL varied linearly with polymer wt% over the range of 4% - 10% (w/v), provided that ligand density was fixed [1]. Thus, we sought to investigate the relationship between macromer concentration (3.5% - 5.0%, <400 – 600 Pa) and cyst formation over 10 days in hydrogels formulated with 2000 μM

RGD and crosslinked with a fast-degrading cysteine-flanked peptide that contains the Coll I-derived sequence, GPQGIWGQ (GPQ-W). Eighteen hours after encapsulation, rounded single cells were incubated with calcein-AM (live) and TOTO-3 iodide (dead) to assess viability. High viability (>85%) was maintained in all conditions (**Figure 3.2b**). Within 48 hours of encapsulation, small, multicellular clusters were visible in gels of low wt% (<5.0% w/v) whereas high wt% gels had only single cells (**Figure 3.2a**)**.** Epithelial cell clusters in 3D culture may form without proliferation via cell migration and aggregation [109, 123]. To determine whether early cluster formation involved proliferation, cells within gels were incubated with an alkyne-modified thymidine analogue, 5-ethynyl-2´-deoxyuridine (EdU). During six-hour incubations on day 2, dividing MDCK II cells incorporated EdU into newly synthesized DNA. Then, after fixation, samples were incubated with an azide-conjugated fluorophore that selectively reacted with the EdU alkyne in a Huisgen 1,3-dipolar cycloaddition and allowed detection of proliferation with fluorescence microscopy. The EdU incorporation assay confirmed widespread proliferation in those cultures where cell clusters were visible. Interestingly, although cell viability was high across all macromer concentrations, there was no cluster formation or proliferation at day 2 in gels with macromer concentration above 4.5% (**Figure 3.2a,c)**.

At day 2, the mean diameter of cellular specimens in 5.0% gels (12.34 ± 0.11 μm) was significantly smaller than objects in other PEG-4MAL gels (>17 μm, $p < 0.0001$), as the feret diameter measurement distinguished single cells in 5.0% gels from the proliferating clusters in all other conditions. Meanwhile, the mean diameter of clusters in Coll I gels exceeded 24 μm, significantly larger than that of all other conditions ($p <$

0.0001) (**Figure 3.3a).** Together, these results indicate that, within a permissive wt% range, PEG-4MAL hydrogels with adhesive ligand and degradable crosslinks support MDCK II proliferation in a 3D context. However, culture of MDCK II in PEG-4MAL hydrogels with wt% of 5.0% and above (data not shown) result in single cells throughout culture, providing no multicellular structures for study. Under these conditions, PEG-4MAL hydrogels with wt% of 3.0% degrade rapidly and disintegrate before cultures are complete (data not shown).

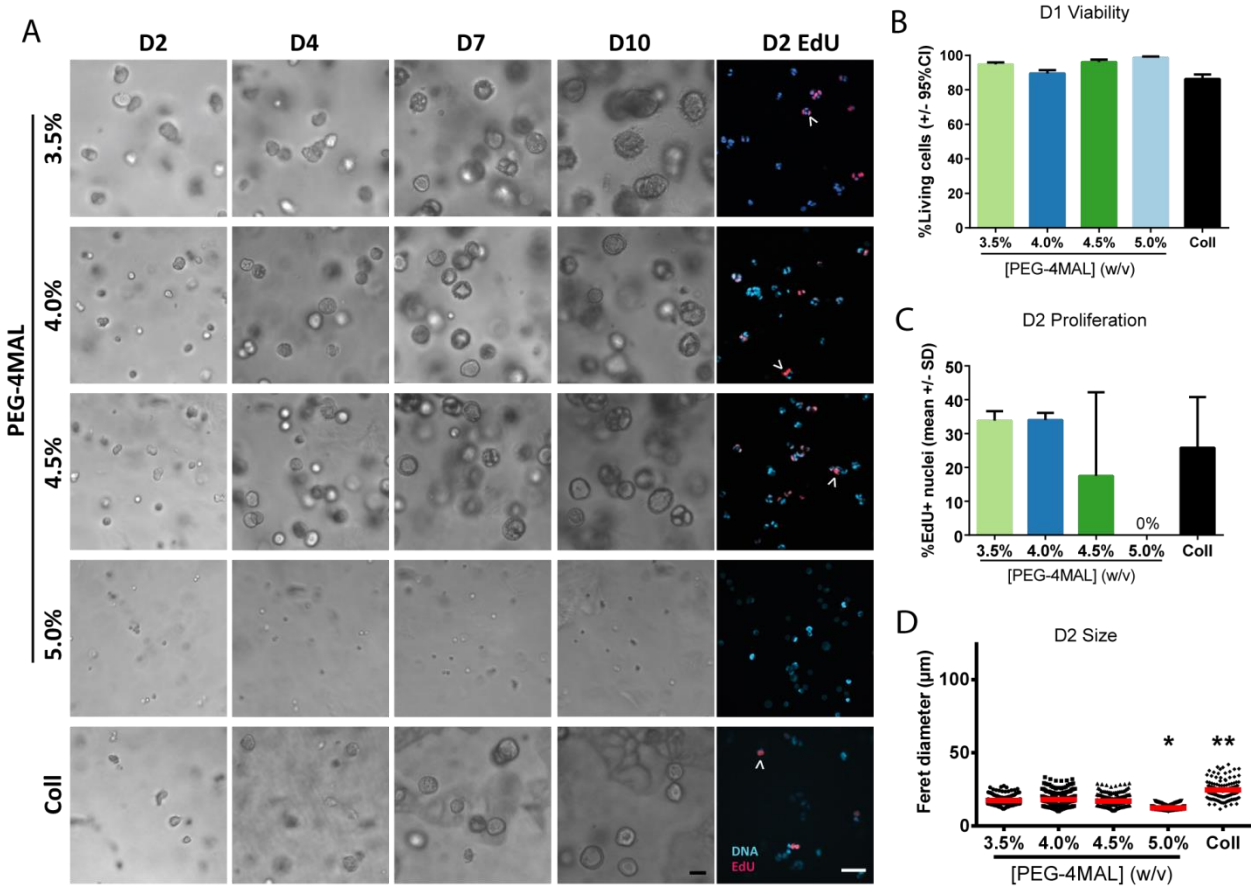

Figure 3.2. PEG-4MAL hydrogels support cyst morphogenesis. a, Single MDCK II cells were cultured in PEG-4MAL hydrogels of different polymer weight percentages and grew into clusters and cysts over 10 days. At day 2, newly synthesized DNA was labeled by incorporation of thymidine analogue EdU and detected by fluorescence microscopy. EdU-positive nuclei indicated with (^). Scale bar 50 µm. b, Quantification of cell

viability by calcein-AM (live) and TOTO-3 iodide (dead) labeling at day 1. At least 503 cells counted per condition. c, Quantification of proliferation from EdU incorporation images. At least 596 nuclei counted per condition. d, Quantification of cyst size. *, 5.0% vs. all other conditions, $p < 0.0001$. **, Coll vs. all other conditions, $p < 0.0001$. Kruskal-Willis test with Dunn's multiple comparisons test. At least 131 objects counted per condition.

At day 5, many clusters in 3.5%, 4.0%, and 4.5% PEG-4MAL gels contained hollow cavities that appeared to be the beginnings of lumens (**Figure 3.3)**. It has been shown in MDCK cysts, and indeed in mammalian epithelial tubes in vivo, that lumen formation occurs by one of three mechanisms, including cavitation and hollowing [5, 119, 123]. In Coll I gels, lumens form predominantly by cavitation, as cells at the interior of spheroids containing more than two cells are cleared via anoikis, a form of apoptosis due to estrangement from ECM. Alternatively, provided an early polarization signal (beta 1 integrin binding of extracellular laminin, for instance), lumens form by hollowing, as fluid-filled vesicles are directed to the interface between cells at the two-cell stage [119, 157]. MDCK cysts in Matrigel^{TM} typically form lumens by hollowing, as there is a strong polarization signal provided by laminin [157]. Additional observations in the literature include simultaneously appearing multiple lumens when signaling involving the small Rho GTPase cdc42 or vesicle trafficking proteins of the Rab family are perturbed [27, 158]. In this instance, the hollowing mechanism is altered such that fluid-filled vesicles condense within cells and at non-central interfaces between cells in a growing cluster. To determine whether growing MDCK II cysts in PEG-4MAL gels contained apoptotic cells, we labeled cleaved caspase-3 in five-day old cysts. Antibody-based detection of cleaved caspase-3 confirmed that 20% – 32% of cysts in PEG-4MAL gels contained apoptotic cells at the time of assay **(Figure 3.3)**. In Coll I gels, 17% of cysts were cleaved-caspase-

3 positive. The fraction of cysts that contained apoptotic cells in PEG-4MAL gels varied inversely with polymer wt%. Fisher's exact test showed the fraction of cleaved caspase-3-positive cysts in 3.5% PEG-4MAL gels was significantly higher than in 4.5% or Coll I gels ($p < 0.0156$). There were no differences in comparisons between 4.0%, 4.5%, and Coll I gels ($p > 0.9999$).

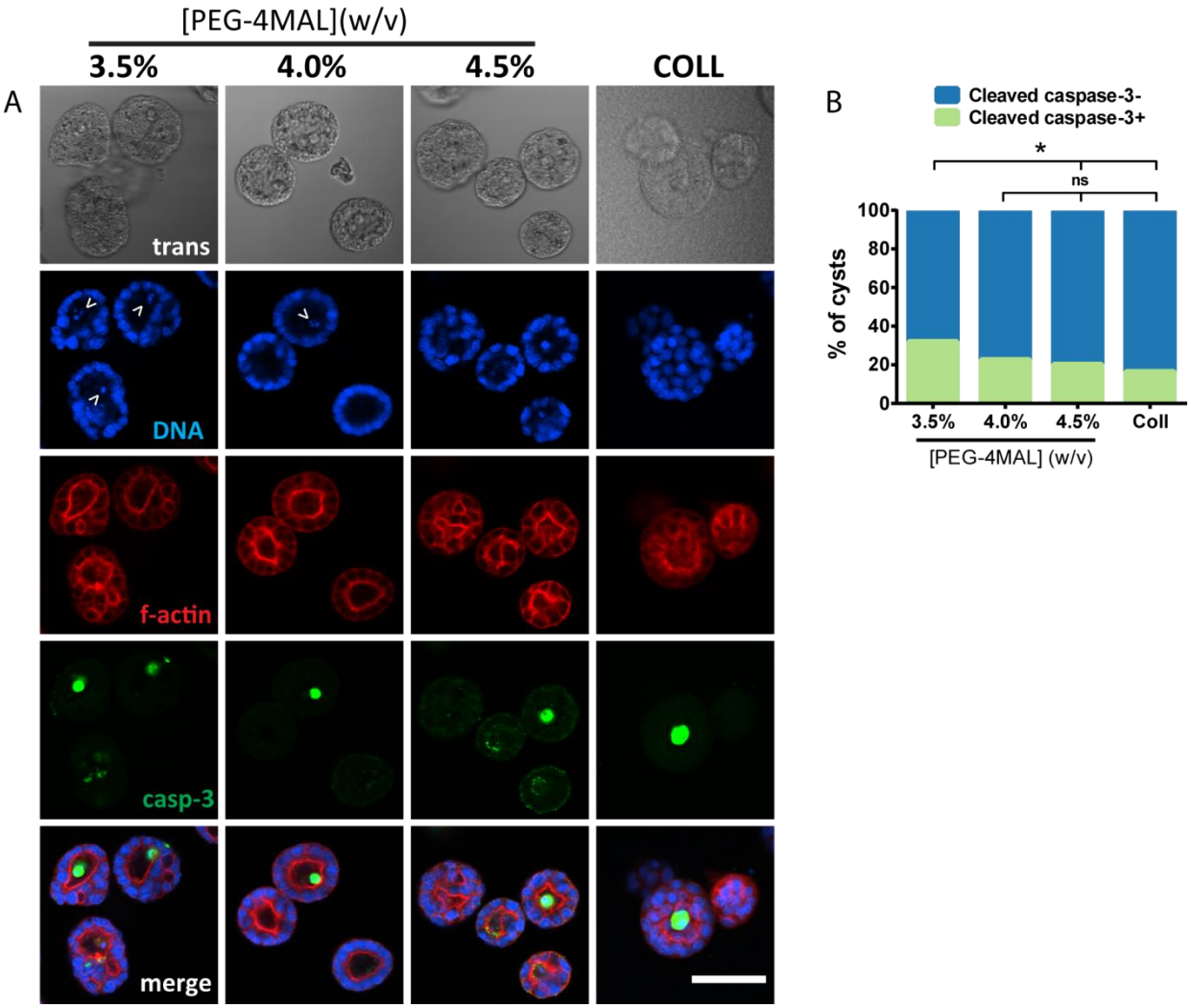

Figure 3.3. Cysts in PEG-4MAL hydrogels contain apoptotic cells. a, MDCK II cysts grown for 5 days in PEG-4MAL hydrogels with 2000 µM RGD and labeled with antibodies against apoptosis marker cleaved caspase-3. Fragmented nuclei indicated by (^). Scale bar 50 µm. b, Quantification of cysts having cleaved caspase-3 labeling at day 5. At least 103 cysts counted per condition.

At day 10, the mean diameters of cysts in 3.5%, 4.0%, and 4.5% PEG-4MAL gels were 58.42 ± 1.30 μm, 58.64 ± 1.14 μm, and 57.34 ± 0.97 μm, respectively (**Figure 3.2a, 3.4b**). However, there was no significant effect of PEG-4MAL wt% on size of cysts ($p > 0.8382$). The mean diameter of cysts in Coll I was significantly than that of PEG-4MAL gels at day 10 (68.95 ± 1.60 μm, $p < 0.0001$).

Establishment and maintenance of apico-basal polarity is a hallmark of epithelia. After 10 days of culture, MDCK II cysts embedded in Coll I gels are fully differentiated [92]. In a physiologically polarized mature cyst, apical polarity markers (e.g., podocalyxin) are segregated exclusively to the interior of the cyst, at the cell surface interfacing the lumen. To investigate the influence of PEG-4MAL wt% (3.5% - 5.0%) on apical polarity phenotypes of resulting cysts, we fixed MDCK II 3D cultures at day 10 and labeled cysts with antibodies against apical polarity marker podocalyxin. Then, we captured cyst cross-sections with a confocal microscope and classified cysts into the following phenotypes: *interior apical polarity*, *exterior apical polarity*, *mixed apical polarity*, and *no apical polarity*. In PEG-4MAL gels, apical polarity phenotypes were modulated by polymer wt%. Whereas only 79% of cysts grown in 3.5% PEG-4MAL gels had internal polarity, 94% and 98% of cysts grown in 4.0% PEG-4MAL and 4.5% PEG-4MAL gels had internal polarity, respectively. In Coll I gels, 97% of cysts had internal apical polarity. Furthermore, in 3.5% PEG-4MAL gels, 7% of cysts had exclusively external (or inverted) apical polarity. In contrast, only 2% of cysts grown in 4.0% PEG-4MAL gels had external polarity and this inverted phenotype was not found in 4.5% PEG-4MAL gels or Coll I gels (**Fig 3.4c.)**. We conducted a chi-squared test to compare the distributions of polarity phenotypes across PEG-4MAL gels of different wt%. In

summary, the distribution of polarity phenotypes in cysts grown in 3.5% PEG-4MAL gels differed significantly from the distributions found in cysts grown in 4.0% and 4.5% PEG-4MAL gels, respectively. Notably, the distribution of apical polarity phenotypes of cysts grown in 4.0% and 4.5% PEG-4MAL did not differ significantly from cysts grown in Coll I gels (**Table 3.1**). This result indicates that (1) PEG-4MAL hydrogels support establishment of apico-basal polarity in a manner similar to Coll I and (2) that the system's weight percentage parameter modulates the apical polarity phenotype. We confirmed that other epithelial polarity markers including tight junction protein ZO-1, apically-oriented golgi matrix protein (GM130), and basolaterally-distributed β-catenin, are properly localized in MDCKII cysts grown in PEG-4MAL hydrogels (**Figure 3.5**).

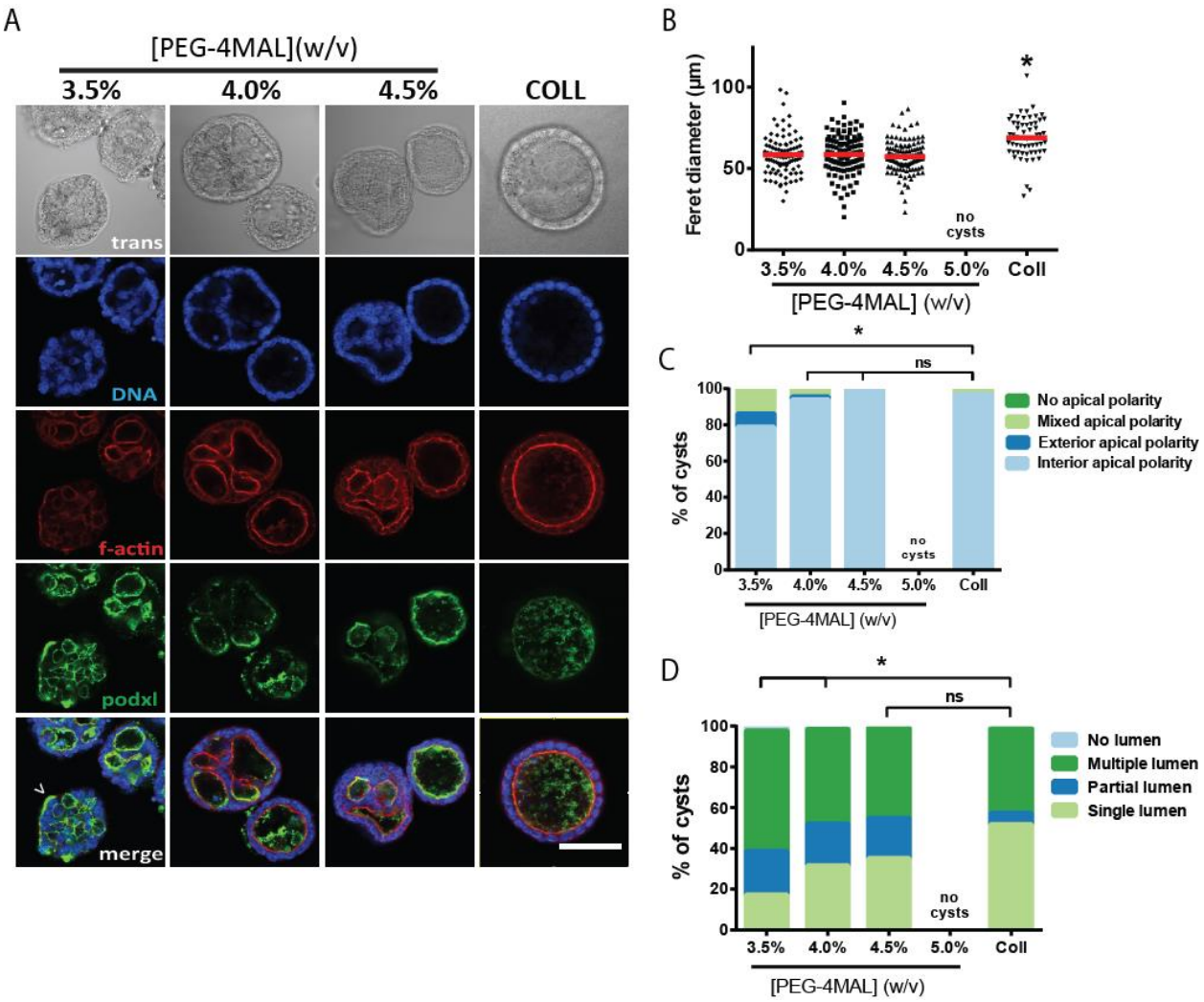

Figure 3.4. PEG-4MAL weight percentage modulates cyst polarity and lumen phenotype. a, MDCK II cysts grown for 10 days and labeled with antibody against apical polarity marker podocalyxin (podxl). Inverted apical polarity indicated by (^). No cysts in 5.0% condition. Scale bar 50 mm. b, Quantification of cyst size at day 10. *, Coll vs. 3.5%, 4.0% or 4.5%: p<0.0001, one-way ANOVA with Tukey's multiple comparison test. Adjusted p value. c, Distribution of apical polarity phenotypes at day 10. At least 89 cysts counted per condition. *, 3.5% vs. Coll: p = 0.0138, ns, 4.0% vs. Coll: p = 0.2289, 4.5% vs. Coll: p = 0.5891, chi-squared test with Bonferroni's correction. d, Distribution of lumen phenotypes at day 10. At least 89 cysts counted per condition. *, 3.5% vs. Coll: p = 3 x 10^-6, 4.0% vs. Coll: p = 0.0198, (ns, 4.5% vs. Coll: p > 0.9999), chi-squared test with Bonferroni's correction.

Table 3.1. PEG-4MAL weight percentage versus apical polarity phenotype distributions.

Comparison	Bonferroni's test for multiple comparisons	X^2	df	P^
3.5% vs. 4.0%	**S**	12.58	3	0.0342
3.5% vs. 4.5%	**S**	22.46	3	0.0003
4.0% vs. 4.5%	NS	1.716	3	1.0000
3.5% vs. Coll	**S**	14.54	3	0.0138
4.0% vs. Coll	NS	0.2289	3	1.0000
4.5% vs. Coll	NS	0.5891	3	1.0000

^P values adjusted for multiple comparisons.

Table 3.2. PEG-4MAL weight percentage versus lumen phenotype phenotype distribution.

Comparison	Bonferroni's test for multiple comparisons	X^2	df	P^
3.5% vs. 4.0%	NS	7.355	3	0.3684
3.5% vs. 4.5%	NS	10.82	3	0.0762
4.0% vs. 4.5%	NS	0.5619	3	1.0000
3.5% vs. Coll	**S**	31.79	3	3×10^{-6}
4.0% vs. Coll	**S**	13.76	3	0.0198
4.5% vs. Coll	NS	0.5891	3	1.0000

^P values adjusted for multiple comparisons.

The cross-section of mature epithelial duct structure is a monolayer of cells surrounding a single, clear lumen. Studies in the literature typically classify MDCK II cysts in terms of lumen phenotypes in response to some genetic or chemical perturbation [5]. We investigated the distribution of cyst phenotypes among *single lumen*, *partial lumen*, *multiple lumen*, and *no lumen* in response to varying polymer wt% (3.5% - 5.0%). Nearly all (>97%) cysts formed in PEG-4MAL gels contained lumens (**Figure 3.4d**). In this respect, cysts in PEG-4MAL gels were comparable to those in Coll I gels. However, fewer than half of cysts in PEG-4MAL gels were characterized by a single clear lumen surrounded by a monolayer of cells, whereas ~51% of cysts in Coll I had single lumen.

Instead, cysts with partially-formed lumens or multiple cavities were dominant in PEG-4MAL gels. Comparing PEG-4MAL gels of different wt%, the low wt% 3.5% PEG-4MAL gels were less likely to have a single lumen than the 4.0% and 4.5% PEG-4MAL gels (17% vs. 31% and 35%, respectively). Likewise, 3.5% gels were more likely to have multiple lumens (59% vs. 46% and 44% for 4.0% and 4.5% gels, respectively) (**Figure 3.4d**). We conducted a chi-squared test to compare the distributions of lumen phenotypes across PEG-4MAL gels of different wt%. Although the trend suggested an increasing incidence of single lumens and decreasing incidence of multiple lumens as wt% increased from 3.5% to 4.5%, the distribution of lumen phenotypes in cysts cultured in 3.5%, 4.0%, and 4.5% PEG-4MAL gels did not differ significantly from each other (**Figure 3.4d.**). However, when lumen phenotype distributions were compared between PEG-4MAL gels and Coll I, we found that 3.5% and 4.0% gels were significantly different from Coll I whereas 4.5% gels did not differ from Coll I **(Table 3.2).** This result indicates that PEG-4MAL hydrogels support lumen formation a manner similar to Coll I.

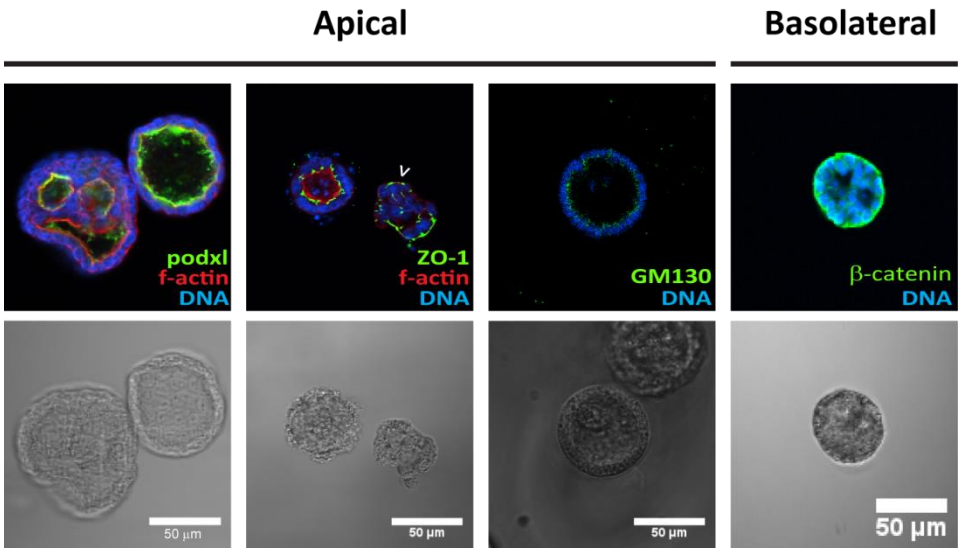

Figure 3.5. MDCKII cysts in PEG-4MAL gels express epithelial polarity markers with physiological localization. ^ indicates external localization of ZO-1 on unpolarized cyst without lumen.

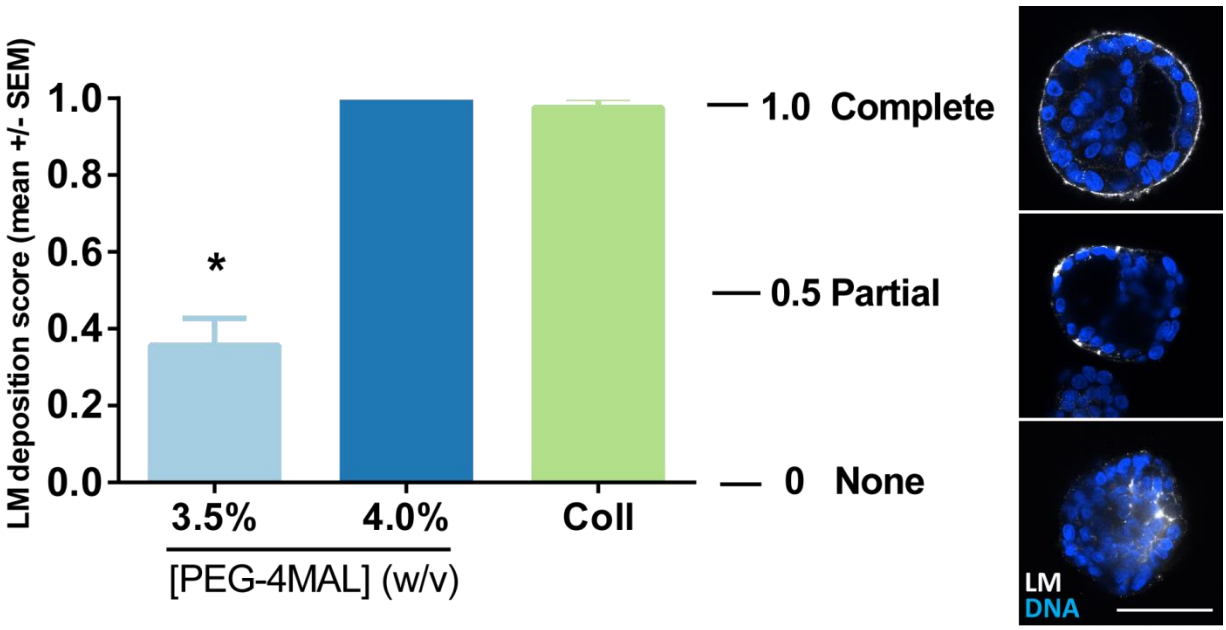

Figure 3.6. PEG-4MAL weight percentage modulates laminin (LM) basement membrane assembly. At day 10, cysts were incubated with an anti-LM antibody prior to fixation to label extracellular LM. Cysts scored on completeness of LM basement membrane. *, 3.5% vs. 4.0% or Coll: $p < 0.0001$, 4.0% vs. Coll: $p > 0.9999$, Kruskal-Willis test with Dunn's multiple comparisons test. 21 cysts counted per condition. Right panel: Representative images from PEG-4MAL gels. Scale bar 50 µm.

As cell-secreted extracellular laminin (LM) has been shown to define the axis of polarity in MDCK II cysts [53, 54], we sought to determine whether the inversion of polarity in 3.5% PEG-4MAL gels could be associated with abnormal LM deposition in the basement membrane. In confocal micrographs of mature MDCK cyst cross sections, we scored the completeness of the LM basement membrane. A continuous layer of LM at the perimeter of the cyst was scored as complete (1.0) whereas absence of the LM layer was scored 0.0 and partial coverage was scored 0.5. We found that nearly all cysts in 4.0% PEG-4MAL gels and Coll I gels had complete LM basement membranes (**Figure 3.6**). However, the mean LM deposition score for cysts in 3.5% gels was less than 0.4, significantly lower than that of 4.0% gels or Coll I gels ($p < 0.0001$), indicating disrupted basement membrane. There was no difference in the LM deposition scores when 4.0% gels and Coll I gels were compared. This result further establishes that PEG-4MAL hydrogels support lumen formation a manner similar to Coll I.

Although variation of PEG-4MAL wt% affects hydrogel properties including elastic modulus, swelling ratio, and crosslink density, it does not systematically alter the hydrogel network structure. However, the molecular weight of the PEG-4MAL macromer can directly affect the distance between crosslinks in the hydrogel network. A macromer with shorter arms has less distance between crosslinks and generally results in higher elastic modulus and decreased swelling [147]. To investigate the influence of network structure on cyst morphogenesis in PEG-4MAL hydrogels, we embedded MDCK II cells in 4.0% (w/v) gels made with 10 kilodalton (kDa) PEG-4MAL or the 20 kDa PEG-4MAL used in previous experiments and assayed proliferation after two days. All gels

were made with 1000 μM RGD. We found that proliferation was completely eliminated in 10 kDa PEG-4MAL gels (**Figure 3.7**). This result was reminiscent of MDCK II cultures in 20 kDa PEG-4MAL gels with wt% exceeding 4.5%, further establishing that a limited set of conditions are required to support MDCK II proliferation in synthetic matrix.

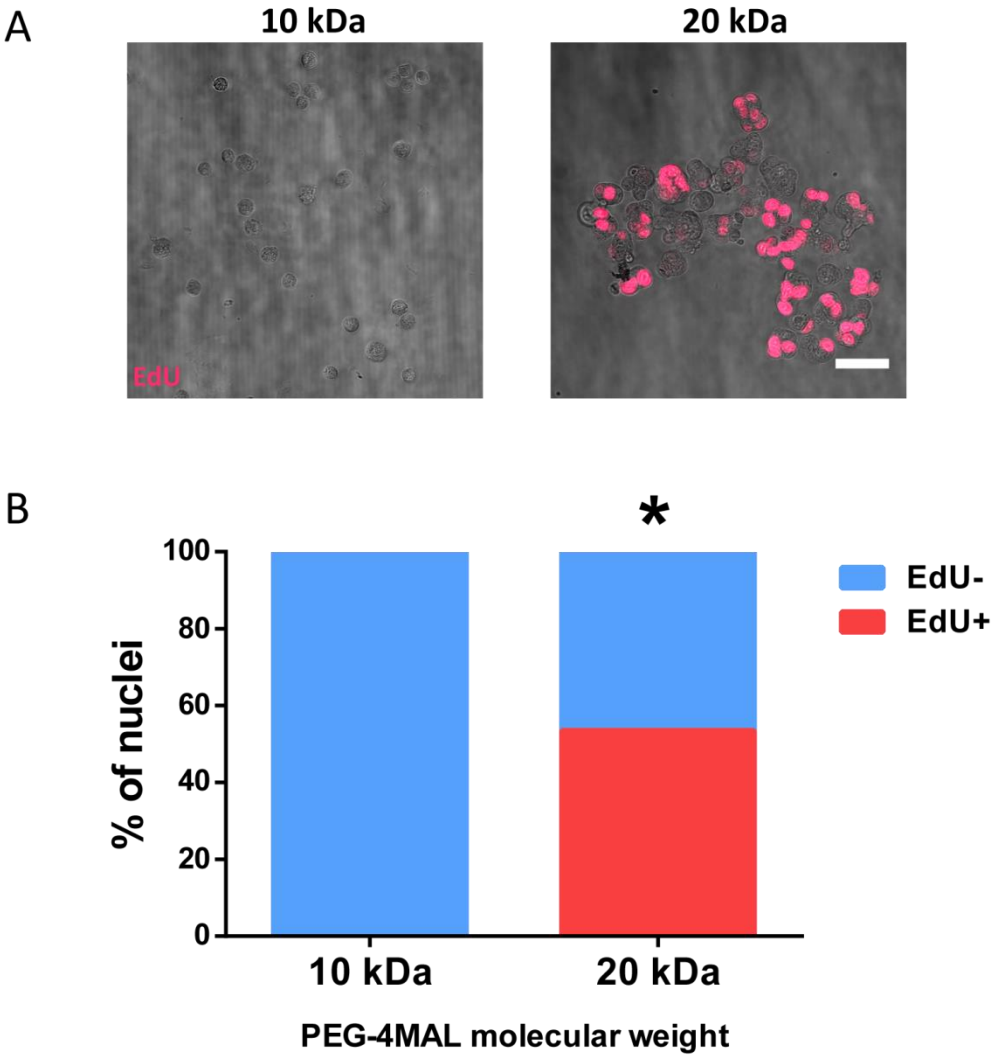

Figure 3.7. PEG-4MAL molecular weight modulates MDCK II cell proliferation. MDCK II cells were cultured in 4.0% (w/v) hydrogels of 10 kDa or 20 kDa PEG-4MAL with 1000 μM RGD and 100% GPQ-W crosslinker for two days. a, Dividing cells were labeled with EdU (red). Representative images. Scale bar 50 μm. b, Quantification of dividing cells. *, Fisher's exact test, $p < 0.0001$. At least 252 nuclei counted per condition.

The preceding results were obtained using gels crosslinked with a fast-degrading, Coll I-derived peptide, "GPQ-W", which contains the protease-sensitive sequence GPQGIWGQ. Hubbell and colleagues have previously shown that single amino acid changes of the protease- sensitive sequence alter the rate at which the peptide is cleaved [130]. In the context of a 4-arm PEG-vinyl sulfone hydrogel, the choice of crosslink peptide sequence influenced fibroblast migration *in vitro* and cranial bone regeneration *in vivo*. Thus, we wondered whether the degradation rate of the crosslink peptide sequence would modulate cyst morphogenesis in PEG-4MAL gels. We cultured MDCK II cells in 4.0% PEG-4MAL hydrogels in which we titrated the concentration of GPQ-W with GPQGIAGQ (GPQ-A) peptide, a peptide that degrades 2 – 7X slower than GPQ-W, depending on the matrix metalloproteinase (MMP) involved [159]. Cyst growth was completely abrogated in gels with 100% GPQ-A (0% GPQ-W), as evidenced by transmitted light images over 10 days (**Figure 3.8**). In fact, as little as 40% GPQ-A (60% GPQ-W), was sufficient to eliminate cyst growth. However, above a threshold GPQ-W concentration of 60%, there were no gross differences in the frequency or size of the epithelial cysts (**Figure 3.8**). Taken together, these results demonstrate that a threshold level of degradability is required for MDCK II proliferation and cyst formation in PEG-4MAL hydrogels.

Next, we sought to determine whether cyst growth in PEG-4MAL hydrogels was dependent upon MMP activity. We encapsulated MDCK II cells in growth-permissive 4.0% PEG-4MAL gels with 100% GPQ-W and incubated the gels in culture media containing broad-spectrum MMP inhibitors GM6001 (25 μm) or MMP inhibitor II

(MMPII) (50 nM). GM6001 is a potent inhibitor of MMP-1, MMP-2, MMP-3, MMP-9, MMP-13, and MMP-14 [160-162]. MMPII is a potent inhibitor of MMP-1, MMP-3, MMP-7, and MMP-9 [163]. Transmitted light images show that cysts grown in the presence of 25 μM GM6001 were smaller and scarcer than those grown in 50 nM MMPII or DMSO (**Figure 3.9a**). Significantly, GM6001 is a potent inhibitor of MMP-2 while MMPII is not. MMP-2 is a gelatinase (cleaves denatured collagen) that is expressed in all parts of the kidney [164]. Thus, the difference between GM6001 and MMPII outcomes in this experiment, with each at a working concentration, is consistent with MMP-2-mediated crosslink degradation. The cysts in MMPII, although large, seem to exhibit filled lumens. We observed similar results when MMPs were inhibited in Coll I gels (**Figure 3.9b**). Together, these results indicate that cyst growth in PEG-4MAL requires MMP activity and a rapidly-degrading crosslink peptide.

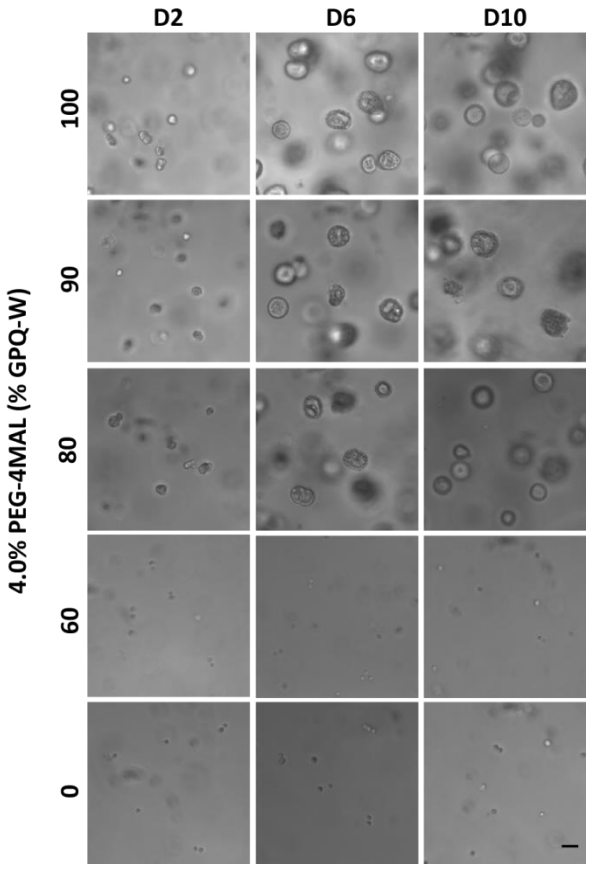

Figure 3.8. Crosslink degradation rate influences cyst growth in PEG-4MAL hydrogels. MDCK II cells were grown for 10 days in 4.0% PEG-4MAL hydrogels with 2000 μM RGD. Fast-degrading (GPQ-) and slow-degrading (GPQ-A) crosslinking peptides were titrated from 0% GPQ-W (100% GPQ-A) to 100% GPQ-W (0% GPQ-A). Scale bar 50 μm.

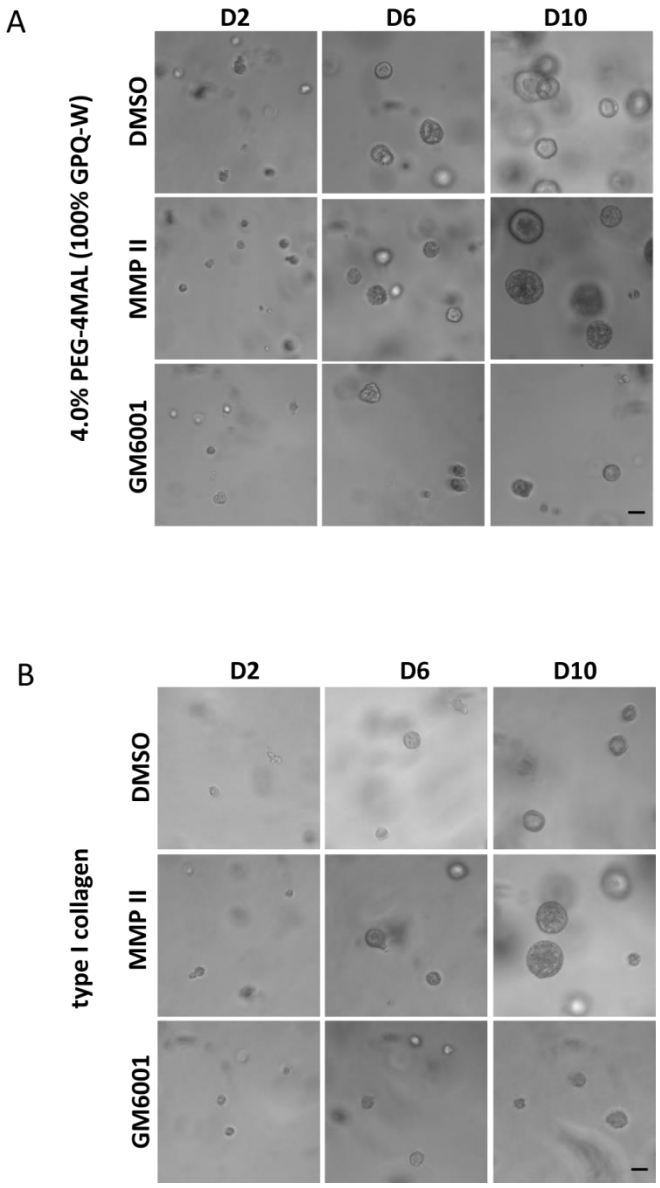

Figure 3.9. MMP inhibition modulates cyst growth in PEG-4MAL hydrogels. MDCK II cells were grown for 10 days in 4.0% PEG-4MAL hydrogels with 2000 μM RGD and fast-degrading crosslinking peptide GPQ-W (a) or Coll I (b) in the presence of 25 μM GM6001 or 50 nM MMPII or 0.5% DMSO. Scale bar 50 μm.

Discussion

Observations in 3D cultures of MDCK II in Coll I and Matrigel^{TM} have established a paradigm of epithelial polarization in which integrin receptors bind specific ECM motifs and subsequently transduce a signal that defines the axis of polarity.

Nevertheless, such approaches are limited by the "as-is" nature of the matrix materials. Furthermore, natural ECMs extracts are characterized by lot-to-lot variability, uncontrolled presentation of adhesive motifs, limited control of mechanical properties, and immunogenic potential when delivered in vivo. As a result, understanding the influence of ECM mechanics and degradation on 3D epithelial morphogenesis remains a major challenge. Therefore, a bioactive matrix with tunable mechanical properties and cell-responsive degradability could be a useful platform for elucidating key influences of ECM properties in tissue morphogenesis. Here, we present a PEG-based bioartificial hydrogel fabricated via well-characterized chemistry under physiological conditions that incorporates adhesive ligands with micromolar precision and allows cell-mediated remodeling of the network via protease-sensitive crosslinks. By culturing MDCK II epithelial cells in these engineered PEG-4MAL matrices over ranges of elastic moduli and crosslink densities, with varying degradation rates, and observing effects on proliferation, cyst size, apical polarity, and lumen phenotype, we demonstrate a platform for modulating MDCK II cyst morphogenesis *in vitro*.

We previously reported Michael-reactive PEG-vinyl sulfone (PEG-4VS)-based hydrogels to modulate MDCK cyst morphogenesis [150]. More recently, a photocrosslinked PEG-acrylate-based hydrogel system was reported to study lung cancer spheroid morphogenesis *in vitro* [143]. However, the PEG-4MAL bioartificial matrix platform has several advantages over other PEG-based matrices for 3D culture epithelial cells. First, the robust Michael addition reaction involving maleimide and a free cysteine on a protein or peptide proceeds rapidly to completion, such that incorporated ligand density is limited only by pipetting precision. Similarly, the efficient reaction between

ligand-functionalized PEG-4MAL and cysteine-flanked crosslinking peptides allows hydrogel formation at wt% as low as 3.0%. This allows cultures in matrices exhibiting a wide range of elastic moduli [1]. Furthermore, the rapid (<15 min) crosslinking in PEG-4MAL system requires only a low concentration of TEA (4 mM) in the PBS buffer. Other systems have required high TEA concentrations (>100 mM), additional buffer additives like HEPES, and photoinitiator-comonomer pairings like eosin Y and 1-vinyl-2 pyrrolidinone (NVP) that complicate adjustment of macromer concentrations [142, 143, 150, 165].

In the current study, we discovered a range of PEG-4MAL wt% (3.5% - 4.5%, w/v) in which embedded MDCK II cells exhibited robust proliferation and cysts development. Below 3.5%, gels degraded rapidly and disintegrated before the cultures were complete. Above 4.5%, cells did proliferate and only remained single cells throughout culture. In the growth-permissive wt% range, we found that cysts grown in 3.5% gels were more likely to exhibit multiple lumens than those cultured in 4.0% and 4.5% gels, in which the classic single lumen cyst was more prevalent. Similarly, 3.5% gels exhibited elevated incidence of cysts whose apical polarity was inverted versus the physiological orientation. Inspection of basement membranes surrounding mature cysts indicated that the departure from physiological cyst phenotype observed in 3.5% gels was associated with disrupted LM basement membrane deposition. Importantly, we identified PEG-4MAL wt% conditions (4.0%, 4.5%) in which encapsulated MDCKII cells proliferate and form polarized cysts with lumens that closely resemble cysts grown in Coll I.

The initial growth of clusters in PEG-4MAL gels raised questions about the mechanism of cluster formation. In 3D cultures of primary human lung alveolar type II cells, hollow, polarized cysts formed from via aggregation without appreciable proliferation or apoptosis [109]. Somewhat similarly, the rate at which MDCK II formed clusters in Matrigel^{TM} scaled with seeding density, ostensibly due to aggregation, with implications for lumen formation [123]. We confirmed that MDCKII clusters grown in PEG-4MAL were forming via proliferation. Although the cell density used here in PEG-4MAL gels (500 cells/μL) is an order of magnitude higher than that of Coll I gels (40 cells/μL), the spacing between single MDCKII cells in highly-swollen PEG-4MAL is sufficient to prevent aggregation. Furthermore, our live cell imaging observations indicate that MDCKII cells in PEG-4MAL do little more than extend short projections and certainly do not migrate over appreciable distances (data not shown). MDCKII cysts in PEG-4MAL followed the morphogenetic pattern observed in Coll I gels, as solid clusters began to exhibit cavities after 4-5 days. Also similar to Coll I, PEG-4MAL gels induced apoptosis in cells at the interior of nascent cysts. These results suggest slow polarization with endogenous secreted LM providing the signal that establishes the axis of polarity [53-55, 123].

Currently, there is great interest in understanding how the mechanics of the microenvironment influence tissue homeostasis, particularly in the cases of epithelial organs where cancer progression has been associated with tissue stiffening [166]. It is well established that most healthy cells maintain a “tensional homeostasis” by generating cytoskeletal tension in response to stresses exerted by the microenvironment [166, 167]. Therefore, the linear relationship between elastic modulus and wt% observed in PEG-

4MAL hydrogels, within the sub-kPa range, presents an attractive opportunity to investigate the influence of matrix mechanics on epithelial morphogenesis. However, for MDCK II cells, the range of cyst growth-permissive wt% is small (3.5% - 4.5%). Nevertheless, within the range analyzed in these studies (3.5% - 5.0%), there is considerable variation in key properties of the matrix. In terms of elastic modulus, 4.0% and 5.0% gels differ by only 200 Pa. (Elastic modulus was not measured for 3.5% gels.) However, there is reason to believe that 3.5% gels have significantly lower elastic modulus than 4.0% gels. The mass swelling ratio of 3.5% gels was three times higher than 4.0% gels and suggests a significantly looser network structure that typically corresponds with a low modulus [1]. Thus, the aberrant polarity and lumen phenotypes observed in 3.5% gels corresponds to a low (<<400 Pa) elastic modulus regime. In contrast, 4.0% and 4.5% gels in a higher (400 – 600 Pa) elastic modulus regime exhibited physiological cyst polarity and lumen phenotypes. We speculate that the high swelling in the 3.5% gel effectively decreases the density of adhesive ligands in the matrix and reduces the adhesive signal presented to the cells. A non-mutually exclusive alternative explanation is that the compliance of the 3.5% gel prevents generation of intracellular forces in response to contractility. The elimination of proliferation at high wt% could be explained by variations in other matrix properties, like crosslink density, that are influenced by wt%.

PEG-4MAL hydrogels are modular systems in which stoichiometric combination of tetra-functional PEG-4MAL macromers and bi-functional crosslinking peptides yields a crosslinked network. Therefore, increasing the concentration (wt%) of PEG-4MAL necessitates an increase in the concentration of crosslinking peptides. In fact, the

concentration of crosslinks in a 5.0% PEG-4MAL gel is more than 60% higher than that of a 3.5% gel, with the same adhesive ligand density. We observed that MDCKII proliferation (but not viability) was eliminated in 5.0% PEG-4MAL gels, whereas 3.5% gels had robust proliferation. Our finding was consistent with earlier findings with mesenchymal cells spreading in PEG-4MAL gels fabricated with a fast-degrading crosslink peptide (GCRDVPMS↓YMRGGDRCG) where viable C2C12 myoblast (mesenchymal) spreading was inversely related to PEG-4MAL wt% [1]. The encapsulated cells are presented with an increasingly difficult burden of local degradation in order to divide or, in the case of mesenchymal cells, to spread. Although elastic moduli of 4.0%, 4.5%, and 5.0% PEG-4MAL gels are similar, we speculate that 5.0% gels exceed a threshold of crosslink density that permits proliferation.

An increase in elastic modulus is observed when a lower molecular weight macromer (having shorter arms) is substituted at a given wt%. Nevertheless, the crosslinking density effect is not avoided, as a decrease in PEG-4MAL molecular weight from 20 kDa to 10 kDa, increases concentration of crosslink peptide by nearly 140%. In our study, MDCK II proliferation was eliminated when embedded in 4.0% 10 kDa PEG-4MAL (vs. 20 kDa) gels. Together, these effects suggest that variation in PEG-4MAL wt% or molecular weight exert tremendous influences on crosslink density. As a result, the behavior of embedded cells may be modulated by the degradability of the crosslinks.

Several groups have shown that degradability is critical parameter for modulating cell behaviors in synthetic matrices [130, 138, 141, 168]. For instance, cell migration is facilitated by local degradation, as cells forge a path through a dense matrix. Notably, Burdick and colleagues showed that degradable hyaluronic acid (HA) hydrogels directed

human mesenchymal stem cell (hMSC) differentiation toward an osteogenic phenotype whereas non-degradable HA hydrogels promoted an adipogenic phenotype independent of elastic modulus. In that instance, degradation allowed local remodeling of the microenvironment to enable assembly of focal adhesions and generation of traction that resulted in osteogenic differentiation [168]. In the present study, we showed that a fast-degrading MMP-cleavable crosslink peptide is required for cyst growth in permissive wt% conditions. Titration of a slower-degrading peptide at 40% of the total crosslinking eliminated MDCK II cell proliferation. Furthermore, inhibition of MMP activity reduced cyst growth rates. Together, these results indicate that matrix degradation strongly influences MDCK II proliferation in PEG-4MAL. A non-mutually exclusive explanation for some of the proliferation-modulation effects attributed to crosslink density would be that, in the cases of increasing wt% or decreasing PEG-4MAL molecular weight, denser hydrogel networks inhibit nutrient diffusion and decreased cellular metabolic function.

Lumen phenotypes in mature MDCKII cysts grown in Coll I gels and Matrigel^{TM} are modulated by apical polarity complexes [123, 158, 169], Rho GTPase functions [27], vesicular trafficking machinery [158, 170], cell-cell adhesion [171, 172], apoptosis mediators [123], and cell seeding density [123]. How PEG-4MAL wt%, with its related effects on elastic modulus and crosslinking density, modulates lumen phenotype is likely related to effects on apico-basal polarity. Just as low PEG-4MAL wt% (3.5%) gels exhibited higher incidence of cysts with multiple lumens versus higher wt% (4.0%, 4.5%) gels, low wt% gels produced cysts with higher incidence of exterior or mixed polarity. Cysts grown from culture of MDCK cells in suspension also exhibit external apical polarity [95-97]. This owes to absence of cell anchorage to matrix via integrin receptors

on the external surface of cyst. As the suspension microenvironment provides no spatial context, the cysts produce an apical surface on the outside and secrete LM into a central lumen, if lumens exist. In this PEG-4MAL culture case, the decreased crosslinking density in the low wt% gels may result in accelerated disintegration of the matrix with its integrin binding ligands. Thus, to some extent, cysts in low wt% gels may have adopted a suspension phenotype. The implications for lumen formation may relate to laminin secretion into the lumen and increased luminal cell survival. In fact, we observed LM staining at the interior of some cysts grown in 3.5% gels (**Figure 3.6, bottom-right panel**). Together, our observations of MDCK II proliferation, cyst polarization, and lumen formation strongly suggest that matrix degradability, which can be modulated by crosslink density, exerts a major influence on epithelial morphogenesis within PEG-4MAL hydrogels. We suppose that increasing cell density from 500 cells/μL to levels used in similar studies (1000-2000 cells/μL) [143, 150, 173] might allow cell proliferation in higher wt% gels and gels made with short-arm macromers, as the secretion of MMPs would be increased.

Conclusions

We have exploited a highly-efficient Michael-reactive PEG macromer to fabricate bioartificial hydrogels that incorporate cell adhesion ligands, permit cell-responsive degradation, and exhibit elastic properties resembling natural ECM extracts. By culturing MDCK II epithelial cells in these engineered PEG-4MAL matrices over a range of polymer wt%, we showed that the elastic modulus, crosslink density and degradability of the matrix effectively modulate cell proliferation and cyst morphogenesis (establishment

of apical polarity and formation of lumens). Furthermore, we demonstrated a flexible platform for modulating epithelial morphogenesis in vitro. In summary, bioartificial matrices stand as an experimental and therapeutic platform offering excellent control of the physical and biological properties of the microenvironment for studies of tissue morphogenesis.

Materials and Methods

Antibodies (and other reagents)

The following primary monoclonal (mAb) and polyclonal (pAb) antibodies were used: Mouse anti-gp135/podocalyxin (supernatant 3F2 1D8, kind gift of G. Ojakian, SUNY Downstate), rabbit anti-laminin (LM) (Sigma-Aldrich, St. Louis, MO). Anti-LM antibody was raised against intact LM-111, consisting of α1-, β1-, and γ1-chains, and may also detect other LM isoforms consisting of those chains (e.g., LM-511) [53, 54]. The following secondary antibodies were used: goat anti-mouse IgG Alexa Fluor 488, goat anti-rat IgG Alexa Fluor 555, goat anti-rabbit IgG Alexa Fluor 488 (Life Technologies, Carlsbad, CA), donkey anti-rabbit IgG Dylight 649 (Thermo Fisher Scientific, Rockford, IL). Nuclei were stained with Hoechst 33342 and filamentous actin was stained with rhodamine phalloidin (Life Technologies). Synthetic adhesive peptide GRGDSPC, and crosslink peptides GCRDGPQGIWGQDRCG and GCRDGPQGIAGQDRCG were obtained from aapptec, (Louisville, KY). MMP inhibitors GM6001 and MMP inhibitor II were obtained from EMD Millipore (Billerica, MA)

Cell culture

Madin-Darby canine kidney (MDCK) strain II epithelial cells (ECACC via Sigma-Aldrich) were maintained in Eagle's minimal essential media (EMEM) (ATCC, Manassas, VA) supplemented with fetal bovine serum (Life Technologies) at 10% (v/v), Penicillin (100 IU/mL, Life Technologies) and streptomycin (100 μg/mL, Invitrogen) and fungizone (Invitrogen).

Three-dimensional cell culture in PEG-maleimide hydrogels

For 5.0% (w/v) hydrogels, four-arm PEG-maleimide (PEG-4MAL) (MW = 22000, Laysan Bio, Arab, AL) was dissolved in diH20 at 12.5% (w/v) and desalted using a 7 kDa MW cutoff column (Zeba, Thermo Fisher Scientific, Waltham, MA). After lyophilization, desalted PEG-4MAL was dissolved in a triethanolamine (TEA) (Sigma-Aldrich) buffer (4 mM in DPBS, pH 7.4) to form a 12.5% solution (w/v) (2.5X the final 5% hydrogel). Dilutions for lower wt% gels were made at this step. Adhesive peptide (G**RGD**SP*C*) was dissolved in TEA (to form 10 mM peptide solution). Two volumes of PEG-4MAL precursor solution was mixed with one volume of peptide solution. The mixture was incubated at room temperature for at least 10 minutes to achieve functionalized PEG-4MAL precursor. Bis-cysteine crosslinking peptide (GCRDGPQG↓IWGQDRCG) (GPQ-W) (↓denotes enzymatic cleavage site) or GCRDGPQG↓IAGQDRCG was dissolved in TEA at concentration that achieves 1:1 maleimide:cysteine ratio after accounting for maleimide groups reacted with adhesive peptide. Actively growing MDCK cells were trypsinized, counted and resuspended at 5x final cell density in ice-cold serum-free EMEM and stored on ice. 12-well silicone isolator sheets (4.5 mm diameter well, 1 mm thick, Grace Bio-Labs, Bend, OR) were pressed onto microscope slides and exposed glass was treated with Sigmacote (Sigma-

Aldrich). To form 20 μL gels, 4 uL of crosslinker solution was pipetted into each well. Then, 4 uL of cell suspension was mixed with 12 μL of functionalized PEG-4MAL precursor solution. 16 μL PEG-cell mixture was then pipetted into well and mixed 10-15 times. Gelation was apparent within 30 seconds. Gels were moved to 37C, 5% CO_2 humidified incubator for 20-25 minutes to facilitate crosslinking. Gels were then swelled in complete growth media and moved to 48-well plate with 0.5 mL complete growth media per well.

Three-dimensional cell culture in type I collagen gels

To prepare a 2 mg/mL neutral type I collagen solution, eight parts type I collagen from bovine tendon (3 mg/ mL, Sigma-Aldrich) was mixed with one part 10X DMEM on ice (see below) and the pH adjusted to 7.2 – 7.6 using 0.1M NaOH. A cell suspension in serum-free media was added to the mixture to dilute the solution to 2 mg/mL type I collagen and result in 40,000 cells/mL. 150 μL of the cell-collagen mixture was added to the wells of an 8-well chambered coverglass. Collagen gel was allowed to solidify for 30 – 45 minutes in a 37° C air incubator. 200 μL complete media added to each well. Alternatively, 75 μL of the cell-collagen mixture was pipetted onto a 6.5 mm polyester permeable support (0.4 μm pore, Corning, Corning, NY) in a 24-well plate. 700 μL complete media was added to the bottom reservoir and 200 μL was added to the top reservoir after gel solidified.

Viability assays

To assay viability of cells within bioartificial matrix: PEG-4MAL gels were moved to 96-well plate, culture medium removed and replaced with 125 μL of 0.5% collagenase I

(1250 U/mL, Worthington Biochemical, Lakewood, NJ), 2 μM calcein-AM (LIVE)(Life Technologies), 1 μM TOTO-3 iodide (DEAD)(Life Technologies) in serum-free EMEM media. Plate incubated at 37° C in 5% CO_2 in humidified incubator for approximately 60 minutes or until hydrogel was completely dissolved and cells settled at bottom of well. For collagen gels, gel was incubated in 2 μM calcein-AM and 1 μM TOTO-3 for 30 minutes and placed in chambered coverglass for imaging. Samples imaged at 10x or 20x with C-1 or C-2 inverted confocal fluorescence microscope (Nikon, Melville, NY) and cells counted with ImageJ macros. For negative control, 0.1% saponin included in assay medium.

Proliferation assays

Proliferation was assayed using the Click-iT EdU Imaging Kit (Life Technologies) with adaptations of manufacturer's instructions. Briefly, 5-ethynyl-2´-deoxyuridine (EdU), a thymidine analogue, was added to hydrogel culture media at 10 μM for 6 – 8 hours. Samples were then fixed and treated with the appropriate kit reagents to label all nuclei with Hoechst 3342 and proliferating nuclei with an Alexa Fluor dye. Then, PEG-4MAL gels were dissolved and mounted in 0.5% collagenase I (1250 U/mL, Worthington Biochemical) in 2% low-melt agarose (Lonza, Walkersville, MD) at 37C in chambered coverglass. After cells and clusters settled to bottom of wells, agarose was allowed to solidify at 4C. For collagen gels, gel was mounted on microscope slide with ProLong Gold (Life Technologies) and #1.5 coverslip. Samples imaged at 10x or 20x with C-1 or C-2 inverted confocal fluorescence microscope (Nikon, Melville, NY) and cells counted with ImageJ macros.

Immunofluorescence labeling of cysts

Gels were washed extensively in PBS+ (3x quickly and 2x 5 minutes) to remove media and fixed in 4% formaldehyde in PBS+ for 15 minutes while rocking at room temperature. After extensive washing in PBS+, gels were incubated 30 minutes in blocking buffer (1% bovine serum albumin, 1% goat serum, 0.1% fish skin gelatin, 0.5% Triton X-100, 0.05% sodium azide in PBS). Meanwhile primary antibodies were diluted in blocking buffer. Mouse anti-gp135 supernatant was used at 1:10 – 1:100 dilution and all others were used at 1:100. In a 48-well plate or 8-well chambered coverglass, 200 μL of primary antibody solution was added to each PEG-4MAL gel and PBS+ added to empty wells for humidity. Plates were sealed with parafilm and placed on orbital shaker at 4C overnight. After extensive washing in blocking buffer, secondary antibodies and nuclear stain were diluted in blocking buffer and added to gels. All fluorescently-labeled secondary antibodies were used at 1:200 dilution, rhodamine phalloidin at 1:50, and DAPI nuclear stain was used at 1:1000 dilution. Secondary antibody incubation proceeded overnight as described for primary antibody. After further washing in blocking buffer, gels were washed in PBS+ and post-fixed for 15 minutes in 4% paraformaldehyde in PBS+. Gels were again washed in PBS+ and stored in PBS+ with sodium azide at 4C protected from light. To label extracellular laminin, the appropriate primary antibody was added to the culture media at 1:50 for four hours prior to fixation.

Cyst collection in agarose gel for imaging

Following immunofluorescence labeling, each gel was placed in well of 8-well chambered coverglass (1.0 thickness, Thermo Fisher Scientific) and 250 μL of 0.1% collagenase I (250 U/mL, Worthington Biochemical) in 2% low-melt agarose (Lonza) in

PBS. After several hours incubation on shaker at 37C, cysts were released to bottom of well and chambers were moved to 4° C refrigerator for agarose to solidify.

Microscopy

Phase contrast images were captured daily during the course of three-dimensional cultures using an inverted microscope (Nikon) and SPOT imaging software (Diagnostic Instruments, Sterling Heights, MI). Fluorescent images for cyst scoring were captured using a C1 or C2 laser scanning confocal microscope with a 20x or 60x objective and EZ-C1 or NIS Elements software (Nikon, Melville, NY). Each field contained up to dozens of cysts. A single z-slice was captured at an appropriate plane. Each image was captured as the merge of four separate channels corresponding to blue, green, red, and transmitted light, respectively.

Quantitation of cyst morphology

For multiplicity of lumens: a cyst cross-section having a single hollow space and outlined by a monolayer of cells was designated as having a *single lumen*, a cyst cross-section having a single hollow space bounded by multiple layers or groups of cells was designated as having a *partial lumen*, a cyst cross-section having multiple hollow spaces was designated as having *multiple lumens*, and a cyst cross-section having no hollow spaces was designated as having *no lumen*.

For polarity: a cyst cross-section in which the interior of lumens are lined with gp135 and the exterior of cyst lacks gp135 possessed *interior apical polarity*, a cyst cross-section in which the interior of lumens lack gp135 and the exterior of cyst is lined with gp135 possessed *exterior apical polarity*, a cyst cross-section in which the interior of lumen and

the exterior of cysts showed similar accumulation of gp135 possessed *mixed apical polarity*. A continuous layer of LM at the perimeter of the cyst was scored as complete (1.0) whereas absence of the LM layer was scored 0.0 and partial coverage was scored 0.5. Cyst size was measured from fluorescent images of cyst cross sections. Minimum and maximum feret diameters were measured for each cysts using ImageJ and the average was reported. See [174].

Statistical Analysis

For continuous variable data, we used one-way ANOVA with Tukey's tests for multiple comparisons, where necessary. For categorical data, we implemented a chi-squared test with Bonferroni's test for multiple comparisons, where necessary (See [175]). GraphPad Prism software (GraphPad, La Jolla, CA) was used to implement analyses.

CHAPTER IV: INFLUENCE OF INCORPORATED ADHESIVE LIGAND CONCENTRATION ON CYST MORPHOGNESIS OF MDCK II EPITHELIAL CELLS IN A BIOARTIFICIAL MATRIX

Summary

Three-dimensional (3D) cell cultures in natural ECM extracts, including type I collagen (Coll I) and Matrigel™, enable observation of epithelial morphogenesis, a hard-wired, multicellular differentiation program that integrates cell-ECM adhesion, cell proliferation, and ECM remodeling to achieve functionally differentiated structures like hollow cysts and tubules [81, 86, 87, 89, 119]. Nevertheless, critical limitations of natural ECM extracts, including clinical incompatibility, lot-to-lot variability and undefined presentation of cell adhesion motifs have motivated development of a synthetic ECM platform for detailed studies. Here, a multi-arm poly (ethylene glycol) (PEG)-maleimide macromer (PEG-4MAL) is covalently functionalized with adhesive peptides and crosslinked with proteolytically-cleavable peptides in the presence of epithelial cells. A highly-efficient Michael-addition reaction enables fabrication of hydrogels with defined quantities of RGD peptide while keeping all other hydrogel properties unchanged [1]. By culturing MDCK II epithelial cells in these engineered PEG-4MAL matrices over a range of incorporated RGD concentration (0 – 2000 μM), we show that cyst size, apical polarity, and lumen phenotypes are remarkably sensitive to adhesive ligand density.

Introduction

Organization of epithelial cells into polarized, 3D tissue structures is critical to the barrier, secretion, and exchange functions of organs including lung, kidney, intestine and

salivary gland. Disruption of the 3D structure or dysregulation of the polarity in epithelial tissues is associated with significant morbidity and mortality [155]. When epithelial cells, including MDCK, are encapsulated in Coll I gels, hollow spherical monolayer structures called cysts form within 10 days and bear the hallmarks of epithelial polarity [92, 95, 96, 156]. Such 3D cultures of epithelial cells in natural ECM extracts have revealed that development and maintenance of intricately ordered epithelial structures (a process termed epithelial morphogenesis) involves coordination cell fate processes including adhesion, migration, differentiation, polarization, and apoptosis. Furthermore, these studies have revealed a powerful role of ECM in a framework of bi-directional signaling where cells embedded in matrix sense the adhesive signals in the matrix while actively remodeling the matrix via proteolytic degradation and secretion of new matrix [24, 35, 53, 65]. Specifically, β1 integrin receptors bind specific ECM motifs and subsequently transduce a signal that culminates in secretion of laminin at the basal surface where β1 integrin binding defines the axis of polarity. The cell surface interfacing the ECM is thus established as "outside" and the opposite cell surface is defined as "inside" [25, 54]. Integrin binding is so critical that blockade of β_1 integrin binding results in major departures from the mature MDCKII cyst phenotype [53]. Thus, 3D culture of epithelial cells in natural ECM extracts is a critical tool for studying development and maintenance of tissue architecture and the implications in organ function and pathogenesis.

Despite progress in these areas, studies of epithelial morphogenesis in natural ECMs are limited by the uncontrolled presentation of adhesive ligands, limited control of matrix structural and mechanical properties, lot-to-lot variability, and concerns over clinical use of animal-derived materials. In contrast, an engineered synthetic matrix that

specifically and precisely presents biological functionality, with tunable elastic properties, could be a useful platform for elucidating key influences of ECM properties in tissue morphogenesis. PEG hydrogels are the gold standard for cell- and tissue-interactive synthetic biomaterials, owing to hydrophilicity that results in highly-swollen gels with tissue-like properties, non-fouling character that presents a "clean slate" to biological systems, and excellent acceptance in vivo [129]. For this reason, cell-encapsulating hydrogels that present cell adhesion ligands and protease-sensitive crosslinking peptides have found broad experimental applications including regulation of cell migration, therapeutic vascularization, and stem cell differentiation [1, 130-133, 136, 152]. We previously showed that PEG-based hydrogel systems could support MDCK cyst morphogenesis [150]. Here, we present a four-arm PEG-maleimide (PEG-4MAL)-based system that offers superior reaction efficiency, a wide range of achievable elastic properties, and cell-responsive degradation as a bioartificial matrix to modulate epithelial morphogenesis. By culturing MDCK II epithelial cells in these engineered PEG-4MAL matrices over a range of adhesive ligand densities and observing dramatic effects on cyst size, apical polarity, and lumen phenotype, we examine the effect of adhesive ligand density on epithelial morphogenesis program.

Results

Many cell fate processes including proliferation, migration, and differentiation are regulated by integrin binding of specific ECM ligands [176]. In fact, beta1 integrin binding to collagen and laminin are critical events in formation of hollow, polarized cysts in collagen gels and Matrigel^{TM} [53-55]. Furthermore, the fibronectin (and laminin-) derived arginine-glycine-aspartate (RGD) tripeptide is bound by integrins αvβ3 and α5β1,

among others, and has been used extensively in engineered systems [177]. RGD density has been shown to modulate cell proliferation, migration, differentiation in a variety of systems [177]. In previous work, we demonstrated that a cysteine-containing cell adhesive peptide (GRGDSPC) can be incorporated into PEG-4MAL gels with high precision. With a reagent that detects free thiols on the unconjugated cysteines, we observed rapid and complete conjugation of GRGDSPC [1]. In contrast, using PEG hydrogels with different reactive groups like vinyl sulfone or acrylate, ligand incorporation was slow and failed to reach completion, even with high concentrations of triethanolamine (TEA) [1]. To understand whether RGD concentration in PEG-4MAL hydrogels influences epithelial cyst development, we cultured MDCK II cells within 4.0% PEG-4MAL gels with 0 – 2000 μM RGD and the fast-degrading crosslink peptide that includes the sequence GPQG↓IWGQ (↓ indicates cleavage site) (**Figure 4.1**). Over 10 days, we assayed cell survival and cell proliferation, measured cyst size, and classified cyst lumen and apical polarity phenotypes. The 4.0% PEG-4MAL parameter was chosen to employ microenvironments in the middle of the proliferation-permitting range (**chapter III**). To avoid a departure from the hydrogel structure used in previous studies within this investigation, we maintained a 2000 μM overall ligand loading. Thus, to vary RGD concentration, we added a quantity of non-adhesive R*D*G peptide equal to the amount that RGD concentration was reduced from 2000 μM. Therefore, in each gel,

$$[RDG] = 2000\ \mu M - [RGD].$$

At day 10, cultures were fixed, labeled with antibodies against apical polarity marker podocalyxin and laminin, stained for f-actin and DNA, and imaged by confocal microscopy (**Figure 4.2a**). The mean feret diameter of cysts ranged from 48.1 ± 1.3 μm

in 0 μM RGD gels to 74.9 ± 1.7 μm in 250 μM RGD gels **(Figure 4.2b.)**. Cysts in 0 μM RGD gels were significantly smaller than cysts in other gels containing as little as 10 μM RGD ($p<0.0004$, ANOVA with post-test corrected by Bonferonni's method). This result indicates that precise control of adhesive ligand presentation in PEG-4MAL hydrogels can modulate MDCK II cyst size.

With a microenvironment that can be precisely tailored to present specific quantities of an integrin-binding ligand, we investigated the effects of RGD incorporation in PEG-4MAL hydrogels on MDCK II cyst apical polarity. Cysts were classified into the following phenotypes: *interior apical polarity*, *exterior apical polarity*, *mixed apical polarity*, and *no apical polarity* (**Figure 4.2d**). Strikingly, the distribution of apical polarity phenotypes underwent a major shift at 250 μM RGD. For gels with low RGD concentration (≤ 100 μM), the majority of cysts had exterior apical polarity, which is inverted relative to the polarity in natural ECMs. In contrast, gels with high RGD concentration (≥ 250 μM) produced cyst populations in which the exterior apical polarity phenotype was rare. Instead, the physiological internal apical polarity phenotype was dominant in high RGD gels. Nevertheless, a small number of cysts with internal apical polarity were present in gels with as little as 50 μM RGD. We conducted a chi-squared test to determine how RGD incorporation in a 4.0% PEG-4MAL hydrogel affected the distribution of apical polarity phenotypes. We found that incorporated RGD concentration of 50 μM or more was sufficient to significantly alter the distribution of apical polarity phenotypes compared to gels with 0 μM RGD ($p<0.0001$). Whereas polarity phenotype differences between 50 μM and 100 μM were not significant ($p=1.0000$), a statistically significant shift in polarity phenotype distributions occurred

between 100 μM and 250 μM ($p<0.0001$). Next, we compared the apical polarity distributions in all concentrations of RGD to the Coll I gel. Notably, the population of cysts in PEG-4MAL gels containing 2000 μM RGD was not significantly different from that in the Coll I gel ($p=0.2388$). These results establish that (1) MDCK II cyst morphogenesis in PEG-4MAL hydrogels is highly sensitive to incorporated RGD concentration and that (2) RGD density in PEG-4MAL hydrogel can be tuned to induce cyst phenotypes resembling those observed in Coll I gels.

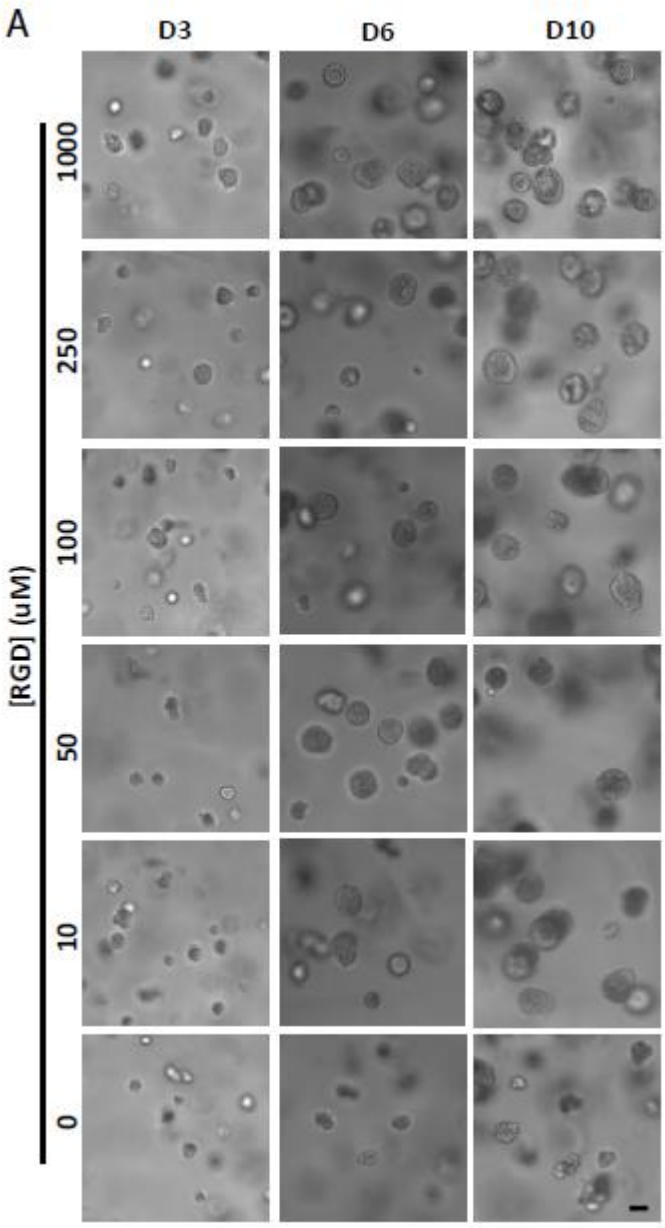

Figure 4.1. Concentration of incorporated RGD in PEG-4MAL hydrogel modulates MDCK II proliferation. a, Single MDCK II cells were cultured in 4.0% PEG-4MAL hydrogels incorporating different amounts of GRGDSPC peptide and grew into clusters and cysts over 10 days. Scale bar 50 μm.

To examine the influence of RGD concentration on the distribution of cyst lumen phenotypes in 4.0% PEG-4MAL gels, we classified 10-day-old cysts among *no lumen,*

partial lumen, *single lumen*, and *multiple lumen* in response to varying RGD concentration (0 – 2000 μM RGD). For gels with low RGD concentration (≤ 100 μM), the majority of cysts had no lumen (**Fig 4.2c.**). In an effect similar to that observed with apical polarity phenotypes in response to RGD concentration, a major shift in the distribution of lumen phenotypes occurred at 250 μM RGD. In gels with high RGD concentration (≥ 250 μM), cysts with no lumen were rare. Whereas cysts with single lumen were completely absent in low RGD gels, single lumen cysts made up a small proportion of the population in high RGD gels. Cysts with multiple lumens were dominant in the high RGD gels (**Fig 4.2c.**). We conducted a chi-squared test to determine how RGD incorporation in a 4.0% PEG-4MAL hydrogel affected the distribution of lumen phenotypes. Incorporated RGD concentration of 50 μM or more was sufficient to significantly alter the distribution of lumen phenotypes compared to gels with 0 μM RGD ($p<0.0001$). Whereas lumen phenotype differences between 50 μM and 100 μM were not significant ($p =1.0000$), a statistically significant shift in lumen phenotype distributions occurred between 100 μM and 250 μM ($p<0.0001$). This result further establishes that MDCK II cyst morphogenesis in PEG-4MAL hydrogels is highly sensitive to incorporated RGD concentration.

Developing MDCK cysts in Coll I assemble a basement membrane such that labeling mature cysts with anti-LM antibodies reveals a thin layer of secreted LM at the periphery of the cyst [53-55, 104]. To determine whether RGD concentration in PEG-4MAL hydrogels modulated LM basement membrane assembly, we labeled extracellular LM in cysts grown in gels presenting 0 – 2000 μM RGD. We observed that LM was patchy or diffuse in gels presenting 0 – 1000 μM RGD. In contrast, cysts in 2000 μM

RGD and Coll I gels exhibited dense and continuous LM basement membranes (**Figure 4.3**). This result further establishes that tuning RGD concentration in PEG-4MAL hydrogels modulates cyst morphogenesis and approximates cyst phenotypes observed in natural ECM.

The importance of β1 integrin binding in MDCK II cyst morphogenesis in Coll I gels is well-established through the use of function-blocking antibodies [53, 103]. Whereas α5β1 integrin binds RGD motifs in the context of FN protein where synergy binding sequences are present, the isolated, linear RGD peptide is primarily bound by αVβ3 [178]. To explore the dependence of cyst morphogenesis in PEG-4MAL matrix on αVβ3 binding, we cultured MDCK II cells in PEG-4MAL in the presence of LM609, an αVβ3 function-blocking antibody. We observed that LM609 caused an inversion of polarity resembling that seen in cultures lacking RGD. Notably, the LM basement membrane was intact and unaffected by LM609 (**Figure 4.4**).

Next, to explore the role of β1 integrin binding in MDCK II cyst morphogenesis in the context of a synthetic matrix presenting only RGD, we cultured MDCK II cells in PEG-4MAL in the presence of AIIB2, a β1 integrin function-blocking antibody. We observed undefined cyst polarity evidenced by diffuse podocalyxin labeling, absent lumen, and diffuse LM basement membrane labeling. Together, these integrin blocking results indicate αVβ3 binding drives physiological cyst polarization in RGD-conjugated PEG-4MAL gels and that β1 binding is required for both polarization and LM basement membrane assembly.

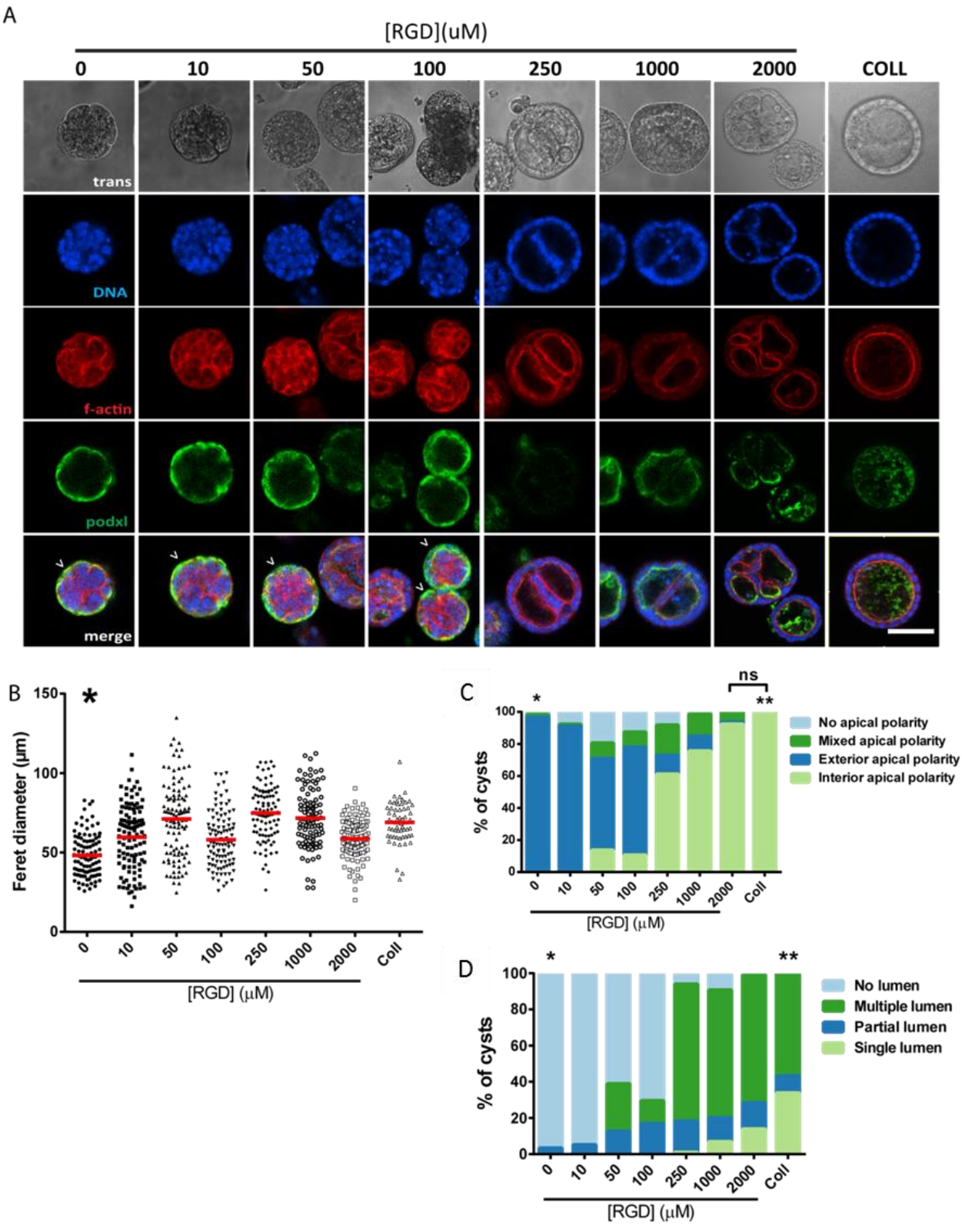

Figure 4.2. Concentration of incorporated RGD in PEG-4MAL hydrogel modulates cyst phenotype and apical polarity. a, MDCK II cysts grown in 4.0% PEG-4MAL for

10 days and labeled with antibody against apical polarity marker podocalyxin (podxl). Inverted apical polarity indicated by (^). Scale bar 50 μm. b, Quantification of cyst size at day 10. At least 62 cysts counted per condition. *, 0 μM RGD vs. every [RGD] (μM) other condition except 2000 μM RGD, $p < 0.05$, one-way ANOVA with Dunnett's multiple comparisons test. c, Distribution of apical polarity phenotypes at day 10. At least 78 cysts counted per condition. *, 0 μM RGD vs. every other condition except 10 μM RGD, $p < 0.0001$. **, Coll vs. every other condition except 2000 μM RGD, $p<0.0001$, chi squared test with Bonferroni's correction for multiple comparisons. d, Distribution of lumen phenotypes at day 10. At least 78 cysts counted per condition. *, 0 μM RGD vs. every other condition except 10 μM RGD, $p < 0.0001$. **, Coll vs. every other condition, $p<0.0001$, chi squared test with Bonferroni's correction for multiple comparisons.

Table 4.1. Incorporated RGD concentration versus apical polarity phenotype distributions.

Comparison	Bonferroni's test for multiple comparisons	X^2	df	P^
0 μM vs. 10 μM	NS	7.266	3	0.7668
0 μM vs. 50 μM	S	91.59	3	$<10^{-6}$
0 μM vs. 100 μM	S	61.06	3	$<10^{-6}$
0 μM vs. 250 μM	S	452.116	3	$<10^{-6}$
0 μM vs. 1000 μM	S	410.2	3	$<10^{-6}$
0 μM vs. 2000 μM	S	543.2	3	$<10^{-6}$
0 μM vs. Coll	S	367.0	3	$<10^{-6}$
50 μM vs. Coll	S	174.4	3	$<10^{-6}$
100 μM vs. Coll	S	179.4	3	$<10^{-6}$
250 μM vs. Coll	S	67.7	3	$<10^{-6}$
1000 μM vs. Coll	S	36.00	3	$<10^{-6}$
2000 μM vs. Coll	NS	9.846	3	0.2388

Chi-squared test. ^P values adjusted for multiple comparisons by Bonferroni's method.

Table 4.2. Incorporated RGD concentration versus lumen phenotype distributions.

Comparison	Bonferroni's test for multiple comparisons	X^2	df	P
0 μM vs. 10 μM	NS	0.5635	3	1.0000
0 μM vs. 50 μM	S	85.03	3	$<10^{-6}$
0 μM vs. 100 μM	S	53.84	3	$<10^{-6}$
0 μM vs. 250 μM	S	528.5	3	$<10^{-6}$
0 μM vs. 1000 μM	S	409.7	3	$<10^{-6}$
0 μM vs. 2000 μM	S	529.0	3	$<10^{-6}$
0 μM vs. Coll	S	430.0	3	$<10^{-6}$
10 μM vs. Coll	S	269.0	3	$<10^{-6}$
50 μM vs. Coll	S	175.3	3	$<10^{-6}$
100 μM vs. Coll	S	210.6	3	$<10^{-6}$
250 μM vs. Coll	S	148.6	3	$<10^{-6}$
1000 μM vs. Coll	S	71.23	3	$<10^{-6}$
2000 μM vs. Coll	S	30.70	3	$<10^{-6}$

Chi-squared test. ^P values adjusted for multiple comparisons by Bonferroni's method.

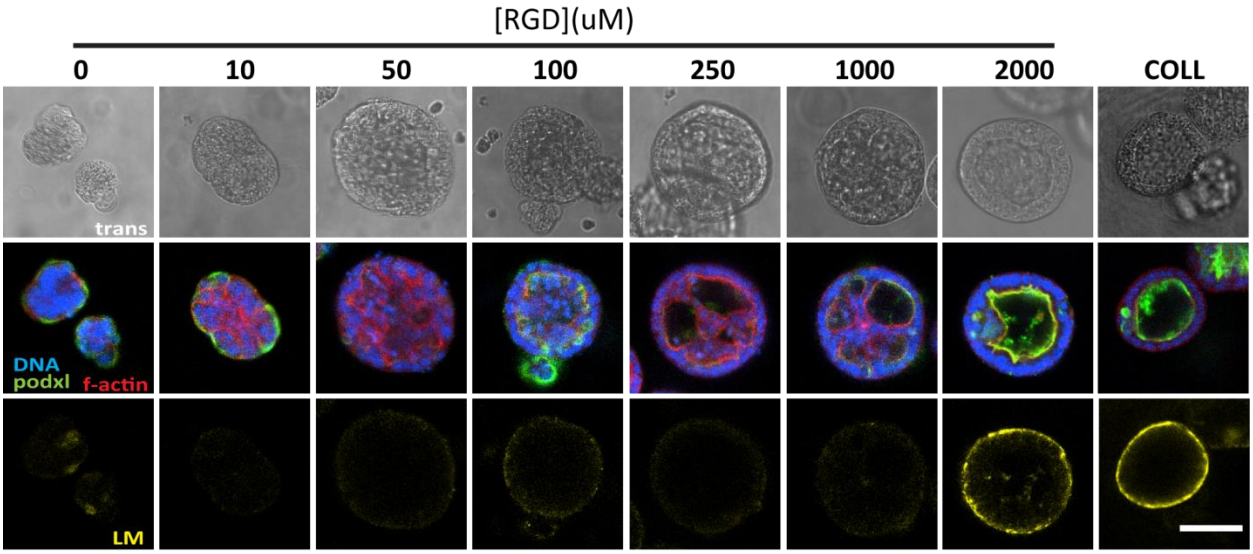

Figure 4.3. Concentration of incorporated RGD in PEG-4MAL hydrogel influences laminin basement membrane deposition. MDCK II cysts grown in 4.0% PEG-4MAL for 10 days and incubated for four hours with antibody against laminin prior to fixation and permeabilization. Representative images. Scale bar 50 μm.

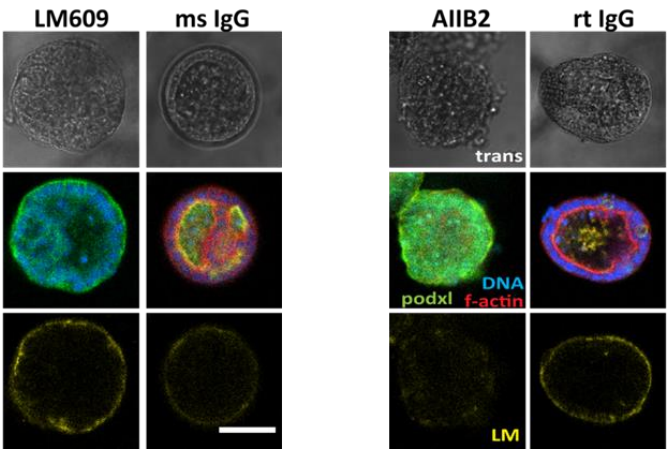

Figure 4.4. Cyst development in PEG-4MAL hydrogel depends on integrin binding. MDCK II cysts grown in 4.0% PEG-4MAL for 10 days in the presence of function-blocking antibodies against β1 integrin (AIIB2, rt IgG) or αVβ3 (LM609, ms IgG) or isotype control antibodies. Representative images. Scale bar 50 μm.

Discussion

Whereas 3D cultures of epithelial cells in natural ECM extracts have elucidated fundamental aspects of morphogenesis of epithelial tissue structures, such approaches are limited by the "as-is" nature of the matrix materials. Natural ECMs extracts are characterized by lot-to-lot variability, uncontrolled presentation of adhesive motifs, limited control of mechanical properties, and immunogenic potential when delivered in vivo. In contrast, a tailorable matrix that specifically and precisely presents biological functionality represents a useful and powerful platform for elucidating key influences of ECM properties in epithelial morphogenesis. Here, we present a PEG-based bioartificial matrix fabricated via well-characterized chemistry under physiological conditions that incorporates adhesive ligands with high precision and allows cell-mediated remodeling of the network via protease-sensitive crosslinks. By culturing MDCK II epithelial cells in these engineered PEG-4MAL matrices over a range of RGD adhesive ligand densities and observing dramatic effects on cyst size, lumen phenotype, and apical polarity, we

demonstrate a platform for modulating epithelial morphogenesis *in vitro*. The robust Michael-addition reaction allows fabrication of PEG-4MAL-based hydrogels with stoichiometric ligand incorporation. By blending in a non-adhesive, scrambled peptide (RDG), we varied RGD concentration over three orders of magnitude without altering the total ligand loading and thus maintained hydrogel structure.

To understand how adhesive ligand density modulates epithelial cyst morphology, we compared cyst size, apical polarity phenotypes and lumen phenotypes of cysts grown in gels presenting a range of adhesive ligand concentrations. This system enabled us to identify RGD concentrations required for physiological apico-basal polarization and lumen formation over 10 days. Strikingly, we observed dramatic phenotypic shifts triggered by RGD concentration increments as small as 10 μM. Although cysts of substantial size grew in gels without RGD, only 10 μM RGD was required to induce a significant increase in cyst size. In contrast, 50 μM or higher concentrations of RGD was required to induce a significant shift in lumen and apical polarity phenotypes versus gels without RGD. Between 100 μM and 250 μM RGD, major phenotypic conversions from *no lumen* to *multiple lumen* cysts and from *external apical polarity* to *internal apical polarity* were observed. LM basement membrane assembly in PEG-4MAL was also modulated by RGD concentration such that high density of RGD promoted formation of basement membranes resembling those in Coll I gels. Blockade of integrin binding using function-blocking antibodies confirmed that αvβ3 binding is sufficient to promote physiological polarization. Surprisingly, αvβ3 blockade had no impact on LM basement membrane assembly. Finally, β1 integrin binding was shown to be critical for both physiological polarization and LM basement membrane assembly.

Presentation of integrin binding ligands is one of the primary modes by which ECM modulates epithelial morphogenesis [28, 176]. Since Pierschbacher and Ruoslahti showed that the cell attachment activity of fibronectin (FN) could be duplicated with small fragments containing the RGD tripeptide, there has been tremendous interest in immobilizing oligopeptides in place of full-length proteins to confer bioactivity to biomaterials [177, 179]. Furthermore, the discovery of integrins and their amino acid binding motifs raised the appeal of peptides for targeting specific receptors to control specific cell responses [180]. Today, oligopeptides offer low cost, easy synthesis, high levels and control of ligand availability, high achievable signal density, and cell surface receptor selectivity.

When integrins bind extracellular ligands, intracellular signals are initiated [181]. In cell cultures on planar substrates, the extent of integrin signaling can be directly controlled by the density of ligand presented on the substrate [182]. In the present study, we embedded MDCK II cells in 3D microenvironments that present specific densities of adhesive ligand. In the absence of RGD, cells grew into cysts with external apical polarity and no lumen. These cysts match those that occur when MDCK II cells are grown in suspension [183]. We hypothesized that, in the absence of RGD, lack of integrin-binding ligands in the extracellular space leaves the cells without an "outside" signal. Thus, the outside of the cyst is established as a free surface (legitimately, in suspension) and the apical membrane components are located there. The matching result demonstrates that the PEG-4MAL hydrogel can encapsulate epithelial cells while presenting a "blank slate" in terms of signaling and spatial cues. The high tethering efficiency of PEG-4MAL allowed us to investigate the dose-response of RGD density.

Incorporation of RGD at 10 μM concentration resulted in a significant increase in cyst size versus gels without RGD. The increase in cyst size most likely indicates increased proliferation, as the cysts in both conditions typically had no lumens (**Figure 4.2b, c**). Integrin binding to RGD has been shown to promote proliferation on engineered surfaces [110, 184]. At RGD concentrations up to 100 μM, cysts with external apical polarity were dominant. However, at 250 μM RGD, a major phenotypic shift was observed, as nearly all cysts had internal apical polarity. Although RGD is bound by a variety of integrins, in the absence of synergistic amino acid sequences found in full-length RGD-containing proteins, RGD is primarily a ligand for integrin αvβ3 [178]. In this study, blockade of αvβ3 binding resulted in inverted cyst polarity and confirmed that integrins sense the RGD ligand in PEG-4MAL to orient polarity in MDCK II cysts. Together these data suggest that a threshold of integrin signaling at the basal surface of the cyst is required for physiological orientation of polarity.

When embedded in Coll I gels, MDCK II cells divide to form clonal clusters of several cells within two days. Then, during days 3-5, the beginnings of a hollow cavity, or lumen, is visible at the center of most clusters, even as cells at the periphery continue to divide. By day 10, a spherical monolayer of cells surrounds a single, fluid-filled lumen, typically [92, 156]. This process has been interrogated for decades, using integrin function-blocking antibodies, alternative natural ECMs including LM-rich Matrigel^{TM}, and myriad loss-of-function and gain-of-function modifications affecting signaling molecules [27, 53, 54, 95, 96, 101]. Together, these studies have exposed a framework in which bi-directional signaling through β1 integrin, with activation of the small GTPase Rac1, organizes secreted LM at the cyst-ECM interface to define an axis of polarity [53-

55]. Then, lumen formation proceeds as cells lacking contact with ECM die via apoptosis [185].

How does the β1-Rac1-LM axis observed in MDCK cyst morphogenesis in collagen inform interpretation of MDCK II cyst morphogenesis in RGD-presenting PEG-4MAL hydrogels? Is the β1-Rac1-LM signaling axis active in PEG-4MAL hydrogels?

It must first be acknowledged that there are several structural and biochemical differences between Coll I and a PEG-4MAL hydrogel. Whereas Coll I is a matrix of protein fibrils bound by non-covalent interactions, PEG-4MAL hydrogel is composed of covalently-crosslinked synthetic polymer chains in a regular meshwork. The resulting mesh size in the collagen gel is on the order of microns (~10.4 μm for 2.0 mg/mL gel [186]) whereas the PEG-4MAL hydrogel mesh size is estimated to be in the tens of nanometers [187]. Furthermore, owing to microns-long fibers and physical crosslinks in collagen gels, cellular tractions may extensively remodel the matrix microstructure. Both systems are sensitive to degradation by a broad range of matrix metalloproteinases (MMPs), as the PEG-4MAL hydrogel is crosslinked with a collagen derived MMP-sensitive peptide. Finally, whereas cell attachment to collagen gels is primarily mediated by integrin α2β1, PEG-4MAL hydrogels in this study exclusively present the RGD peptide, a ligand primarily bound by integrin αVβ3. Although RGD sites are present in Coll I, they are typically hidden from integrin binding [67].

In spite of these differences, mature cysts grown in PEG-4MAL with high RGD concentration resemble those grown in Coll I and follow a similar development pattern over 10 days (see Chapter III). In Coll I gels, cysts with external apical polarity result when β1 integrin binding is blocked using function-blocking antibody AIIB2 [53].

However, the inversion of polarity involves more than missing spatial cues. First, blockade of β1 integrin binding results in decreased Rac1 activation and increased RhoA activation. Then, the increased RhoA activity imposes its effects through ROCK I and myosin II activities. Forcing Rac1 activation with a constitutively active construct prevents the inversion of polarity [55]. It would be interesting to see whether inverted polarity in PEG-4MAL gels could be prevented by inhibition of RhoA effectors.

Along with β1 integrin and Rac1, the third component of polarity orientation in collagen gels is LM secretion and assembly into the basement membrane. When β1 integrin binding is blocked by AIIB2, or a dominant negative Rac1 is expressed in MDCK, inverted cyst polarity is accompanied by an incomplete LM basement membrane, although synthesis and secretion of laminin are normal [53-55]. Addition of exogenous laminin-111, which self assembles *in vitro*, partially restores internal apical polarity [54, 188]. In PEG-4MAL gels with high concentration of RGD, a thin layer of secreted LM is visible in at the periphery of 10-day-old cysts (**Figure 4.3**). Interestingly, blocking αVβ3 integrin binding caused external apical polarity but did not disrupt the LM basement membrane assembly. How can αVβ3 signaling be such a potent modulator of cyst polarity without discernibly influencing LM basement membrane assembly? This observation is consistent with a model in which polarity is stabilized early in cyst development such that LM basement membrane assembly proceeds later in culture without affecting polarity. In fact, Mostov and colleagues acknowledge that β1 function-blocking antibody AIIB2 is ineffective in inverting cyst polarity when added after day three of culture in Coll I gels [55].

In contrast to the αVβ3 blocking experiment, blocking β1 integrin binding in PEG-4MAL gels with RGD prevented physiological polarization and disrupted LM basement membrane assembly (**Figure 4.4**). The β1 integrin blocking result is consistent with the observations of Matlin and Mostov in MDCK 2D and 3D cultures, respectively [53, 99, 103]. Importantly, these findings affirm a central role of β1 integrin signaling in MDCK II cyst morphogenesis in the context of a microenvironment that does not initially present β1 integrin-binding ligands. We presume that the cell-secreted LM basement membrane provides sufficient signaling through β1 integrin to promote physiological cyst polarization.

Conclusions

We have exploited a highly-efficient Michael-reactive PEG macromer to fabricate bioartificial hydrogels that incorporate cell adhesion ligands, permit cell-responsive degradation, and exhibit elastic properties resembling natural ECM extracts. In culturing MDCK II epithelial cells in these engineered PEG-4MAL matrices over a range of incorporated RGD concentration, we showed that cyst size, apical polarity, and lumen phenotypes are remarkably sensitive to adhesive ligand density. Thus, we conclude that a threshold level αVβ3 integrin signaling, via binding RGD, is required for establishment of internal apical polarity. Furthermore, our findings affirm a central role of β1 integrin signaling in orientation of polarity and assembly of LM basement matrix during cyst morphogenesis.

Materials and Methods

Antibodies (and other reagents)

The following primary monoclonal (mAb) and polyclonal (pAb) antibodies were used: Mouse anti-gp135/podocalyxin (supernatant 3F2 1D8, kind gift of G. Ojakian, SUNY Downstate), rabbit anti-laminin (LM) (Sigma-Aldrich, St. Louis, MO). Anti-LM antibody was raised against intact LM-111, consisting of α1-, β1-, and γ1-chains, and may also detect other LM isoforms consisting of those chains (e.g., LM-511) [53, 54]. Mouse anti-αVβ3 integrin function blocking mAb (LM609, EMD Millipore, Billerica, MA), rat anti-β1 integrin function blocking mAb (AIIB2, proclin-free developed by Caroline H. Damsky and obtained from the Developmental Studies Hybridoma Bank developed under the auspices of the NICHD and maintained by The University of Iowa, Department of Biology, Iowa City, IA 52242), rat IgG1 isotype control mAb (RTK2071, Biolegend, San Diego, CA), mouse IgG1 isotype control mAb (MOPC-21, Biolegend, San Diego, CA) . The following secondary antibodies were used: goat anti-mouse IgG Alexa Fluor 488, goat anti-rat IgG Alexa Fluor 555, goat anti-rabbit IgG Alexa Fluor 488, donkey anti-rabbit IgG Dylight 649 (Thermo Fisher Scientific, Rockford, IL). Nuclei were stained with Hoechst 33342 and filamentous actin was stained with rhodamine phalloidin (Life Technologies). Synthetic adhesive peptides GRGDSPC, GR*D*GSPC, and crosslink peptide GCRDGPQGIWGQDRCG were obtained from aapptec, Louisville, KY.

Cell culture

Madin-Darby canine kidney (MDCK) strain II epithelial cells (ECACC via Sigma-Aldrich) were maintained in Eagle's minimal essential media (EMEM) (ATCC, Manassas, VA) supplemented with fetal bovine serum (Life Technologies) at 10% (v/v),

Penicillin (100 IU/mL, Life Technologies) and streptomycin (100 μg/mL, Invitrogen) and fungizone (Invitrogen).

Three-dimensional cell culture in PEG-maleimide hydrogels

For 5.0% (w/v) hydrogels, four-arm PEG-maleimide (PEG-4MAL) (MW = 22000, Laysan Bio, Arab, AL) was dissolved in diH20 at 12.5% (w/v) and desalted using a 7 kDa MW cutoff column (Zeba, Thermo Fisher Scientific, Waltham, MA). After lyophilization, desalted PEG-4MAL was dissolved in a triethanolamine (TEA) (Sigma-Aldrich) buffer (4 mM in DPBS, pH 7.4) to form a 12.5% solution (w/v) (2.5x times that of the final 5% hydrogel). Dilutions for lower wt% gels were made at this step. Adhesive peptide (G**RGD**SP*C*) or non-adhesive peptide (G**RDG**SP*C*) or combination was dissolved in TEA (to form 10 mM peptide solution). Two volumes of PEG-4MAL precursor solution was mixed with one volume of peptide solution. The mixture was incubated at room temperature for at least 10 minutes to achieve functionalized PEG-4MAL precursor. Rapidly-degrading bis-cysteine crosslinking peptide (GCRDGPQG↓IWGQDRCG) ("GPQ") (↓denotes enzymatic cleavage site) was dissolved in TEA at concentration that achieves 1:1 maleimide:cysteine ratio after accounting for maleimide groups reacted with adhesive peptide. Actively growing MDCK cells were trypsinized, counted and resuspended at 5x final cell density in ice-cold serum-free EMEM and stored on ice. 12-well silicone isolator sheets (4.5 mm diameter well, 1 mm thick, Grace Bio-Labs, Bend, OR) were pressed onto microscope slides and exposed glass was treated with Sigmacote (Sigma-Aldrich). To form 20 μL gels, 4 uL of crosslinker solution was pipetted into each well. Then, 4 uL of cell suspension was mixed with 12 μL of functionalized PEG-4MAL precursor solution. 16

μL PEG-cell mixture was then pipetted into well and mixed 10-15 times. Gelation was apparent within 30 seconds. Gels were moved to 37C, 5% CO_2 humidified incubator for 20-25 minutes to facilitate crosslinking. Gels were then swelled in complete growth media and moved to 48-well plate with 0.5 mL complete growth media per well. For studies with integrin function-blocking antibodies, cells were pre-incubated (30 min, rocking, room temp) in 0.1% bovine serum albumin in serum free EMEM containing antibodies. AIIB2 (anti-β1) was used at 8 μg/mL, LM609 (anti- αVβ3) and isotype controls were used at 10 μg/mL.

Three-dimensional cell culture in type I collagen gels

To prepare a 2 mg/mL neutral type 1 collagen solution, eight parts type I collagen from bovine tendon (3 mg/ mL, Sigma-Aldrich) was mixed with one part 10X DMEM on ice (see below) and the pH adjusted to 7.2 – 7.6 using 0.1M NaOH. A cell suspension in serum-free media was added to the mixture to dilute the solution to 2 mg/mL type I collagen and result in 40,000 cells/mL. 150 uL of the cell-collagen mixture was added to the wells of an 8-well chambered coverglass. Collagen gel was allowed to solidify for 30 – 45 minutes in a 37C air incubator. 200 μL complete media added to each well. Alternatively, 75 uL of the cell-collagen mixture was pipetted onto a 6.5 mm polyester permeable support (0.4 μm pore, Corning, Corning, NY) in a 24-well plate. 700 uL complete media was added to the bottom reservoir and 200 uL was added to the top reservoir after gel solidified.

Immunofluorescence labeling of cysts

Gels were washed extensively in PBS+ (3x quickly and 2x 5 minutes) to remove media and fixed in 4% formaldehyde in PBS+ for 15 minutes while rocking at room temperature. After extensive washing in PBS+, gels were incubated 30 minutes in blocking buffer (1% bovine serum albumin, 1% goat serum, 0.1% fish skin gelatin, 0.5% Triton X-100, 0.05% sodium azide in PBS). Meanwhile primary antibodies were diluted in blocking buffer. Mouse anti-gp135 supernatant was used at 1:10 – 1:100 dilution and all others were used at 1:100. In a 48-well plate or 8-well chambered coverglass, 200 μL of primary antibody solution was added to each PEG-4MAL gel and PBS+ added to empty wells for humidity. Plates were sealed with parafilm and placed on orbital shaker at 4C overnight. After extensive washing in blocking buffer, secondary antibodies and nuclear stain were diluted in blocking buffer and added to gels. All fluorescently-labeled secondary antibodies were used at 1:200 dilution, rhodamine phalloidin at 1:50, and DAPI nuclear stain was used at 1:1000 dilution. Secondary antibody incubation proceeded overnight as described for primary antibody. After further washing in blocking buffer, gels were washed in PBS+ and post-fixed for 15 minutes in 4% paraformaldehyde in PBS+. Gels were again washed in PBS+ and stored in PBS+ with sodium azide at 4C protected from light. To label extracellular laminin, the appropriate primary antibody was added to the culture media at 1:50 for four hours prior to fixation.

Cyst collection in agarose gel for imaging

Following immunofluorescence labeling, each gel was placed in well of 8-well chambered coverglass (1.0 thickness, Thermo Fisher Scientific) and 250 μL of 0.1% collagenase I (250 U/mL, Worthington Biochemical) in 2% low-melt agarose (Lonza, Walkersville, MD) in PBS. After several hours incubation (shaking?) at 37C, cysts were

released to bottom of well and chambers were moved to 4C refrigerator for agarose to solidify.

Microscopy

Phase contrast images were captured daily during the course of three-dimensional cultures using an inverted microscope (Nikon) and SPOT imaging software (Diagnostic Instruments, Sterling Heights, MI). Fluorescent images for cyst scoring were captured using a C1 or C2 laser scanning confocal microscope with a 20x or 60x objective and EZ-C1 or NIS Elements software (Nikon, Melville, NY). Each field contained up to dozens of cysts. A single z-slice was captured at an appropriate plane. Each image was captured as the merge of four separate channels corresponding to blue, green, red, and transmitted light, respectively.

Quantitation of cyst morphology

For multiplicity of lumens: a cyst cross-section having a single hollow space and outlined by a monolayer of cells was designated as having a *single lumen*, a cyst cross-section having a single hollow space bounded by multiple layers or groups of cells was designated as having a *partial lumen*, a cyst cross-section having multiple hollow spaces was designated as having *multiple lumens*, and a cyst cross-section having no hollow spaces was designated as having *no lumen*.

For polarity: a cyst cross-section in which the interior of lumens are lined with gp135 and the exterior of cyst lacks gp135 possessed *interior apical polarity*, a cyst cross-section in which the interior of lumens lack gp135 and the exterior of cyst is lined with gp135 possessed *exterior apical polarity*, a cyst cross-section in which the interior of lumen and

the exterior of cysts showed similar accumulation of gp135 possessed *mixed apical polarity*. Cyst size was measured from fluorescent images of cyst cross sections. Minimum and maximum feret diameters were measured for each cysts using ImageJ and the average was reported. See ([174]).

Statistical Analysis

For continuous variable data, we used one-way ANOVA with Tukey's tests for multiple comparisons, where necessary. For categorical data, we implemented a chi-squared test with Bonferroni's test for multiple comparisons, where necessary (See [175]). GraphPad Prism software (GraphPad, La Jolla, CA) was used to implement analyses.

CHAPTER V: SUMMARY AND FUTURE DIRECTIONS

Overall Summary

How the 3D multicellular tissue structures that comprise the functional units of organs including the kidney, lung, and breast, are formed, maintained and repaired is a topic of intense research. Interest is driven by the implications of epithelial tissue assembly and homeostasis for cancer progression and prospective regenerative therapies. The studies described in this thesis manipulated physical and biochemical aspects of the microenvironment in which epithelial morphogenesis occurs. 3D cell cultures in natural ECM extracts, including type I collagen (Coll I), have enabled observation of epithelial morphogenesis, a hard-wired, multicellular differentiation program that integrates cell-ECM adhesion, cell proliferation, and ECM remodeling to achieve functionally differentiated structures like hollow cysts and tubules [154]. Nevertheless, critical limitations of natural ECM extracts, including clinical incompatibility, lot-to-lot variability and undefined presentation of cell adhesion motifs motivated development of engineered ECM mimics for detailed studies. PEG-based hydrogels offer tunable, tissue-like elastic properties, modular incorporation of cell adhesion peptides and cell-responsive degradation, and an excellent record in the clinic. Therefore, chapter III demonstrated culture of MDCK II epithelial cells in cell-adhesive PEG hydrogels with tunable elastic properties, crosslink density, and degradability. The influence of matrix physical and biochemical properties on MDCK II cyst morphogenesis was quantitatively evaluated using this system.

Currently, there is great interest in understanding how the mechanics of the microenvironment influence tissue homeostasis, particularly in the cases of epithelial organs where cancer progression has been associated with tissue stiffening [166]. Therefore, the linear relationship between elastic modulus and polymer wt% observed in PEG-4MAL hydrogels, within the sub-kPa range, presents an attractive opportunity to investigate the influence of matrix mechanics on epithelial morphogenesis.

Presentation of integrin binding ligands is one of the primary modes by which ECM modulates epithelial morphogenesis [28, 176]. Elucidation of the amino acid binding motifs bound by particular integrins allows use of oligopeptides for targeting specific receptors to control specific cell responses [180]. Furthermore, oligopeptides offer low cost, easy synthesis, high levels and control of ligand availability, high achievable signal density, and cell surface receptor selectivity.

In this thesis, we hypothesized that the polymer wt% of a synthetic matrix and the concentration of adhesive peptides presented therein would modulate MDCK II cell proliferation and cyst morphogenesis. Cell proliferation within PEG-4MAL hydrogels was assayed using an antibody-free, fluorescently-detected thymidine analogue, while cyst size, apico-basal polarity, lumen formation and basement membrane assembly were quantified following confocal immunofluorescence imaging.

Polymer weight percentage influences cyst morphogenesis through effects on elastic modulus, crosslink density and gel degradability

It is well established that most healthy cells maintain a "tensional homeostasis" by generating cytoskeletal tension in response to stresses exerted by the microenvironment

[166, 167]. Even in what are considered static tissues, cells are subject to hydrostatic pressure and respond to changes in matrix mechanics. In the mammary gland, for instance, the bi-layered epithelium lining the ducts and alveoli is subject to outward pressure during milk production. These cells respond with contractility that forces milk out of the alveoli and into the larger ducts toward the nipple [166]. Mammary tumors are often detected as stiffened regions of otherwise soft tissue. Furthermore, tumor stiffness may ultimately be correlated with increased morbidity in human breast cancer [167]. On the tissue level, mammary epithelial cells (MECs) respond to stiffening of their microenvironment with increased stiffness of the cellular cortex. In tumors, this results in enhanced ability to migrate through dense basement membranes and to metastasize to distant sites. *In vitro*, immortalized human MECs cultured in soft ECM extracts like Coll I or reconstituted basement membranes like Matrigel^{TM} form polarized spherical acini that resemble alveolar end buds. However, when the microenvironment is progressively stiffened, the small, spherical, polarized acini give way to larger structures with destabilized cell-cell junctions, perturbed polarity, disrupted lumen formation, and elevated extracellular signal-regulated kinase (ERK) signaling [111].

In PEG-4MAL hydrogels, the elastic modulus of the matrix varies linearly with polymer wt% over the range 4.0% – 10% (w/v) (400 – 1500 Pa) [1]. In chapter III, we sought to determine how elastic properties of the PEG-4MAL matrix influenced MDCK II cell proliferation and cyst morphogenesis. We found that the cell growth-permissive range of the PEG-4MAL matrix with these cells was limited to 3.5% - 4.5%. Nevertheless, we observed dramatic differences in apico-basal polarity and lumen phenotypes as wt% was varied. As will be discussed later, we concluded that the

differences in cyst phenotypes are best attributed to shifts in elastic modulus and crosslink density that accompany wt% changes and potentially affect the adhesive signaling and degradability of the hydrogel, respectively

Future studies can potentially overcome the limited set of PEG-4MAL molecular weight and wt% configurations that permit MDCK II proliferation and therefore access a wider range of elastic moduli. To do this, immature MDCK II clusters or mature cysts may be generated growth-permissive PEG-4MAL gels and then collected and re-embedded in gels that do not permit proliferation of single cells. PEG-4MAL hydrogels are rapidly dissolved in collagenase solutions without compromising cell viability. Subsequent washing and gentle pelleting may produce a cluster or cyst suspension that may be readily re-embedded in new gels. As immature cell clusters in PEG-4MAL typically have external (inverted) apical polarity (data not shown), inversion of polarity during transplantation would not be a significant concern. In the case of mature cysts with assembled basement membranes, it will be important to determine whether polarity and basement membrane integrity could be maintained during transplantation.

Several groups have shown that degradability is critical parameter for modulating cell behaviors in synthetic matrices [130, 138, 141, 168]. In the PEG-4MAL system, as used in this thesis, variations in polymer wt% cause dramatic changes in crosslink density. Thus, increases in PEG-4MAL wt% increased crosslink density and, as a result, encapsulated cells were presented with an increasingly difficult burden of local degradation in order to divide. Directly modulating matrix degradability with slow-degrading crosslink peptides or with soluble MMP inhibitors at an otherwise growth-

permissive PEG-4MAL wt% provided further evidence that rapid local degradation is required for cyst development.

PEG-4MAL wt% also influences hydrogel swelling. This indicates an effect on the mesh size of the hydrogel network. For 4.0% gels, we estimate a theoretical mesh size of ~35 nm, nearly three orders of magnitude smaller than that of Coll I gels. Lower molecular weight PEG-4MAL would have even smaller mesh size. Thus, there is reason to believe that high wt% PEG-4MAL may inhibit nutrient diffusion. Ongoing studies will assay bulk gel degradation and estimate diffusion coefficients.

Threshold of RGD density, is required for establishment of internal apical polarity

Since Pierschbacher and Ruoslahti showed that the cell attachment activity of fibronectin (FN) could be duplicated with small fragments containing the RGD tripeptide, there has been tremendous interest in immobilizing oligopeptides in place of full-length proteins to confer bioactivity to biomaterials [177, 179]. The robust Michael-type addition reaction between maleimide and thiols allows incorporation of precise quantities of cysteine-containing peptides in PEG-4MAL hydrogels. In this thesis, precision functionalization allowed us to show that increments of RGD concentration as small as 10 μM modulate cyst size. Titrating RGD concentration from 0 – 2000 μM indicated that a threshold level of integrin binding is required for physiological orientation of apico-basal polarity. Function-blocking antibody incubation suggested that signaling through αVβ3 integrin specifically mediated polarization. Further antibody blocking showed that β1 integrin signaling was also required polarization and LM basement membrane assembly. Together, these findings suggest that the β1 integrin –LM signaling axis

established in Coll I gels is an appropriate paradigm for interpreting cyst morphogenesis results in PEG-4MAL.

Nevertheless, future studies will adapt protocols to evaluate intracellular signaling involving Rho GTPases within PEG-4MAL. In 2D systems, threshold levels of ECM ligand binding cause integrin receptor clustering and formation of focal adhesion complexes [182]. These complexes subsequently act as signaling hubs as factors like focal adhesion kinase (FAK) and others are recruited. Ultimately, focal adhesions are linked to the cytoskeleton and allow the cell to exert significant forces across the membrane onto the ECM. Thus, in future work, it will be important to determine whether RGD binding by αVβ3 initiates assembly of focal adhesions and integrin signaling.

Our findings in this thesis have reinforced the notion that, during cyst morphogenesis, MDCK II cells bind extracellular LM using β1 integrin to orient an axis of polarity. We made these observations using RGD peptides to provide an initial integrin binding signal that apparently stimulated LM secretion and eventual β1 integrin binding. However, in LM-rich basement membranes extracts like Matrigel^{TM}, a pre-assembled LM basement membrane promotes rapid MDCK II cyst polarization and lumen formation (at the two-cell stage) without cell death [123]. Furthermore, addition of soluble LM-111 or basement membrane extract to cultures of MDCK II in non-ideal microenvironments results in enhanced cyst polarization and lumen formation [53, 55, 154]. It is known that particular LM isoforms are involved in specific cell behaviors [189]. For instance, following kidney tubule injury, denuded tubules are repopulated by neighboring cells that secrete and migrate on LM-332 to fill holes in the epithelial monolayer [31, 52, 190]. However, LM-332 is also implicated in elevated cell adhesion and migration in

polycystic kidney disease [61, 191]. Over the last decade, Nomizu and colleagues have developed high-throughput screening techniques to identify bioactive peptides from LM-111, LM-511, and LM-332 [192-196]. As the hydrogel-forming Michael-type addition reaction used here can incorporate essentially any peptide that contains a free cysteine, we are interested in using the PEG-4MAL system to investigate the influence of specific LM peptide domains on cyst morphogenesis.

Future Directions

Investigating interplay between cell-ECM forces and cyst morphogenesis

In spite of limitations in the current study, PEG-4MAL hydrogels are uniquely suited to study of matrix mechanical effects in MDCK II cyst morphogenesis. In fact, we have exploited the excellent optical transparency and water-like refractive properties of PEG-4MAL to measure cyst-generated tractions. We encapsulated MDCK II cells along with 200 nm fluorescent beads in PEG-4MAL gels and observed bead displacements with live cell imaging. When a two-day-old MDCK II cyst, not yet having a lumen, was ablated with sodium azide, we observed a dramatic positive displacement of surrounding beads, indicating that the living cyst had contracted the gel locally (**Figure 5.1a**). Interestingly, we observed that larger cysts with lumens collapsed upon ablation, suggesting that mature cysts exert pressure on the surrounding matrix (data not shown). To calculate traction forces, we modeled the system as an infinite elastic solid with a pressurized spherical cavity and found that matrix displacement field is described by

$$u = \frac{3Pa^3}{4Er^2}$$

where u is matrix displacement (meters), P is pressure (Pa), E is elastic modulus (Pa), a is cyst radius (meters), and r is distance from center of cyst (meters) [197]. We measured bead displacements (to visualize matrix displacement) using ImageJ Mosaic plugin [198] and employed a least-squares fit with E = 500 Pa (for 4.0% PEG-4MAL hydrogel) and cyst radius of 17 μm to calculate a pressure or, in this case, a traction force of 273 Pa (**Figure 5.1**). This calculated force is in excellent agreement with those calculated by others for multicellular epithelial tissues (150 Pa for rapidly-proliferating lung carcinoma spheroids) and appropriately smaller than those calculated for wound-closing fibroblasts (1700 Pa, NIH 3T3) [199]. Notably, the spherical symmetry of the cyst dramatically simplifies the otherwise computationally intensive calculations required for highly-spread mesenchymal cells.

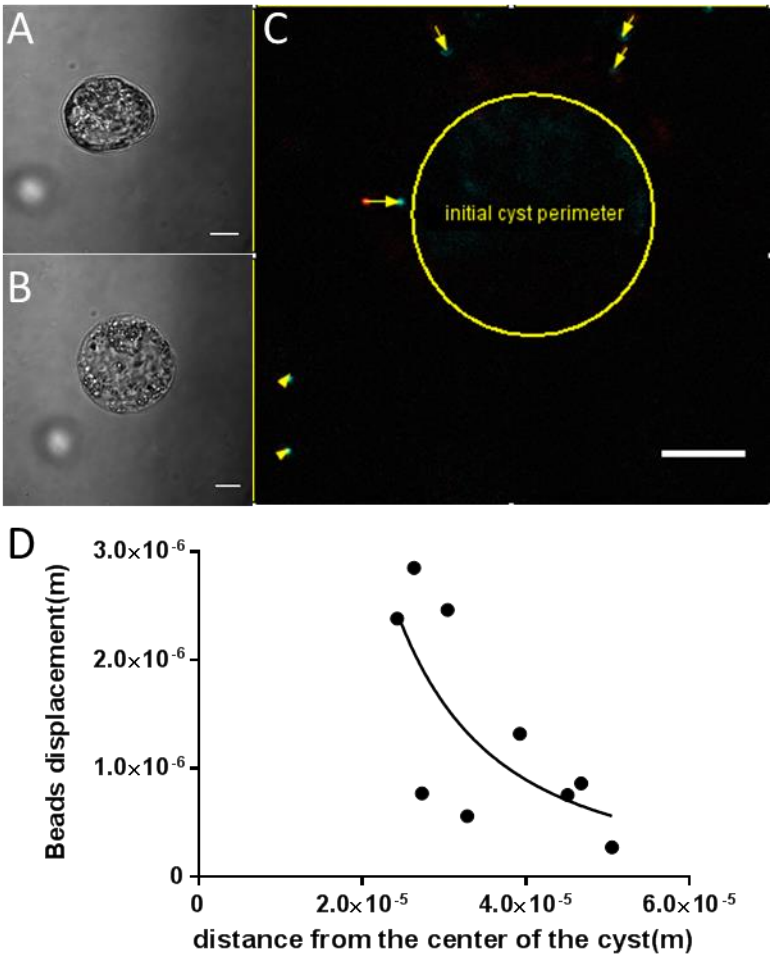

Figure 5.1. Fluorescent particle tracking in PEG-4MAL hydrogel reveals mechanical behavior of multicellular cysts. Live cell imaging of solid cyst (a) revealed expansion of cyst perimeter after destruction with sodium azide (b). c, Arrows indicate displacement of beads due to cyst contractility prior to sodium azide treatment. d, Least squares fit of bead displacement versus initial distance from cyst. Scale bars 10 μm.

Given these promising preliminary results, future work will investigate the influences of integrin binding, matrix elastic properties, and cellular contractile machinery on cyst tractions. First, to investigate the evolution of forces exerted upon the ECM during cyst development from single cells to mature structures, cells embedded within cyst growth-permissive PEG-4MAL hydrogels, will be ablated with SDS at various time points. We expect that the magnitude of cellular tractions will decrease from

a maximum in small, solid clusters to a minimum when lumen formation is complete. In mature cysts with single lumen, we expect that polarized fluid transport into the lumen will result in a positive pressure on the matrix. It will also be interesting to see how the existence of partial or multiple lumens influence cyst tractions. Next, to determine how cell-ECM adhesion modulates cyst generated forces, we will culture MDCK II cells in PEG-4MAL matrices presenting a range of RGD concentrations. By controlling the number of integrin-ligand bonds, we expect that cyst tractions will scale with RGD concentration and provide further illustrate the influence of integrin-signaling in MDCK cyst morphogenesis. Recent studies with MDCK II in Coll I gels have shown that extracellular LM, signaling through β1 integrin, reduces RhoA activation and its downstream affects through ROCK I and myosin II [55]. In this thesis, we showed that the PEG-4MAL system with RGD promotes robust proliferation without β1 integrin ligand presentation but nevertheless relies on β1 signaling, likely through binding LM, to enable apico-basal cyst polarity. Therefore, it will be interesting to see whether the inverted apico-basal polarity that we observed upon β1 integrin blockade is associated with elevated contractility. In an orthogonal approach, these experiments could employ PEG-4MAL matrices engineered to present active LM-derived peptides to directly, and perhaps dose-dependently, regulate RhoA activation and cell-exerted matrix contraction.

This proposed work is potentially transformative in that it will yield multicellular tissue traction profiles in three-dimensions enabled by rationally-designed biomimetic materials that feature precise tuning of the mechanics and biochemical properties of the microenvironment.

Other very recent contributions have employed highly-specialized equipment and analytical techniques to study single cell mechanobiology within synthetic matrices or cell sheet mechanics upon 2D materials. However, this proposal enables mechano-biological characterization of *actively developing* 3D tissue rudiments in a medium where cell-matrix interactions, elastic properties, and structural evolution (degradation and ECM deposition) may be precisely tuned or monitored. This system yields multicellular traction force profiles arising from a vast space of tissue morphogenetic phases and microenvironmental configurations that provide insights into developmental processes and disease states.

Modulating epithelial polarity with dynamic microenvironments

An emerging strategy for investigating cell responses to changes in the microenvironment involves dynamic ligand presentation. One approach employs engineered adhesive peptides whose integrin binding domains are concealed by light-sensitive "cage" molecules. Upon irradiation with specific wavelengths of light, the cage is removed and the adhesive motif is exposed. García and del Campo have pioneered use of these caged-RGD reagents to dynamically regulate cell adhesion, migration, and differentiation on surfaces [200, 201]. In this thesis, we observed that MDCK II cells grown in PEG-4MAL gels presenting low (< 250 μM) concentration of RGD grew into clusters without lumens with inverted apical polarity over 10 days. Several studies have established that pools of integrins are expressed on the apical surfaces of epithelia, with implications for polarity reversal upon exposure to the appropriate ECM ligands [24, 101, 103]. Thus, it would be interesting to see whether delayed exposure of caged-RGD in a

PEG-4MAL matrix would rectify inverted apico-basal polarity. Future work could also make use of built-in fluorescence recovery after photobleaching (FRAP) modules on confocal microscopes to locally expose cell adhesion ligands and explore how regional differences in integrin binding influence cyst polarity.

Conclusions

Epithelial morphogenesis is a hard-wired, multicellular differentiation program that dynamically integrates microenvironmental cues to coordinate cell fate processes including adhesion, migration, proliferation, and polarization. Thus, epithelial morphogenesis is an instructive mode of tissue assembly, maintenance, and repair. Recently, limitations of natural ECM extracts have motivated development of a synthetic ECM platform for detailed studies. In this thesis, PEG-4MAL was covalently functionalized with adhesive peptides and crosslinked with proteolytically-cleavable structural peptides in the presence of epithelial cells. The highly-efficient Michael-addition reaction enabled fabrication of hydrogel with elastic properties resembling natural ECMs [1]. By culturing MDCK II epithelial cells in these engineered PEG-4MAL matrices over a range of polymer wt% and RGD peptide concentration, we showed that the biochemical and physical properties of the matrix, particularly integrin signaling via ligand binding, elastic modulus, and matrix degradability, effectively modulate establishment of apico-basal polarity and lumen phenotypes in 3D cyst structures.

REFERENCES

1. Phelps, E.A., et al., *Maleimide Cross-Linked Bioactive PEG Hydrogel Exhibits Improved Reaction Kinetics and Cross-Linking for Cell Encapsulation and In Situ Delivery.* Advanced Materials, 2012. **24**(1): p. 64-70.

2. Bottinger, E.P., *TGF-beta in renal injury and disease.* Seminars in Nephrology, 2007. **27**(3): p. 309-320.

3. Liano, F., et al., *Epidemiology of acute renal failure: A prospective, multicenter, community-based study.* Kidney International, 1996. **50**(3): p. 811-818.

4. Thadhani, R., M. Pascual, and J.V. Bonventre, *Acute Renal Failure.* N Engl J Med, 1996. **334**(22): p. 1448-1460.

5. Bryant, D.M. and K.E. Mostov, *From cells to organs: building polarized tissue.* Nature Reviews Molecular Cell Biology, 2008. **9**(11): p. 887-901.

6. Humphreys, B.D., et al., *Intrinsic epithelial cells repair the kidney after injury.* Cell Stem Cell, 2008. **2**(3): p. 284-291.

7. Venkatachalam, M.A., et al., *ISCHEMIC DAMAGE AND REPAIR IN RAT PROXIMAL TUBULE - DIFFERENCES AMONG S1, S2, AND S3 SEGMENTS.* Kidney International, 1978. **14**(1): p. 31-49.

8. Zuk, A. and K.S. Matlin, *Induction of a laminin isoform and alpha 3beta 1-integrin in renal ischemic injury and repair in vivo.* Am J Physiol Renal Physiol, 2002. **283**(5): p. F971-984.

9. Ubelmann, F., et al., *Enterocyte loss of polarity and gut wound healing rely upon the F-actin–severing function of villin.* Proceedings of the National Academy of Sciences, 2013. **110**(15): p. E1380-E1389.

10. Wynn, T.A., *Cellular and molecular mechanisms of fibrosis.* The Journal of Pathology, 2008. **214**(2): p. 199-210.

11. Thannickal, V.J., et al., *Mechanisms of Pulmonary Fibrosis.* Annual Review of Medicine, 2004. **55**(1): p. 395-417.

12. Lutolf, M.P. and J.A. Hubbell, *Synthetic biomaterials as instructive extracellular microenvironments for morphogenesis in tissue engineering.* Nature Biotechnology, 2005. **23**(1): p. 47-55.

13. Bard, J., *Morphogenesis : the cellular and molecular processes of developmental anatomy*. Developmental and cell biology series, 23. 1992, Cambridge [England]: Cambridge University Press.

14. O'Brien, L.E., M.M.P. Zegers, and K.E. Mostov, *Opinion - Building epithelial architecture: insights from three-dimensional culture models.* Nature Reviews Molecular Cell Biology, 2002. **3**(7): p. 531-537.

15. Hartsock, A. and W.J. Nelson, *Adherens and tight junctions: Structure, function and connections to the actin cytoskeleton.* Biochimica Et Biophysica Acta-Biomembranes, 2008. **1778**(3): p. 660-669.

16. Jou, T.S., E.E. Schneeberger, and W.J. Nelson, *Structural and functional regulation of tight junctions by RhoA and Rac1 small GTPases.* Journal of Cell Biology, 1998. **142**(1): p. 101-115.

17. Perez-Moreno, M., C. Jamora, and E. Fuchs, *Sticky Business: Orchestrating Cellular Signals at Adherens Junctions.* Cell, 2003. **112**(4): p. 535-548.

18. Shin, K., V.C. Fogg, and B. Margolis, *Tight junctions and cell polarity*, in *Annual Review of Cell and Developmental Biology*. 2006. p. 207-235.

19. Cereijido, M., et al., *Tight junction and polarity interaction in the transporting epithelial phenotype.* Biochimica Et Biophysica Acta-Biomembranes, 2008. **1778**(3): p. 770-793.

20. Kowalczyk, A.P. and K.J. Green, *Structure, Function, and Regulation of Desmosomes*, in *Molecular Biology of Cadherins*, F. VanRoy, Editor. 2013. p. 95-118.

21. Farkas, A.E., C.T. Capaldo, and A. Nusrat, *Regulation of epithelial proliferation by tight junction proteins*, in *Barriers and Channels Formed by Tight Junction Proteins Ii*, M. Fromm and J.D. Schulzke, Editors. 2012. p. 115-124.

22. Apodaca, G., L.I. Gallo, and D.M. Bryant, *Role of membrane traffic in the generation of epithelial cell asymmetry.* Nat Cell Biol, 2012. **14**(12): p. 1235-1243.

23. Mostov, K.E., M. Verges, and Y. Altschuler, *Membrane traffic in polarized epithelial cells.* Current Opinion in Cell Biology, 2000. **12**(4): p. 483-490.

24. Akhtar, N. and C.H. Streuli, *An integrin–ILK–microtubule network orients cell polarity and lumen formation in glandular epithelium.* Nat Cell Biol, 2013. **15**(1): p. 17-27.

25. Drubin, D.G. and W.J. Nelson, *Origins of cell polarity.* Cell, 1996. **84**(3): p. 335-344.

26. Roignot, J., X. Peng, and K. Mostov, *Polarity in Mammalian Epithelial Morphogenesis.* Cold Spring Harbor Perspectives in Biology, 2013. **5**(2).

27. Martin-Belmonte, F., et al., *PTEN-mediated apical segregation of phosphoinositides controls epithelial morphogenesis through Cdc42.* Cell, 2007. **128**(2): p. 383-97.

28. Hynes, R.O., *The Extracellular Matrix: Not Just Pretty Fibrils.* Science, 2009. **326**(5957): p. 1216-1219.

29. Nelson, C.M. and J. Tien, *Microstructured extracellular matrices in tissue engineering and development.* Current Opinion in Biotechnology, 2006. **17**(5): p. 518-523.

30. Ekblom, M., et al., *Laminin Isoforms and Epithelial Development.* Annals of the New York Academy of Sciences, 1998. **857**(Morphogenesis: Cellular Interactions): p. 194-211.

31. Mak, G.Z., et al., *Regulated synthesis and functions of laminin 5 in polarized Madin-Darby canine kidney epithelial cells.* Molecular Biology of the Cell, 2006. **17**(8): p. 3664-3677.

32. Sasaki, T., R. Fässler, and E. Hohenester, *Laminin: the crux of basement membrane assembly.* The Journal of Cell Biology, 2004. **164**(7): p. 959-963.

33. Timpl, R. and J.C. Brown, *Supramolecular assembly of basement membranes.* BioEssays, 1996. **18**(2): p. 123-132.

34. Hamill, K.J., et al., *Laminin deposition in the extracellular matrix: a complex picture emerges.* J Cell Sci, 2009. **122**(Pt 24): p. 4409-17.

35. Wang, H., et al., *Rotational motion during three-dimensional morphogenesis of mammary epithelial acini relates to laminin matrix assembly.* Proceedings of the National Academy of Sciences, 2012.

36. Fox, J.W., et al., *Recombinant nidogen consists of three globular domains and mediates binding of laminin to collagen type IV.* Embo J, 1991. **10**(11): p. 3137-46.

37. Mayer, U., E. Kohfeldt, and R. Timpl, *Structural and Genetic Analysis of Laminin-Nidogen Interaction.* Annals of the New York Academy of Sciences, 1998. **857**(Morphogenesisi: Cellular Interactions): p. 130-142.

38. Cheng, Y.S., et al., *Self-assembly of laminin isoforms.* Journal of Biological Chemistry, 1997. **272**(50): p. 31525-31532.

39. Kalluri, R., *Basement membranes: structure, assembly and role in tumour angiogenesis.* Nature Reviews. Cancer, 2003. **3**(6): p. 422-433.

40. Kleinman, H.K., et al., *Basement membrane complexes with biological activity.* Biochemistry, 1986. **25**(2): p. 312-318.

41. Kleinman, H.K., et al., *ISOLATION AND CHARACTERIZATION OF TYPE-IV PROCOLLAGEN, LAMININ, AND HEPARAN-SULFATE PROTEOGLYCAN FROM THE EHS SARCOMA.* Biochemistry, 1982. **21**(24): p. 6188-6193.

42. Orkin, R.W., et al., *MURINE TUMOR PRODUCING A MATRIX OF BASEMENT-MEMBRANE.* Journal of Experimental Medicine, 1977. **145**(1): p. 204-220.

43. Aumailley, M., et al., *A simplified laminin nomenclature.* Matrix Biology, 2005. **24**(5): p. 326-332.

44. Miner, J.H. and P.D. Yurchenco, *LAMININ FUNCTIONS IN TISSUE MORPHOGENESIS.* Annual Reviews of Cell and Developmental Biology, 2004. **20**: p. 255-284.

45. Tashiro, K., et al., *THE RGD CONTAINING SITE OF THE MOUSE LAMININ A CHAIN IS ACTIVE FOR CELL ATTACHMENT, SPREADING, MIGRATION AND NEURITE OUTGROWTH.* Journal of Cellular Physiology, 1991. **146**(3): p. 451-459.

46. Goldfinger, L.E., M.S. Stack, and J.C.R. Jones, *Processing of laminin-5 and its functional consequences: Role of plasmin and tissue-type plasminogen activator.* Journal of Cell Biology, 1998. **141**(1): p. 255-265.

47. Odenthal, U., et al., *Molecular analysis of laminin N-terminal domains mediating self-interactions.* Journal of Biological Chemistry, 2004. **279**(43): p. 44504-44512.

48. Cohen, M.W., et al., *Laminin-induced clustering of dystroglycan on embryonic muscle cells: Comparison with agrin-induced clustering.* Journal of Cell Biology, 1997. **136**(5): p. 1047-1058.

49. Colognato, H. and P.D. Yurchenco, *The laminin alpha 2 expressed by dystrophic dy(2J) mice is defective in its ability to form polymers.* Current Biology, 1999. **9**(22): p. 1327-1330.

50. DeHart, G.W., K.E. Healy, and J.C.R. Jones, *The role of alpha 3 beta 1 integrin in determining the supramolecular organization of laminin-5 in the extracellular matrix of keratinocytes.* Experimental Cell Research, 2003. **283**(1): p. 67-79.

51. deHart, G.W. and J.C.R. Jones, *Myosin-mediated cytoskeleton contraction and Rho GTPases regulate laminin-5 matrix assembly.* Cell Motility and the Cytoskeleton, 2004. **57**(2): p. 107-117.

52. Sehgal, B.U., et al., *Integrin beta 4 regulates migratory behavior of keratinocytes by determining laminin-332 organization.* Journal of Biological Chemistry, 2006. **281**(46): p. 35487-35498.

53. Yu, W., et al., *Beta1-integrin orients epithelial polarity via Rac1 and laminin.* Mol Biol Cell, 2005. **16**(2): p. 433-45.

54. O'Brien, L.E., et al., *Rac1 orientates epithelial apical polarity through effects on basolateral laminin assembly.* Nature Cell Biology, 2001. **3**(9): p. 831-838.

55. Yu, W., et al., *Involvement of RhoA, ROCK I and myosin II in inverted orientation of epithelial polarity.* EMBO Rep, 2008. **9**(9): p. 923-929.

56. Leiss, M., et al., *The role of integrin binding sites in fibronectin matrix assembly in vivo.* Current Opinion in Cell Biology, 2008. **20**(5): p. 502-507.

57. Wierzbicka-Patynowski, I. and J.E. Schwarzbauer, *The ins and outs of fibronectin matrix assembly.* Journal of Cell Science, 2003. **116**(16): p. 3269-3276.

58. Timpl, R., et al., *Laminin--a glycoprotein from basement membranes.* Journal of Biological Chemistry, 1979. **254:**: p. 9933-9937.

59. Klein, G., et al., *ROLE OF LAMININ A-CHAIN IN THE DEVELOPMENT OF EPITHELIAL-CELL POLARITY.* Cell, 1988. **55**(2): p. 331-341.

60. Miner, J.H. and C. Li, *Defective glomerulogenesis in the absence of laminin alpha 5 demonstrates a developmental role for the kidney glomerular basement membrane.* Developmental Biology, 2000. **217**(2): p. 278-289.

61. Joly, D., et al., *beta(4) integrin and laminin 5 are aberrantly expressed in polycystic kidney disease - Role in increased cell adhesion and migration.* American Journal of Pathology, 2003. **163**(5): p. 1791-1800.

62. Nguyen, N.M. and R.M. Senior, *Laminin isoforms and lung development: All isoforms are not equal.* Developmental Biology, 2006. **294**(2): p. 271-279.

63. Ryan, M.C., et al., *Targeted Disruption of the LAMA3 Gene in Mice Reveals Abnormalities in Survival and Late Stage Differentiation of Epithelial Cells.* The Journal of Cell Biology, 1999. **145**(6): p. 1309-1324.

64. Urich, D., et al., *Lung-specific loss of the laminin α3 subunit confers resistance to mechanical injury.* Journal of Cell Science, 2011. **124**(17): p. 2927-2937.

65. Hynes, R.O., *Integrins: Bidirectional, allosteric signaling machines.* Cell, 2002. **110**(6): p. 673-687.

66. Matlin, K.S., B. Haus, and A. Zuk, *Integrins in epithelial cell polarity: using antibodies to analyze adhesive function and morphogenesis.* Methods, 2003. **30**(3): p. 235-46.

67. van der Flier, A. and A. Sonnenberg, *Function and interactions of integrins.* Cell and Tissue Research, 2001. **305**(3): p. 285-298.

68. Rienhoff, W., *Development and growth of the metanephros or permanent kidney in chick embryos.* John's Hopkins Hosp Bull, 1922. **33**: p. 392-406.

69. Saxén, L., T. Vainio, and S. Toivonen, *Effect of polyoma virus on mouse kidney rudiment in vitro.* Journal of the National Cancer Institute, 1962. **29**(3): p. 597-631.

70. Heath, J.K., *MORPHOGENESIS OF MAMMARY-GLAND.* Nature, 1977. **265**(5595): p. 587-587.

71. Kratochw.K, *ORGAN SPECIFICITY IN MESENCHYMAL INDUCTION DEMONSTRATED IN EMBRYONIC DEVELOPMENT OF MAMMARY GLAND OF MOUSE.* Developmental Biology, 1969. **20**(1): p. 46-&.

72. Kratochwil, K. and P. Schwartz, *TISSUE INTERACTION IN ANDROGEN RESPONSE OF EMBRYONIC MAMMARY RUDIMENT OF MOUSE - IDENTIFICATION OF TARGET TISSUE FOR TESTOSTERONE.* Proceedings of the National Academy of Sciences of the United States of America, 1976. **73**(11): p. 4041-4044.

73. Sakakura, T., Y. Nishizuka, and C.J. Dawe, *MESENCHYME-DEPENDENT MORPHOGENESIS AND EPITHELIUM-SPECIFIC CYTODIFFERENTIATION IN MOUSE MAMMARY-GLAND.* Science, 1976. **194**(4272): p. 1439-1441.

74. Gaush, C.R., W.L. Hard, and T.F. Smith, *CHARACTERIZATION OF AN ESTABLISHED LINE OF CANINE KIDNEY CELLS (MDCK).* Proceedings of the Society for Experimental Biology and Medicine, 1966. **122**(3): p. 931-&.

75. Dukes, J., P. Whitley, and A. Chalmers, *The MDCK variety pack: choosing the right strain.* BMC Cell Biology, 2011. **12**(1): p. 43.

76. Debnath, J., S.K. Muthuswamy, and J.S. Brugge, *Morphogenesis and Oncogenesis of MCF-10A mammary epithelial acini grown in three-dimensional basement membrane cultures.* Methods, 2003. **30**: p. 256-268.

77. Delie, F. and W. Rubas, *A human colonic cell line sharing similarities with enterocytes as a model to examine oral absorption: Advantages and limitations of the Caco-2 model.* Critical Reviews in Therapeutic Drug Carrier Systems, 1997. **14**(3): p. 221-286.

78. Rousset, M., *THE HUMAN-COLON CARCINOMA CELL-LINES HT-29 AND CACO-2 - 2 INVITRO MODELS FOR THE STUDY OF INTESTINAL DIFFERENTIATION.* Biochimie, 1986. **68**(9): p. 1035-1040.

79. Leighton, J., *ANATOMIC EVIDENCE OF TRANSPORT FUNCTION BY ADENOCARCINOMAS AND A SUGGESTED ROLE OF TRANSPORT IN THE SPREAD OF CANCER*.* Annals of the New York Academy of Sciences, 1981. **372**(Hormonal Regulation of Epithelial Transport of Ions and Water): p. 455-464.

80. McAteer, J.A., A.P. Evan, and K.D. Gardner, *MORPHOGENETIC CLONAL GROWTH OF KIDNEY EPITHELIAL-CELL LINE MDCK.* Anatomical Record, 1987. **217**(3): p. 229-239.

81. Bennett, D.C., *MORPHOGENESIS OF BRANCHING TUBULES IN CULTURES OF CLONED MAMMARY EPITHELIAL-CELLS.* Nature, 1980. **285**(5767): p. 657-659.

82. Bennett, D.C., B.L. Armstrong, and S.M. Okada, *RECONSTITUTION OF BRANCHING TUBULES FROM 2 CLONED MAMMARY CELL-TYPES IN CULTURE.* Developmental Biology, 1981. **87**(1): p. 193-199.

83. Hall, H.G., D.A. Farson, and M.J. Bissell, *LUMEN FORMATION BY EPITHELIAL-CELL LINES IN RESPONSE TO COLLAGEN OVERLAY - A MORPHOGENETIC MODEL IN CULTURE.* Proceedings of the National Academy of Sciences of the United States of America-Biological Sciences, 1982. **79**(15): p. 4672-4676.

84. Yang, J., et al., *SUSTAINED GROWTH AND 3-DIMENSIONAL ORGANIZATION OF PRIMARY MAMMARY-TUMOR EPITHELIAL-CELLS EMBEDDED IN COLLAGEN GELS.* Proceedings of the National Academy of Sciences of the United States of America, 1979. **76**(7): p. 3401-3405.

85. Yang, J., et al., *SUSTAINED GROWTH IN PRIMARY CULTURE OF NORMAL MAMMARY EPITHELIAL-CELLS EMBEDDED IN COLLAGEN GELS.* Proceedings of the National Academy of Sciences of the United States of America-Biological Sciences, 1980. **77**(4): p. 2088-2092.

86. McAteer, J.A., et al., *POLARIZED EPITHELIAL CYSTS INVITRO - A REVIEW OF CELL AND EXPLANT CULTURE SYSTEMS THAT EXHIBIT EPITHELIAL CYST FORMATION.* Scanning Microscopy, 1988. **2**(3): p. 1739-1763.

87. Montesano, R., et al., *IDENTIFICATION OF A FIBROBLAST-DERIVED EPITHELIAL MORPHOGEN AS HEPATOCYTE GROWTH-FACTOR.* Cell, 1991. **67**(5): p. 901-908.

88. Montesano, R., G. Schaller, and L. Orci, *INDUCTION OF EPITHELIAL TUBULAR MORPHOGENESIS INVITRO BY FIBROBLAST-DERIVED SOLUBLE FACTORS.* Cell, 1991. **66**(4): p. 697-711.

89. Pollack, A.L., R.B. Runyan, and K.E. Mostov, *Morphogenetic mechanisms of epithelial tubulogenesis: MDCK cell polarity is transiently rearranged without loss of cell-cell contact during scatter factor hepatocyte growth factor-induced tubulogenesis.* Developmental Biology, 1998. **204**(1): p. 64-79.

90. Dyer, R. and J. Ruby, *ELECTRON MICROSCOPE OBSERVATIONS OF ATTACHMENT OF CULTURED CELLS TO A RECONSTITUTED COLLAGEN MATRIX.* Anatomical Record, 1963. **145**(2): p. 224-&.

91. Grinnell, F. and M.K. Feld, *Fibronectin adsorption on hydrophilic and hydrophobic surfaces detected by antibody binding and analyzed during cell adhesion in serum-containing medium.* Journal of Biological Chemistry, 1982. **257**(9): p. 4888-4893.

92. O'Brien, L.E., et al., *Morphological and biochemical analysis of Rac1 in three-dimensional epithelial cell cultures.* Methods Enzymol, 2006. **406**: p. 676-91.

93. Chambard, M., J. Gabrion, and J. Mauchamp, *INFLUENCE OF COLLAGEN GEL ON THE ORIENTATION OF EPITHELIAL-CELL POLARITY - FOLLICLE FORMATION FROM ISOLATED THYROID-CELLS AND FROM PREFORMED MONOLAYERS.* Journal of Cell Biology, 1981. **91**(1): p. 157-166.

94. Greenburg, G. and E.D. Hay, *EPITHELIA SUSPENDED IN COLLAGEN GELS CAN LOSE POLARITY AND EXPRESS CHARACTERISTICS OF MIGRATING MESENCHYMAL CELLS.* Journal of Cell Biology, 1982. **95**(1): p. 333-339.

95. Wang, A.Z., G.K. Ojakian, and W.J. Nelson, *STEPS IN THE MORPHOGENESIS OF A POLARIZED EPITHELIUM .1. UNCOUPLING THE ROLES OF CELL CELL AND CELL SUBSTRATUM CONTACT IN ESTABLISHING PLASMA-MEMBRANE POLARITY IN MULTICELLULAR EPITHELIAL (MDCK) CYSTS.* Journal of Cell Science, 1990. **95**: p. 137-151.

96. Wang, A.Z., G.K. Ojakian, and W.J. Nelson, *STEPS IN THE MORPHOGENESIS OF A POLARIZED EPITHELIUM .2. DISASSEMBLY AND ASSEMBLY OF PLASMA-MEMBRANE DOMAINS DURING REVERSAL OF EPITHELIAL-CELL POLARITY IN MULTICELLULAR EPITHELIAL (MDCK) CYSTS.* Journal of Cell Science, 1990. **95**: p. 153-165.

97. Wang, A.Z., et al., *DETERMINANTS OF APICAL MEMBRANE FORMATION AND DISTRIBUTION IN MULTICELLULAR EPITHELIAL MDCK CYSTS.* American Journal of Physiology, 1994. **267**(2): p. C473-C481.

98. Grant, M.R., et al., *Simulating Properties of In Vitro Epithelial Cell Morphogenesis.* PLoS Comput Biol, 2006. **2**(10): p. e129.

99. Schoenenberger, C.A., et al., *Integrin expression and localization in normal MDCK cells and transformed MDCK cells lacking apical polarity.* J Cell Sci, 1994. **107 (Pt 2)**: p. 527-41.

100. Saelman, E.U.M., P.J. Keely, and S.A. Santoro, *LOSS OF MDCK CELL ALPHA-2-BETA-1 INTEGRIN EXPRESSION RESULTS IN REDUCED CYST FORMATION, FAILURE OF HEPATOCYTE GROWTH-FACTOR SCATTER FACTOR-INDUCED BRANCHING MORPHOGENESIS, AND INCREASED APOPTOSIS.* Journal of Cell Science, 1995. **108**: p. 3531-3540.

101. Ojakian, G.K. and R. Schwimmer, *REGULATION OF EPITHELIAL-CELL SURFACE POLARITY REVERSAL BY BETA(1)-INTEGRINS.* Journal of Cell Science, 1994. **107**: p. 561-576.

102. Schwimmer, R. and G.K. Ojakian, *THE ALPHA-2-BETA-1 INTEGRIN REGULATES COLLAGEN-MEDIATED MDCK EPITHELIAL MEMBRANE REMODELING AND TUBULE FORMATION.* Journal of Cell Science, 1995. **108**: p. 2487-2498.

103. Zuk, A. and K.S. Matlin, *Apical beta 1 integrin in polarized MDCK cells mediates tubulocyst formation in response to type I collagen overlay.* Journal of Cell Science, 1996. **109**: p. 1875-1889.

104. Jiang, S.T., et al., *Role of fibronectin deposition in cystogenesis of Madin-Darby canine kidney cells.* Kidney International, 1999. **56**(1): p. 92-103.

105. Kleinman, H.K. and G.R. Martin. *Matrigel: basement membrane matrix with biological activity*. in *Seminars in cancer biology*. 2005. Elsevier.

106. Ivanov, A.I., et al., *Myosin II regulates the shape of three-dimensional intestinal epithelial cysts.* J Cell Sci, 2008. **121**(Pt 11): p. 1803-14.

107. Jaffe, A.B., et al., *Cdc42 controls spindle orientation to position the apical surface during epithelial morphogenesis.* The Journal of Cell Biology, 2008. **183**(4): p. 625-633.

108. Zhang, X., et al., *The [alpha]2 and [alpha]3 integrins are required for morphologic differentiation of an intestinal epithelial cell line.* Surgery, 2003. **133**(4): p. 429-437.

109. Yu, W., et al., *Formation of cysts by alveolar type II cells in three-dimensional culture reveals a novel mechanism for epithelial morphogenesis.* Mol Biol Cell, 2007. **18**(5): p. 1693-700.

110. Debnath, J. and J.S. Brugge, *Modelling glandular epithelial cancers in three-dimensional cultures.* Nat Rev Cancer, 2005. **5**(9): p. 675-688.

111. Paszek, M., et al., *Tensional homeostasis and the malignant phenotype.* Cancer Cell, 2005. **8**: p. 241-254.

112. Ekblom, P., et al., *INVITRO SEGREGATION OF THE METANEPHRIC NEPHRON.* Developmental Biology, 1981. **84**(1): p. 88-95.

113. Nelson, W.J., *Adaptation of core mechanisms to generate cell polarity.* Nature, 2003. **422**(6933): p. 766-774.

114. Joberty, G., et al., *The cell-polarity protein Par6 links Par3 and atypical protein kinase C to Cdc42.* Nat Cell Biol, 2000. **2**(8): p. 531-9.

115. Kroschewski, R., A. Hall, and I. Mellman, *Cdc42 controls secretory and endocytic transport to the basolateral plasma membrane of MDCK cells.* Nat Cell Biol, 1999. **1**(1): p. 8-13.

116. Maehama, T. and J.E. Dixon, *The tumor suppressor, PTEN/MMAC1, dephosphorylates the lipid second messenger, phosphatidylinositol 3,4,5-trisphosphate.* J Biol Chem, 1998. **273**(22): p. 13375-8.

117. Musch, A., et al., *cdc42 regulates the exit of apical and basolateral proteins from the trans-Golgi network.* Embo J, 2001. **20**(9): p. 2171-9.

118. Rescher, U., et al., *Annexin 2 is a phosphatidylinositol (4,5)-bisphosphate binding protein recruited to actin assembly sites at cellular membranes.* J Cell Sci, 2004. **117**(Pt 16): p. 3473-80.

119. Lubarsky, B. and M.A. Krasnow, *Tube morphogenesis: Making and shaping biological tubes.* Cell, 2003. **112**(1): p. 19-28.

120. Lipschutz, J.H., et al., *Exocyst is involved in cystogenesis and tubulogenesis and acts by modulating synthesis and delivery of basolateral plasma membrane and secretory proteins.* Molecular Biology of the Cell, 2000. **11**(12): p. 4259-4275.

121. Vegasalas, D.E., P.J.I. Salas, and E. Rodriguezboulan, *MODULATION OF THE EXPRESSION OF AN APICAL PLASMA-MEMBRANE PROTEIN OF MADIN-DARBY CANINE KIDNEY EPITHELIAL-CELLS - CELL CELL-INTERACTIONS CONTROL THE APPEARANCE OF A NOVEL INTRACELLULAR STORAGE COMPARTMENT.* Journal of Cell Biology, 1987. **104**(5): p. 1249-1259.

122. Vegasalas, D.E., P.J.I. Salas, and E. Rodriguezboulan, *EXOCYTOSIS OF VACUOLAR APICAL COMPARTMENT (VAC) - A CELL CELL CONTACT CONTROLLED MECHANISM FOR THE ESTABLISHMENT OF THE APICAL PLASMA-MEMBRANE DOMAIN IN EPITHELIAL-CELLS.* Journal of Cell Biology, 1988. **107**(5): p. 1717-1728.

123. Martin-Belmonte, F., et al., *Cell-polarity dynamics controls the mechanism of lumen formation in epithelial morphogenesis.* Curr Biol, 2008. **18**(7): p. 507-13.

124. Debnath, J., et al., *The role of apoptosis in creating and maintaining luminal space with normal and oncogene-expressing mammary acini.* Cell, 2002. **111**(1): p. 29-40.

125. Currie, L.J., J.R. Sharpe, and R. Martin, *The use of fibrin glue in skin grafts and tissue-engineered skin replacements: A review.* Plastic and Reconstructive Surgery, 2001. **108**(6): p. 1713-1726.

126. Patino, M.G., et al., *Collagen as an Implantable Material in Medicine and Dentistry.* Journal of Oral Implantology, 2002. **28**(5): p. 220-225.

127. Silva, G.A., et al., *Selective differentiation of neural progenitor cells by high-epitope density nanofibers.* Science, 2004. **303**(5662): p. 1352-1355.

128. DeForest, C.A. and K.S. Anseth, *Advances in Bioactive Hydrogels to Probe and Direct Cell Fate.* Annual Review of Chemical and Biomolecular Engineering, 2012. **3**(1): p. 421-444.

129. Zhu, J., *Bioactive modification of poly(ethylene glycol) hydrogels for tissue engineering.* Biomaterials, 2010. **31**(17): p. 4639-4656.

130. Lutolf, M.P., et al., *Synthetic matrix metalloproteinase-sensitive hydrogels for the conduction of tissue regeneration: Engineering cell-invasion characteristics.* Proceedings of the National Academy of Sciences of the United States of America, 2003. **100**(9): p. 5413-5418.

131. Lutolf, M.P., et al., *Cell-Responsive Synthetic Hydrogels.* Advanced Materials, 2003. **15**(11): p. 888-892.

132. Gobaa, S., et al., *Artificial niche microarrays for probing single stem cell fate in high throughput.* Nature Methods, 2011. **8**(11): p. 949-955.

133. Ranga, A. and M.P. Lutolf, *High-throughput approaches for the analysis of extrinsic regulators of stem cell fate.* Current Opinion in Cell Biology, 2012. **24**(2): p. 236-244.

134. Schwartz, M.P., et al., *A synthetic strategy for mimicking the extracellular matrix provides new insight about tumor cell migration.* Integr Biol (Camb), 2010. **2**(1): p. 32-40.

135. Gobin, A.S. and J.L. West, *Cell migration through defined, synthetic extracellular matrix analogues.* Faseb Journal, 2002. **16**(3): p. 751-+.

136. Phelps, E.A., et al., *Bioartificial matrices for therapeutic vascularization.* Proc Natl Acad Sci U S A, 2010. **107**(8): p. 3323-8.

137. Fisher, J.P., et al., *PHOTOINITIATED POLYMERIZATION OF BIOMATERIALS.* Annual Review of Materials Research, 2001. **31**(1): p. 171-181.

138. Kloxin, A.M., et al., *Photodegradable Hydrogels for Dynamic Tuning of Physical and Chemical Properties.* Science, 2009. **324**(5923): p. 59-63.

139. Polizzotti, B.D., B.D. Fairbanks, and K.S. Anseth, *Three-dimensional biochemical patterning of click-based composite hydrogels via thiolene photopolymerization.* Biomacromolecules, 2008. **9**(4): p. 1084-1087.

140. Hahn, M.S., et al., *Photolithographic patterning of polyethylene glycol hydrogels.* Biomaterials, 2006. **27**(12): p. 2519-2524.

141. Hahn, M.S., J.S. Miller, and J.L. West, *Three-dimensional biochemical and biomechanical patterning of hydrogels for guiding cell behavior.* Advanced Materials, 2006. **18**(20): p. 2679-+.

142. Michael, V.T., et al., *Effective tuning of ligand incorporation and mechanical properties in visible light photopolymerized poly(ethylene glycol) diacrylate hydrogels dictates cell adhesion and proliferation.* Biomedical Materials, 2013. **8**(2): p. 025001.

143. Gill, B.J., et al., *A synthetic matrix with independently tunable biochemistry and mechanical properties to study epithelial morphogenesis and EMT in a lung adenocarcinoma model.* Cancer Research, 2012.

144. Lutolf, M.P., et al., *Systematic modulation of Michael-type reactivity of thiols through the use of charged amino acids.* Bioconjug Chem, 2001. **12**(6): p. 1051-6.

145. Friedman, M., J.F. Cavins, and J.S. Wall, *Relative Nucleophilic Reactivities of Amino Groups and Mercaptide Ions in Addition Reactions with α,β-Unsaturated Compounds1,2.* Journal of the American Chemical Society, 1965. **87**(16): p. 3672-3682.

146. Heggli, M., et al., *Michael-Type Addition as a Tool for Surface Functionalization.* Bioconjugate Chemistry, 2003. **14**(5): p. 967-973.

147. Lutolf, M.P. and J.A. Hubbell, *Synthesis and physicochemical characterization of end-linked poly(ethylene glycol)-co-peptide hydrogels formed by Michael-type addition.* Biomacromolecules, 2003. **4**(3): p. 713-22.

148. Rizzi, S.C. and J.A. Hubbell, *Recombinant protein-co-PEG networks as cell-adhesive and proteolytically degradable hydrogel matrixes. Part I: Development and physicochemical characteristics.* Biomacromolecules, 2005. **6**(3): p. 1226-38.

149. Rizzi, S.C., et al., *Recombinant protein-co-PEG networks as cell-adhesive and proteolytically degradable hydrogel matrixes. Part II: biofunctional characteristics.* Biomacromolecules, 2006. **7**(11): p. 3019-29.

150. Chung, I.M., et al., *Bioadhesive hydrogel microenvironments to modulate epithelial morphogenesis.* Biomaterials, 2008. **29**(17): p. 2637-45.

151. Shikanov, A., et al., *Hydrogel network design using multifunctional macromers to coordinate tissue maturation in ovarian follicle culture.* Biomaterials, 2011. **32**(10): p. 2524-2531.

152. Phelps, E.A., et al., *Vasculogenic bio-synthetic hydrogel for enhancement of pancreatic islet engraftment and function in type 1 diabetes.* Biomaterials, 2013. **34**(19): p. 4602-4611.

153. Salimath, A.S., et al., *Dual Delivery of Hepatocyte and Vascular Endothelial Growth Factors via a Protease-Degradable Hydrogel Improves Cardiac Function in Rats.* Plos One, 2012. **7**(11).

154. Rodríguez-Fraticelli, A.E., et al., *Cell confinement controls centrosome positioning and lumen initiation during epithelial morphogenesis.* The Journal of Cell Biology, 2012. **198**(6): p. 1011-1023.

155. Wang, C.-C., L. Jamal, and K.A. Janes, *Normal morphogenesis of epithelial tissues and progression of epithelial tumors.* Wiley Interdisciplinary Reviews: Systems Biology and Medicine, 2012. **4**(1): p. 51-78.

156. McAteer, J.A., et al., *MDCK cysts: An in vitro model of epithelial cyst formation and growth.* Methods in Cell Science, 1986. **10**(4): p. 245-248.

157. Ferrari, A., et al., *ROCK-mediated contractility, tight junctions and channels contribute to the conversion of a preapical patch into apical surface during isochoric lumen initiation.* Journal of Cell Science, 2008. **121**(21): p. 3649-3663.

158. Torkko, J.M., et al., *Depletion of apical transport proteins perturbs epithelial cyst formation and ciliogenesis.* Journal of Cell Science, 2008. **121**(8): p. 1193-1203.

159. Patterson, J. and J.A. Hubbell, *Enhanced proteolytic degradation of molecularly engineered PEG hydrogels in response to MMP-1 and MMP-2.* Biomaterials, 2010. **31**(30): p. 7836-7845.

160. Grobelny, D., L. Poncz, and R.E. Galardy, *Inhibition of human skin fibroblast collagenase, thermolysin, and Pseudomonas aeruginosa elastase by peptide hydroxamic acids.* Biochemistry, 1992. **31**(31): p. 7152-4.

161. Galardy, R.E., et al., *Inhibition of angiogenesis by the matrix metalloprotease inhibitor N-[2R-2-(hydroxamidocarbonymethyl)-4-methylpentanoyl)]-L-tryptophan methylamide.* Cancer Res, 1994. **54**(17): p. 4715-8.

162. Solorzano, C.C., et al., *A matrix metalloproteinase inhibitor prevents processing of tumor necrosis factor alpha (TNF alpha) and abrogates endotoxin-induced lethality.* Shock, 1997. **7**(6): p. 427-31.

163. Pikul, S., et al., *Discovery of Potent, Achiral Matrix Metalloproteinase Inhibitors.* Journal of Medicinal Chemistry, 1998. **41**(19): p. 3568-3571.

164. Catania, J.M., G. Chen, and A.R. Parrish, *Role of matrix metalloproteinases in renal pathophysiologies.* American Journal of Physiology - Renal Physiology, 2007. **292**(3): p. F905-F911.

165. Shih, H. and C.-C. Lin, *Visible-Light-Mediated Thiol-Ene Hydrogelation Using Eosin-Y as the Only Photoinitiator.* Macromolecular Rapid Communications, 2013. **34**(3): p. 269-273.

166. Butcher, D.T., T. Alliston, and V.M. Weaver, *A tense situation: forcing tumour progression.* Nat Rev Cancer, 2009. **9**(2): p. 108-122.

167. DuFort, C.C., M.J. Paszek, and V.M. Weaver, *Balancing forces: architectural control of mechanotransduction.* Nat Rev Mol Cell Biol, 2011. **12**(5): p. 308-319.

168. Khetan, S., et al., *Degradation-mediated cellular traction directs stem cell fate in covalently crosslinked three-dimensional hydrogels.* Nature Materials, 2013. **12**(5): p. 458-465.

169. Kim, M., et al., *Polarity proteins PAR6 and aPKC regulate cell death through GSK-3β in 3D epithelial morphogenesis.* Journal of Cell Science, 2007. **120**(14): p. 2309-2317.

170. Desclozeaux, M., et al., *Active Rab11 and functional recycling endosome are required for E-cadherin trafficking and lumen formation during epithelial morphogenesis.* American Journal of Physiology-Cell Physiology, 2008. **295**(2): p. C545-C556.

171. Desclozeaux, M., et al., *Active Rab11 and functional recycling endosome are required for E-cadherin trafficking and lumen formation during epithelial morphogenesis.* Am J Physiol Cell Physiol, 2008. **295**(2): p. C545-56.

172. Troxell, M.L., et al., *Mutant cadherin affects epithelial morphogenesis and invasion, but not transformation.* J Cell Sci, 2001. **114**(Pt 6): p. 1237-46.

173. Raza, A., C.S. Ki, and C.-C. Lin, *The influence of matrix properties on growth and morphogenesis of human pancreatic ductal epithelial cells in 3D.* Biomaterials, 2013. **34**(21): p. 5117-5127.

174. Francus, P., *Image Analysis, Sediments and Paleoenvironments*. 2004: Springer.

175. Zar, J.H., *Biostatistical analysis*. 1999: Prentice Hall.

176. Streuli, C.H., *Integrins and cell-fate determination.* J Cell Sci, 2009. **122**(2): p. 171-177.

177. Hersel, U., C. Dahmen, and H. Kessler, *RGD modified polymers: biomaterials for stimulated cell adhesion and beyond.* Biomaterials, 2003. **24**(24): p. 4385-4415.

178. Petrie, T.A., et al., *Integrin specificity and enhanced cellular activities associated with surfaces presenting a recombinant fibronectin fragment compared to RGD supports.* Biomaterials, 2006. **27**(31): p. 5459-5470.

179. Pierschbacher, M.D. and E. Ruoslahti, *CELL ATTACHMENT ACTIVITY OF FIBRONECTIN CAN BE DUPLICATED BY SMALL SYNTHETIC FRAGMENTS OF THE MOLECULE.* Nature, 1984. **309**(5963): p. 30-33.

180. Ruoslahti, E. and M.D. Pierschbacher, *NEW PERSPECTIVES IN CELL-ADHESION - RGD AND INTEGRINS.* Science, 1987. **238**(4826): p. 491-497.

181. Schlaepfer, D.D., et al., *INTEGRIN-MEDIATED SIGNAL-TRANSDUCTION LINKED TO RAS PATHWAY BY GRB2 BINDING TO FOCAL ADHESION KINASE.* Nature, 1994. **372**(6508): p. 786-791.

182. Garcia, A.J. and D. Boettiger, *Integrin-fibronectin interactions at the cell-material interface: initial integrin binding and signaling.* Biomaterials, 1999. **20**(23-24): p. 2427-2433.

183. Liu, K.D., et al., *Rac1 is required for reorientation of polarity and lumen formation through a PI 3-kinase-dependent pathway.* American Journal of Physiology-Renal Physiology, 2007. **293**(5): p. F1633-F1640.

184. Wu, W., et al., *β1-Integrin is required for kidney collecting duct morphogenesis and maintenance of renal function.* American Journal of Physiology - Renal Physiology, 2009. **297**(1): p. F210-F217.

185. Frisch, S.M. and H. Francis, *DISRUPTION OF EPITHELIAL CELL-MATRIX INTERACTIONS INDUCES APOPTOSIS.* Journal of Cell Biology, 1994. **124**(4): p. 619-626.

186. Arevalo, R.C., J.S. Urbach, and D.L. Blair, *Size-Dependent Rheology of Type-I Collagen Networks.* Biophysical Journal, 2010. **99**(8): p. L65–L67.

187. Peppas, N.A., et al., *Hydrogels in Biology and Medicine: From Molecular Principles to Bionanotechnology.* Advanced Materials, 2006. **18**(11): p. 1345-1360.

188. Coleman, M.L., C.J. Marshall, and M.F. Olson, *RAS and RHO GTPases in G1-phase cell-cycle regulation.* Nature Reviews Molecular Cell Biology, 2004. **5**(5): p. 355-366.

189. Miner, J.H. and P.D. Yurchenco, *Laminin functions in tissue morphogenesis.* Annu Rev Cell Dev Biol, 2004. **20**: p. 255-84.

190. Greciano, P.G., et al., *Laminin 511 partners with laminin 332 to mediate directional migration of Madin–Darby canine kidney epithelial cells.* Molecular Biology of the Cell, 2012. **23**(1): p. 121-136.

191. Joly, D., et al., *Laminin 5 Regulates Polycystic Kidney Cell Proliferation and Cyst Formation.* Journal of Biological Chemistry, 2006. **281**(39): p. 29181-29189.

192. Mochizuki, M., et al., *Laminin-1 peptide-conjugated chitosan membranes as a novel approach for cell engineering.* Faseb Journal, 2003. **17**(3): p. 875-+.

193. Hozumi, K., et al., *Cell adhesive peptide screening of the mouse laminin alpha1 chain G domain.* Arch Biochem Biophys, 2010. **503**(2): p. 213-22.

194. Hozumi, K., et al., *Reconstitution of laminin-111 biological activity using multiple peptide coupled to chitosan scaffolds.* Biomaterials, 2012. **33**(17): p. 4241-50.

195. Katagiri, F., et al., *Identification of active sequences in the L4a domain of laminin alpha5 promoting neurite elongation.* Biochemistry, 2012. **51**(24): p. 4950-8.

196. Yamada, Y., et al., *Laminin active peptide/agarose matrices as multifunctional biomaterials for tissue engineering.* Biomaterials, 2012. **33**(16): p. 4118-25.

197. Bower, A.F., *Applied Mechanics of Solids*. 2009, Boca Raton, FL, USA: CRC Press.

198. Sbalzarini, I. and P. Koumoutsakos, *Feature point tracking and trajectory analysis for video imaging in cell biology.* Journal of Structural Biology, 2005. **151**: p. 182-195.

199. Legant, W.R., et al., *Measurement of mechanical tractions exerted by cells in three-dimensional matrices.* Nature Methods, 2010. **7**: p. 969-971.

200. Salierno, M.J., A.J. García, and A. del Campo, *Photo-Activatable Surfaces for Cell Migration Assays.* Advanced Functional Materials, 2013. **doi: 10.1002/adfm.201300902**.

201. Weis, S., et al., *Dynamic cell-adhesive microenvironments and their effect on myogenic differentiation.* Acta Biomaterialia, 2013. **9**(9): p. 8059-8066.

VITA

NDUKA O. ENEMCHUKWU

ENEMCHUKWU was born in Boston, Massachusetts, USA to a pair of Nigerian immigrants who met at Northeastern University while pursuing degrees in pharmacy. He is their third child of six and the first of their three sons. By age five, his family moved to Mount Dora, Florida. He graduated from Mount Dora High School in 2001. As a youth, Enemchukwu excelled in spelling and participated in interscholastic sports including basketball, cross-country, tennis, and track and field. He was active in student government and community service and a participant in American Legion's Florida Boys' State. Enemchukwu earned an SB in Materials Science and Engineering with a minor in Applied International Studies at Massachusetts Institute of Technology (MIT) in 2005. At MIT, he held leadership roles in MIT Campus Crusade for Christ and MIT Black Students Union and completed an internship at Hitachi Chemical in Tsukuba, Japan with the MIT Japan Program. After a year internship with Campus Crusade for Christ following his graduation from MIT, Enemchukwu continued his studies at Georgia Institute of Technology. At Georgia Tech, he held leadership roles in the Black Graduate Students' Association and the Fellowship of Christian Graduate Students and was an instructor in the LEAD Summer Engineering Program for high school students. In Atlanta, he has been an active member of his church, Assembly of Truth Family Worship Center, and cultural organizations including Umu Igbo Unite and Nnewi Union Atlanta. In 2012, Enemchukwu married Chinyere Uzomba, with whom he enjoys cooking, dancing, and ministry activities.